Lateral carbon export from the southern Benguela upwelling system

Prepared by:
Neil C. Swart

Department of Physical Oceanography
University of Cape Town

This dissertation is submitted to the University of Cape Town
in fulfilment of the academic requirements
for the Degree of Master of Science in Physical Oceanography

January 2008

Abstract

The objective of this study was to quantify the lateral export of organic carbon from the continental shelf of the southern Benguela upwelling system to the open ocean. The flux is potentially important because the Benguela is one of the most productive and biogeochemically active ecosystems in the global ocean. Furthermore, a significant fraction of oceanic carbon storage is modulated through the biological pump mechanism, and on millennial timescales the global ocean regulates atmospheric concentrations of carbon dioxide. The current study builds on previous work, and examines both the physical and biogeochemical aspects of the lateral carbon flux from the southern Benguela. Multiple physical mechanisms capable of inducing cross-shelf advection were examined, including dynamic interaction with Agulhas Rings and upwelling front instability, however the bottom boundary layer (BBL) was the focus. The vertical extent, cross-shelf distribution and flow characteristics of the BBL were made using historical hydrographic and current meter data. The BBL was a persistent feature of the southern Benguela shelf and slope. Recording current meter records from several positions confirmed the theoretical proposition that off-shelf flow would occur during poleward flow regimes. Particular regions, most notably the Cape Canyon, experienced unprecedented off-shelf velocities at all times, highlighting such regions as conduits of shelf-ocean exchange. The characteristics of internal tide propagation over the bathymetry of the southern Benguela, critical to vertical mixing, were examined for the first time. The semi-diurnal internal tide was found to preferentially dissipate its energy on the upper continental slope, potentially becoming bottom trapped and generating significant baroclinic velocities. Such energy dissipation and turbulent mixing would be critically important for sediment resuspension, bottom nepheloid layer formation and lateral advection. Diurnal internal tides were likely to be transmitted onto the shelf, where they were recognized as a mechanism modulating bottom mixing.

The biogeochemistry of the water column in the southern Benguela was considered using *in situ* cruise data. Active denitrification was identified on the basis of a nitrogen deficit, highlighting the importance of this process in the southern system, and raising concerns over the generic use of Redfield stoichiometry. All biogeochemical variables displayed a distinct seasonal signal. Concentrations of POC in summer were considerably higher than those observed on other continental shelves, and strong horizontal gradients with the open ocean suggest that a significant shelf-ocean exchange could occur under favourable flow conditions. A significant aspect of this study is the documentation of the first known reliable estimates of DOC in the southern Benguela, which show it to be the dominant carbon pool. DOC concentrations were remarkably high for an upwelling system, likely as a result of the large primary production, and also exhibit strong horizontal gradients and lateral export potential. An outstanding result was the identification of the bottom nepheloid layer as a biogeochemical hot spot, being the preferential site of oxygen deficiency, denitrification, organic matter accumulation and the region of strongest horizontal gradients.

Recognizing its importance, the bottom nepheloid layer (BNL) was characterized in its vertical extent and cross-shelf distribution for the first time in the southern Benguela using historical optical backscatter data. The optical data were significantly correlated with measured *in situ* POC concentrations. The BNL was ubiquitous over the shelf and slope, was not seasonal, and it was maintained through lateral advection rather than vertical input of particulate matter. A turbidity time series shows pulses of particulate matter propagating across the shelf in time and entering the deep ocean. Through a cross-shelf carbon flux model it was possibly to quantify the annual lateral export flux of POC from the southern Benguela continental shelf to the deep ocean. The result indicated that the vast majority of organic carbon was oxidized on the continental shelf, and that only a small fraction (<1%) of primary production was exported seaward of the shelf break as POC. Despite the small magnitude of the lateral POC flux, it was in good agreement with geological rates of organic carbon accumulation on the upper continental slope. The potential lateral DOC flux was estimated as an order of magnitude greater than the POC flux, but still a negligible fraction

of total primary production. Thus it seems that the system cannot play a significant role in modulating atmospheric carbon dioxide levels on time scales of human relevance.

Preface

The work herein comprises an MSc dissertation in Physical Oceanography, completed at the University of Cape Town, under the supervision of Dr Howard Waldron. The thesis is organised into four chapters, each independent in its own right, followed by a conclusion, as follows:

The introduction consists of a literature review which attempts to define precisely the importance of the global carbon cycle, the role of the ocean in this cycle, and specifically the contribution of the marine biota and continental margins. The introduction also serves to introduce the study region, the southern Benguela, and to review previous carbon flux studies which have been undertaken in the area. A statement of the working hypothesis of this research project concludes the first chapter.

Chapter 2 is an examination of the physical mechanisms which are most important in modulating lateral carbon fluxes on continental margins, with specific observations from the Benguela. It is presented near the beginning of the thesis in order to set the physical context for the remainder of the work, yet it was not a major focus of the project.

The third chapter concerns the biogeochemistry of the water column in the study region, based on measured variables, and is the foundation on which most of the assertions made in the thesis are based.

The fourth and final chapter delves into historical data sets, and attempts to address the principal theme of the thesis regarding the quantity of organic carbon exported from the southern Benguela system, and it is an applied modeling approach.

Declaration

I declare that this thesis is my own work. Where collaboration with other people has taken place, or material generated by other researchers is included, the parties and/or material are indicated in the acknowledgements or references as appropriate. This work is being submitted for the Master of Science Degree in Physical Oceanography at the University of Cape Town. It has not been submitted to any other university for any other degree or examination.

Neil C. Swart

Date

Acknowledgements

I was personally supported financially through the David and Elaine Potter Fellowship, administered by UCT, for which I am most grateful, since without it I would not have been able to complete a MSc. The running costs of the research project were kindly provided from the Benguela Ecology Programme grant from the NRF. A semester exchange at Scripps Institution of Oceanography vastly improved the quality of this project. I would like to dearly thank my host there, Lihini Aluwihare, for her hospitality and assistance. I'm grateful to the other SIO faculty who also gave me valuable advice, most notably Peter Franks and Jen Mackinnon. The IAPO office and UCT made the exchange possible logistically and financially, for which I thank them, particularly Sharon Turner. My supervisor, Howard Waldron, conceived of the project, and inspired many of the earlier ideas and research strategies which made the study a success. I would also like to thank Howard for helping with the current meter logistics, and spending three beer-less days at sea helping me to filter water. The UCT oceanography department was my home and the people my friends and advisors for the last two years, and it was great. The CSIR (Pedro Monteiro; Eugene Mabille), IMT (Carl Waiman, Pepedi, Skoller) and MCM (Larry Hutchings; Franklin Frantz) all helped in developing, and deploying an ADCP mooring, for which they are each thanked. The in situ data which form the foundation of this thesis comes from the SHBML, which is Larry Hutchings initiative. Furthermore, Larry allowed my participation on several cruises to collect my own data, and provided much useful discussion on the Benguela. The historical SHBML was provided thanks to the efforts of Marcel van den Berg and Christine Illert at MCM - I am grateful. Marten Gründlingh and Ursula Von St Ange at SADCO gave me access to

the RCM data and helped with my numerous queries, for which I thank them. Some of the results of this work were reported at the Continental Margins conference in Shanghai, China, September 2007. It was an IMBER/LOICZ meeting, and my attendance was sponsored by SCOR, facilitated through the IMBER IPO to whom I would like to say Xie Xie very much. I would mostly like to thank my parents, Allan and Joan, and sister Michelle for their support, over all the years. Its greatly appreciated, and I certainly wouldn't have survived without it. Then, to all the raggeds, now displaced around the world, whose incorrigible behaviour and excessive lager consumption made the last 6 years in Cape Town truly worthwhile, muchos gracias.

Contents

List of Figures

List of Tables

Chapter 1

Introduction

1.1 The carbon cycle in context: Global climate and atmospheric CO_2 during the last 540 million years

1.1.1 The modern context

Since the late 19th century it has been recognized that increasing the concentrations of greenhouse gasses (GHG) in the atmosphere could potentially lead to global warming through an enhanced greenhouse effect (Sarmiento, 1993). Meanwhile since the beginning of the industrial revolution, human activities have released greenhouse gasses into the atmosphere, principally carbon dioxide derived from fossil fuel emissions and land use changes (Sarmiento, 1993; Siegenthaler and Sarmiento, 1993; Schimel et al., 2000; Solomon et al., 2007). The resulting rise in atmospheric carbon dioxide concentrations, which has been directly measured since 1957 (Figure 1.1), has thus become a matter of central concern to modern society. (Schimel et al., 2000; Keeling et al., 2005; Solomon et al., 2007). The rapid increase in CO_2 concentrations since $\approx$1800 is undoubtedly due to anthropogenic emissions (Keeling et al., 2005; Solomon et al., 2007). This is known because the rate of atmospheric increase in CO_2 has been less than the fossil fuel input, implying that the oceans and terrestrial biosphere (and all other sources of natural variation such as volcanoes) have together been a net sink of CO_2

during this period (Figure 1.2) (Siegenthaler and Sarmiento, 1993; Schimel et al., 2000). The link between anthropogenic emissions and atmospheric accumulation is further supported by the fact that the difference in CO_2 concentrations between the Northern Hemisphere (NH) and Southern Hemisphere (SH) has been increasing in time - an expected consequence of the higher emissions in the NH (Siegenthaler and Sarmiento, 1993).

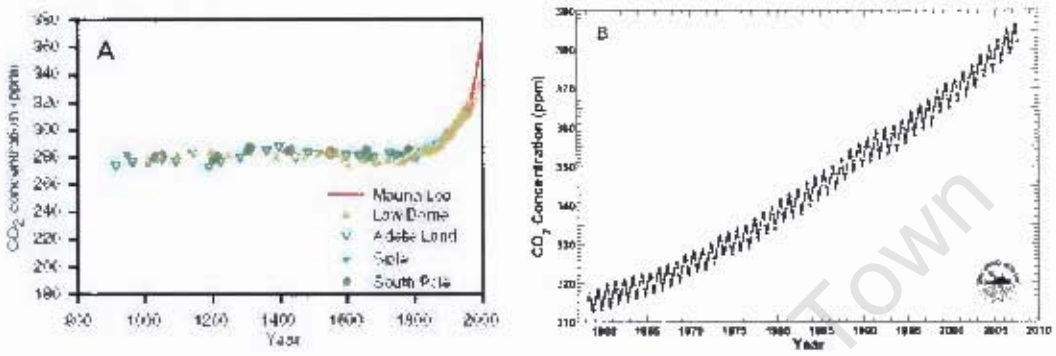

Figure 1.1: Atmospheric CO_2 concentrations over various timescales. **A** (Atmospheric) CO_2 concentration in various Antarctic ice cores for the past millennium, showing steady concentrations of approximately 280 ppm prior to 1800, and the extremely rapid increase associated with the industrial revolution thereafter. Recent atmospheric measurements at Mauna Loa are shown in red for comparison [from Prentice et al 2001 Figure 3.2]. **B** Monthly average atmospheric carbon dioxide concentration versus time at Mauna Loa Observatory, Hawaii (20°N, 156°W) where CO_2 concentration is in parts per million in the mole fraction (p.p.m.). The curve is a fit to the data based on a stiff spline plus a 4 harmonic fit to the seasonal cycle with a linear gain factor. Data from Scripps CO2 Program (http://scripps.co2.ucsd.edu). Last updated August 2007.

The question arises as to how significant the recent modern anthropogenic CO_2 perturbation is in respect to past changes, and how likely it is that such changes can have a marked influence on global climate. We can address these questions through a consideration of atmospheric CO_2 and climate over the Phanerozoic eon, the period of the last 540 million years.

1.1.2 Climate and atmospheric CO_2 during the Phanerozoic eon

Reconstructions of distant past atmospheric CO_2 concentrations (Figure 1.3) can be made through carbon cycle models (Berner and Kothavala, 2001; Bergman et al., 2004), or using geochemical proxies (Royer et al., 2004), both of which are in good agreement. On these multimillion year timescales, CO_2 levels are controlled by an interplay between the silicate-carbonate cycle (vulcanism/tectonics and weathering) and the organic matter cycle

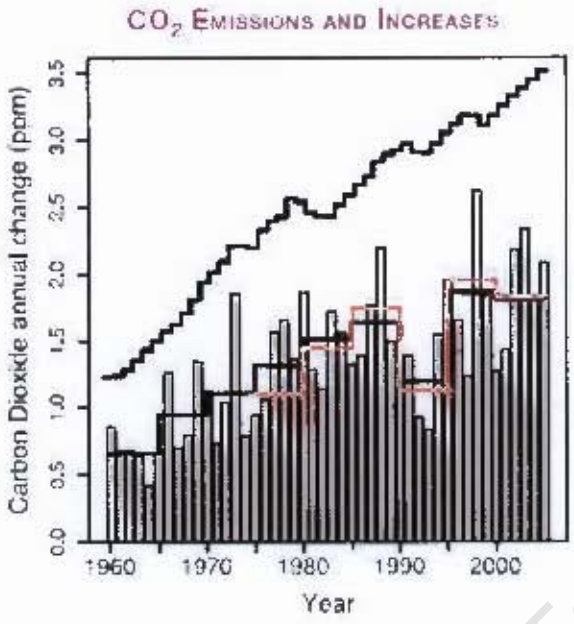

Figure 1.2: Annual changes in global mean CO_2 concentration (grey bars) and their five-year means from two different measurement networks (red and lower black stepped lines). The five-year means smooth out short-term perturbations associated with strong ENSO events in 1972, 1982, 1987 and 1997. Uncertainties in the five-year means are indicated by the difference between the red and lower black lines and are of order 0.15 ppm. The upper stepped line shows the annual increases that would occur if all fossil fuel emissions stayed in the atmosphere and there were no other emissions (From Solomon et al. (2007) Figure T.S.3).

(photosynthesis/sedimentation and diagenesis/respiration) (Berner, 2005). The major features of the record are the very high atmospheric CO_2 concentrations (>20 times modern levels) of the early Phanerozoic, the massive decrease during the Devonian period (≈400 Ma) caused by the rise of large land plants (Berner and Kothavala, 2001; Berner, 2005), the secondary CO_2 maxima in the Triassic and Jurassic (≈200 Ma), and the sustained decrease in atmospheric CO_2 over the last 150 million years (Berner and Kothavala, 2001; Ghosh et al., 2005).

Over Phanerozoic timescales geological evidence of glacial deposits provides a robust, albeit coarse, record of global temperatures. There is a pronounced glacial extent during two periods, the Permian-Carboniferous (≈300 Ma) and the recent (30 - 0 Ma) Cenozoic (see Figure 1.3). It is particularly relevant to note that both the major glaciations correspond to periods of low atmospheric CO_2 (<500 ppm), implying that atmospheric CO_2 concentrations controlled global climate through the greenhouse effect over geological time (Royer et al.,

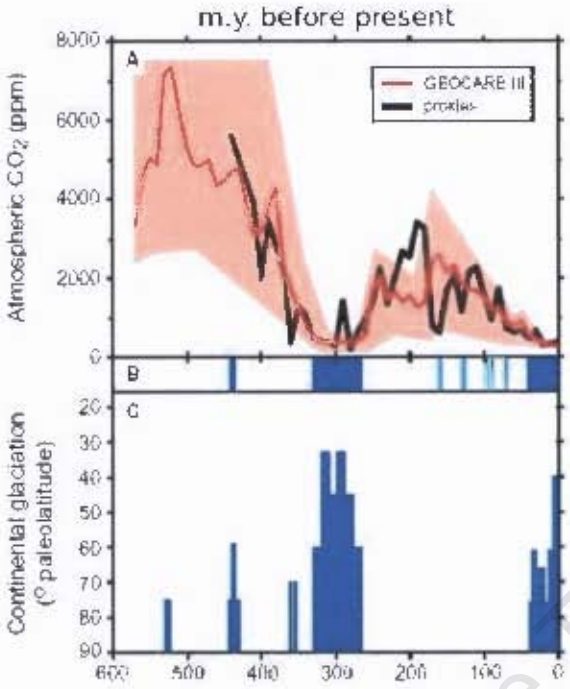

Figure 1.3: Atmospheric CO_2 and latitudinal extent of glaciation over the Phanerozoic.
(A) CO_2 concentrations from GEOCARBIII model (originally from Berner and Kothavala (2001)) and various proxy data. 10 m.y. time steps are used in both curves. Shaded area represents range of error for model predictions (B) Glacials (dark blue) and cool periods (light blue). (C) Latitudinal extent of direct glacial evidence (tillites, striated bedrock, etc. throughout the Phanerozoic; from Royer et al. (2004) Figure 2).

2004), although some scientists prefer to invoke celestial forcing (Shaviv and Veizer, 2003).

For the period of the Cenozoic (last 65 million years) higher resolution oxygen isotope records are available as a temperature proxy (Figure 1.4) and reveal complex trends, cycles and aberrations in global climate (Zachos et al., 2001). While the major trend is a general cooling over the Cenozoic, traditionally attributed to decreasing atmospheric CO_2 concentrations and changing planetary albedo (Fedorov et al., 2006), various other climatic perturbations and cycles are evident. The cyclic phenomena evident in the $\delta^{18}O$ records, particularly during glaciated climate states, are driven by changes in insolation, caused by slight variations in three of earths orbital parameters (eccentricity, obliquity and precession), which are referred to as the Milankovitch cycles (Figure 1.5) (Zachos et al., 2001; Huybers and Wunsch, 2005). A striking feature of the record is the amplification of the Milankovitch cycles, which begins around 3 Ma, and become particularly pronounced in the last 1 Ma, where the extreme points

of the oscillations represent cool glacial and warm interglacial states (Fedorov et al., 2006).

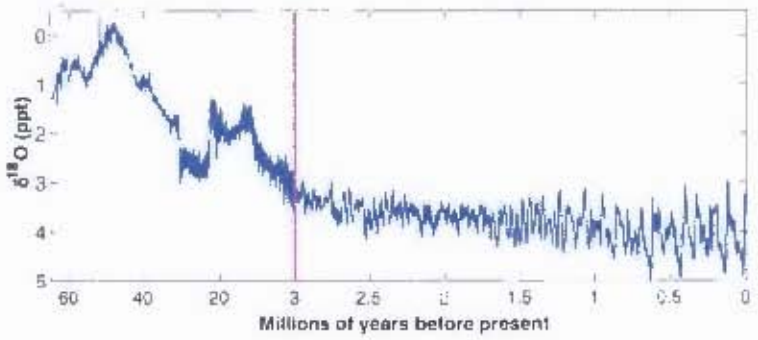

Figure 1.4: Cenozoic $\delta^{18}O$.

Variations in $\delta^{18}O$ over the past 60 million years. Higher values of $\delta^{18}O$ indicate colder climate (greater global ice volume). The gradual cooling over the past 50 million years is evident. Note that the time scale changes at 3 Ma. The Milankovitch cycles are modest in amplitude up to 3 Ma but then start amplifying (from Fedorov et al. (2006) Figure 1).

By far the best records of past climatic changes have been provided by ice core data, which can reveal local temperature (through $\delta^{18}O$ or δD), and atmospheric trace gas concentrations, the latter of which are recorded in air bubbles trapped within the ice (Petit et al., 1999; EPICA members, 2004). The most comprehensive of these records come from Antarctica, with detailed information available for the last 420 kyr (Figure 1.7, Petit et al., 1999), and temperature data spanning the last 8 glacial cycles (740 kyr) (EPICA members, 2004). The predominant climate pattern is a saw-toothed sequence, with warm interglacial periods, slowly giving way to cool glacial conditions, and then a rapid return to interglacial warm conditions (Petit et al., 1999; EPICA members, 2004). Shallow marine $\delta^{18}O$ records confirm that these cycles are not only confined to the polar regions, but are indeed a global phenomenon (Veizer et al., 2000).

Perhaps the most remarkable aspect of the glacial interglacial cycles is the tight coherence between shifts in temperature and atmospheric concentrations of the greenhouse gasses (Petit et al., 1999; EPICA members, 2004; Blunier et al., 2005). The atmospheric CO_2 concentration fluctuated from 180 p.p.m. during glacials to 280-300 p.p.m. during interglacials. The radiative forcing caused by such a shift amplifies the original small orbital forcing (Milankovitch) signal, and can account for nearly half of the observed temperature change, when considered with further amplifying feedbacks being supplied by water vapour, clouds and ice albedo

(Petit et al., 1999; Blunier et al., 2005). These records then imply that climatic variations on glacial-interglacial timescales are strongly coupled with greenhouse gas concentrations (Petit et al., 1999; Sigman and Boyle, 2000; Watson et al., 2000), although the causes of these fluctuations is a matter of hot debate, and correlation does not imply causality (Roe and Allen, 1999; Sigman and Boyle, 2000; Fedorov et al., 2006; Marinov et al., 2006; Toggweiler et al., 2006; Lamy et al., 2007; Toggweiler, in press).

If one chooses instead to focus on shorter timescales, it becomes apparent that superimposed on the glacial-interglacial cycles, rapid climatic oscillations occur on the sub-millennial timescale (Figure 1.6) (Alley, 2000; Blunier and Brook, 2001). Rapid warmings, occurring within a decade, and subsequent slow cooling are referred to as Dansgaard-Oeschger (D-O) events (Blunier et al., 2005). Such instances of rapid climatic variability also peculiarly seem to be out of phase between the two hemispheres, and as such are referred to as the bi-polar see-saw (Blunier and Brook, 2001) and are likely caused by changes in the global ocean meridional overturning circulation (Alley, 2000; Blunier and Brook, 2001; Pahnke and Zahn, 2005; Lamy et al., 2007).

1.1.3 The modern context revisited: Implications for the future

Evidence of recent global climate change has been thoroughly documented by the Intergovernmental Panel on Climate Change (IPCC). This includes the observations that global surface air temperatures have risen by $\approx 0.75\,^{\circ}C$ since 1860 (Figure 1.8), the thermal content of the ocean has increased, there has been a massive decrease in the extent of mountain glaciers, the Arctic ice cap has reduced in extent and thickness as has sea ice, global sea level has risen at an unprecedented rate (Figure 1.9), atmospheric circulation patterns have been modified and there has been an increase in severe weather events (IPCC, 2001; Solomon et al., 2007). The major difficulty is attributing such changes to anthropogenic forcing, as opposed to natural variability in the climate system. The IPCC approaches this problem using coupled Ocean-Atmosphere General Circulation Models (GCMs), and conclude that the currently observed changes can only be accounted for when anthropogenic forcing is taken

into account (Figure 1.10; Solomon et al., 2007).

The GCMs tend to be run at fairly poor spatial and temporal resolution, and furthermore, certain of the fundamental physical processes which control global climate, such as clouds, are not well understood, while others are only represented through parametrization (e.g. see the errors associated with clouds in Figure 1.12; IPCC, 2001). Thus there is a fair degree of uncertainty in the climate projections of these models under increasing atmospheric CO_2 concentrations (Figure 1.11). However, what is clear is that in both the recent and distant geological past, global climate has been strongly correlated with atmospheric CO_2 concentrations (Petit et al., 1999; Royer et al., 2004). Current atmospheric CO_2 concentrations of $\approx$380 p.p.m., have been unsurpassed in the last 420 ky, are are likely the highest in the last 20 million years (Petit et al., 1999; IPCC, 2001). Perhaps more importantly, the paleorecord reveals that in the past one million years the global climate system has become highly sensitive to feedbacks, and prone to dramatic and rapid shifts (Alley, 2000; Zachos et al., 2001; Blunier et al., 2005; Fedorov et al., 2006). Thus, it seems that we are pushing a volatile system, and perhaps the most pertinent concern is that we are not exactly sure of how it will respond (Philander, pers. comm; Broeker, 2003). Under the circumstances, gaining a solid scientific understanding of the carbon cycle and its controls is key.

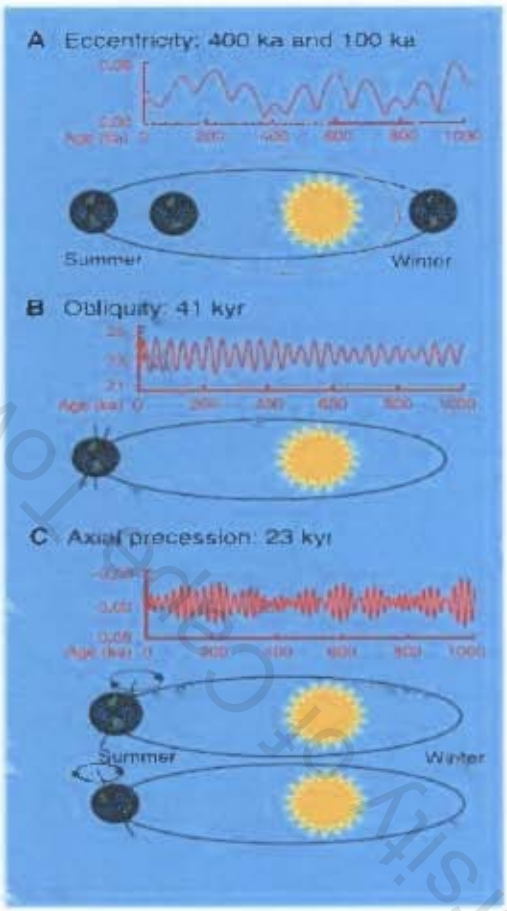

Figure 1.5: Milankovitch orbital forcings on insolation.

Primary orbital components are displayed. The gravitational forces exerted by other celestial bodies affect Earths orbit. As a result, the amount and, more importantly, the distribution of incoming solar radiation oscillate with time. There are three orbital perturbations with −ve periods. eccentricity (at 400 and 100 ky), obliquity (41 ky), and precession (23 and 19 ky). (A) Eccentricity refers to the shape of Earths orbit around the sun, varying from near circular to elliptical. This effect on insolation is very small, however, and by itself should not account for changes in Earths climate during the past. (B) Obliquity refers to the tilt of Earths axis relative to the plane of the ecliptic varying between 22.1° and 24.5°. A high angle of tilt increases the seasonal contrast, most effectively at high latitudes (e.g., winters in both hemispheres will be colder and summers hotter as obliquity increases). (C) Precession refers to the wobble of the axis of rotation describing a circle in space with a period of 26 ky. Modulated by orbital eccentricity, precession determines where on the orbit around the sun (e.g., with relation to aphelion or perihelion) seasons occur, thereby increasing the seasonal contrast in one hemisphere and decreasing it in the other. The effect is largest at the equator and decreases with increasing latitude. The periods of the precessional signal modulated by eccentricity are 23 and 19 ky, the periods observed in geological records [from Zachos et al. (2001) Figure 1].

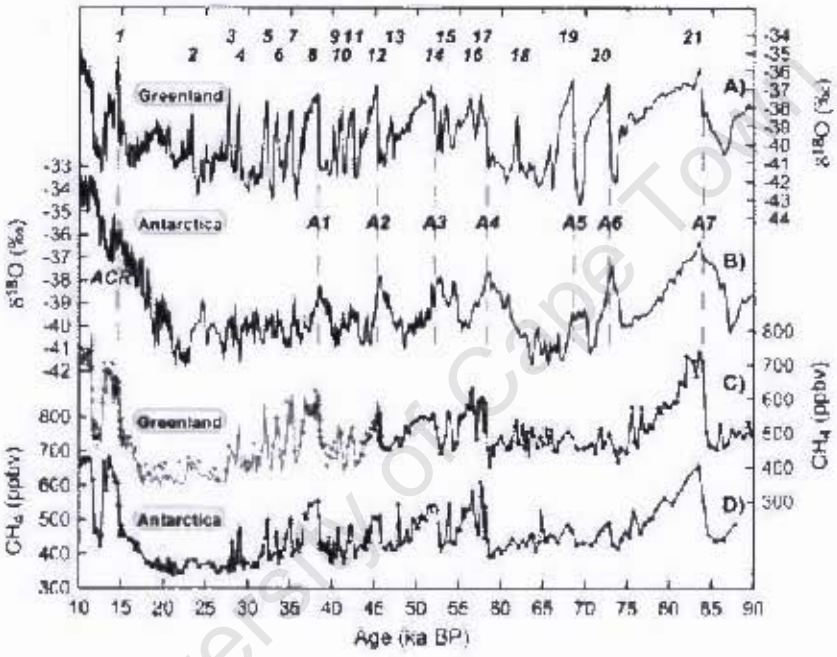

Figure 1.6: Isotopic and CH_4 data from Greenland and Antarctica on the GISP2 time scale. Dashed lines indicate the onset of major D-O events. (A) $\delta^{18}O_{ice}$ from GISP2, Greenland (16). (B) $\delta^{18}O_{ice}$ from Byrd Station, West Antarctica (23). (C) CH_4 data from GISP2 and GRIP. Crosses and dots are from GISP2; the solid gray line is from GRIP (2, 8). The solid line runs through the data used for the synchronization: GISP2 (black line) up to 45.5 ka and GRIP data (gray line) from 45.5 ka to the Holocene. (D) CH4 data from Byrd Station (from Blunier and Brook (2001) Figure 1).

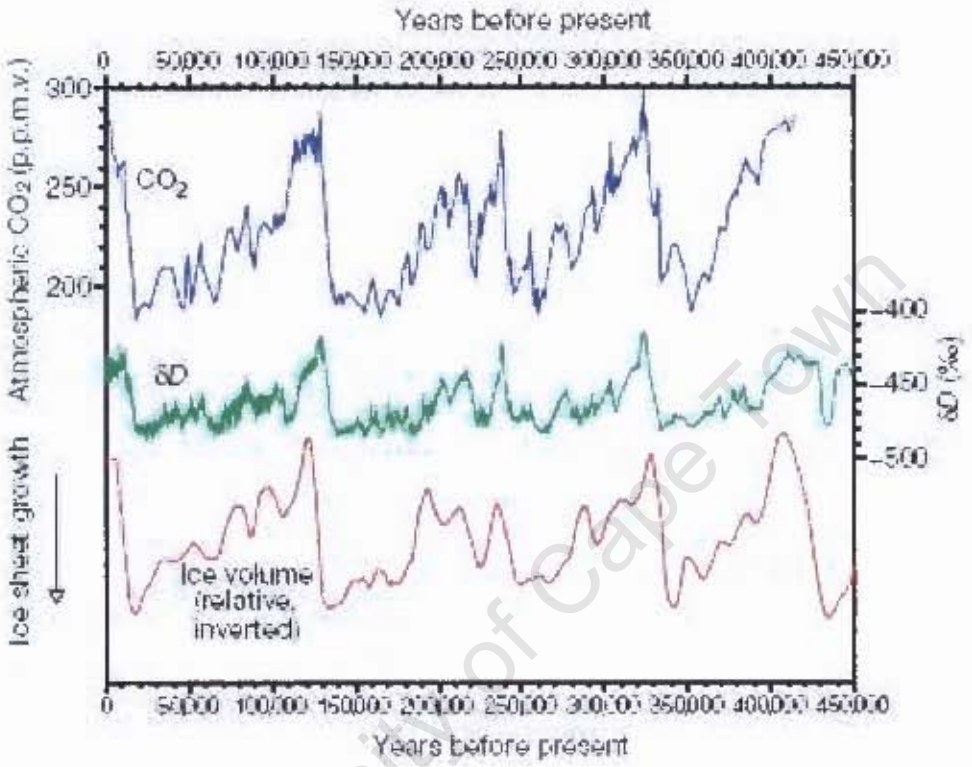

Figure 1.7: Vostok time series and ice volume.

The history of atmospheric CO_2 (blue) back to 420 kyr ago as recorded by the gas content in the Vostok ice core from Antarctica. The ratio of deuterium to hydrogen in ice (expressed as the term δD; green) provides a record of air temperature over Antarctica, with more negative δD values corresponding to colder conditions. Maximum glacial-interglacial temperature variations were around 12°C. The history of global ice volume based on benthic foraminiferal oxygen isotope data from deep-sea sediment cores is plotted as relative sea level (red), so that ice ages (peaks in continental ice volume) appear as sea level minima, with a full glacial/interglacial amplitude for sea level change of about 120m. During peak glacial periods, atmospheric CO_2 is 80±100 p.p.m.v. lower than during peak interglacial periods, with upper and lower limits that are reproduced in each of the 100-kyr cycles. Ice core records, including the Vostok record shown here, indicate that atmospheric CO_2 was among the early parameters to change at the termination of glacial maxima, roughly in step with Southern Hemisphere warming and preceding the decline in Northern Hemisphere ice volume (adapted from Sigman and Boyle (2000) Figure 1; Vostok data originally from Petit et al. (1999)).

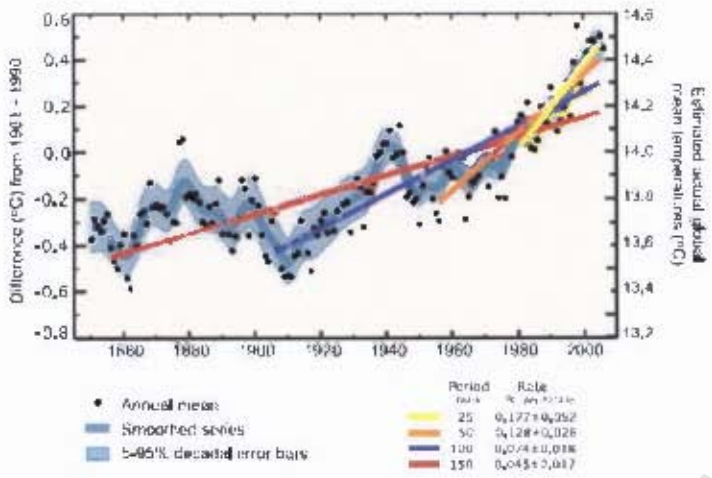

Figure 1.8: Annual global mean temperatures (black dots) with linear fits to the data. The left hand axis shows temperature anomalies relative to the 1961 to 1990 average and the right hand axis shows estimated actual temperatures, both in °C. Linear trends are shown for the last 25 (yellow), 50 (orange), 100 (purple) and 150 years (red). The smooth blue curve shows decadal variations, with the decadal 90% error range shown as a pale blue band about that line. The total temperature increase from the period 1850 to 1899 to the period 2001 to 2005 is 0.76°C ± 0.19°C (from Solomon et al. (2007) Figure T.S. 6).

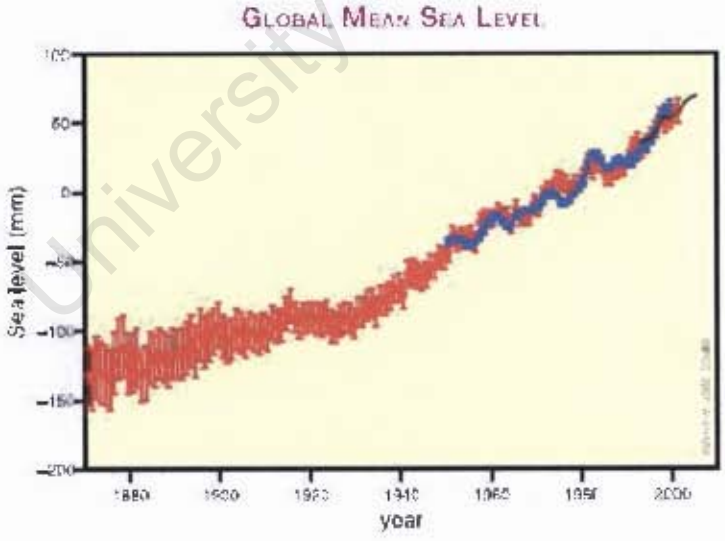

Figure 1.9: Annual averages of the global mean sea level.

Sea level based on reconstructed sea level fields since 1870 (red), tide gauge measurements since 1950 (blue) and satellite altimetry since 1992 (black). Units are in mm relative to the average for 1961 to 1990. Error bars are 90% confidence intervals (from Figure Solomon et al. (2007) T.S. 18).

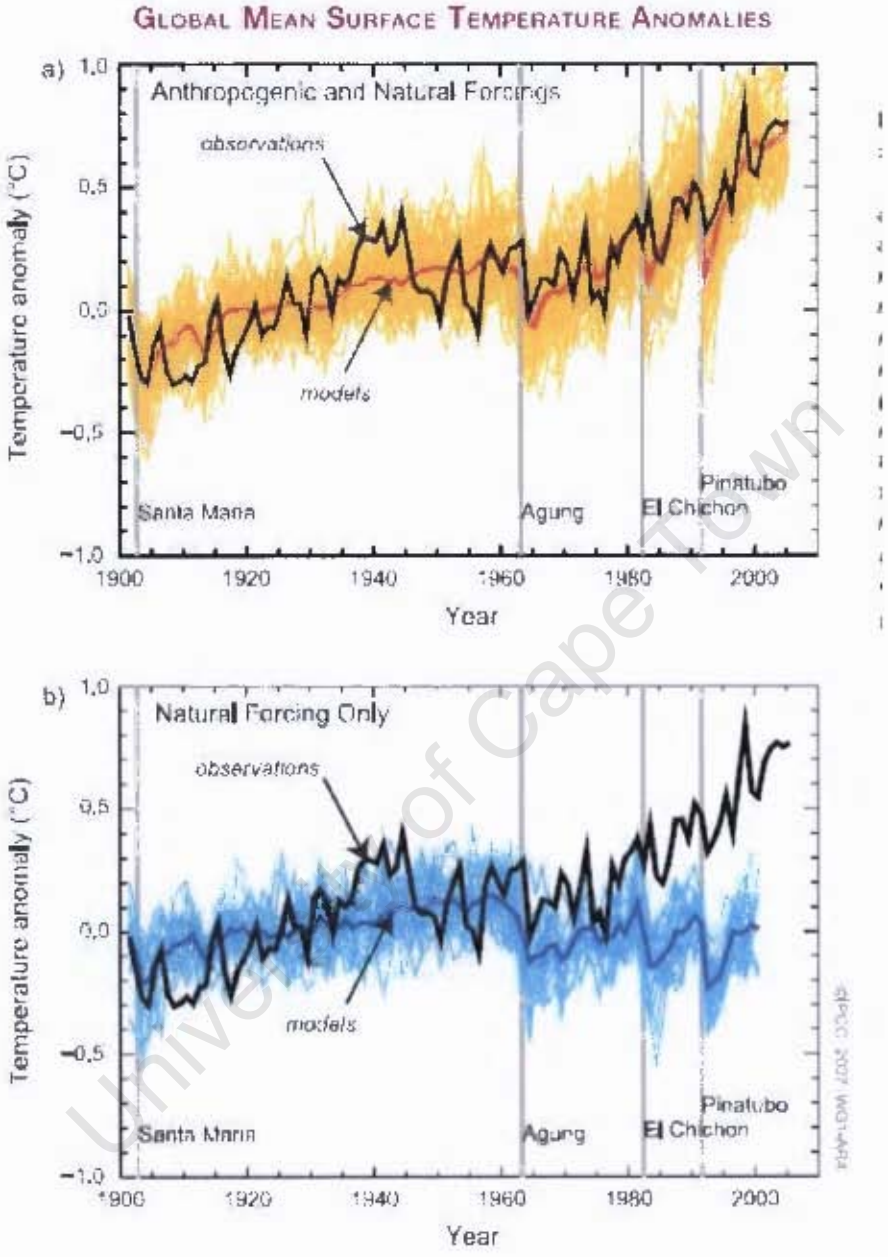

Figure 1.10: Global mean surface temperature anomalies

(a) Global mean surface temperature anomalies relative to the period 1901 to 1950, as observed (black line) and as obtained from simulations with both anthropogenic and natural forcings. The thick red curve shows the multi-model ensemble mean and the thin yellow curves show the individual simulations. Vertical grey lines indicate the timing of major volcanic events. (b) As in (a), except that the simulated global mean temperature anomalies are for natural forcings only. The thick blue curve shows the multi-model ensemble mean and the thin lighter blue curves show individual simulations. Each simulation was sampled so that coverage corresponds to that of the observations (from Solomon et al. (2007) Figure T.S.23).

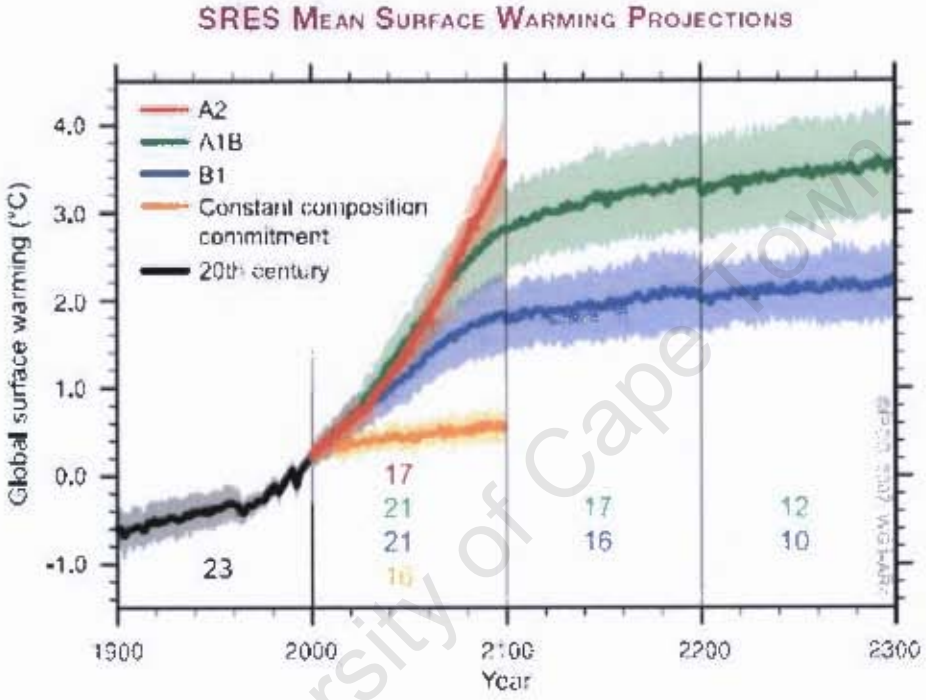

Figure 1.11: Multi-model means of surface warming (compared to the 1980-1999 base period) for the SRES scenarios A2 (red), A1B (green) and B1 (blue), shown as continuations of the 20th-century simulation. The latter two scenarios are continued beyond the year 2100 with forcing kept constant. An additional experiment, in which the forcing is kept at the year 2000 level is also shown (orange). Linear trends from the corresponding control runs have been removed from these time series. Lines show the multi-model means, shading denotes the ±1 standard deviation range. Discontinuities between different periods have no physical meaning and are caused by the fact that the number of models that have run a given scenario is different for each period and scenario (numbers indicated in Figure). For the same reason, uncertainty across scenarios should not be interpreted from this Figure (from Solomon et al. (2007) Figure T.S.32).

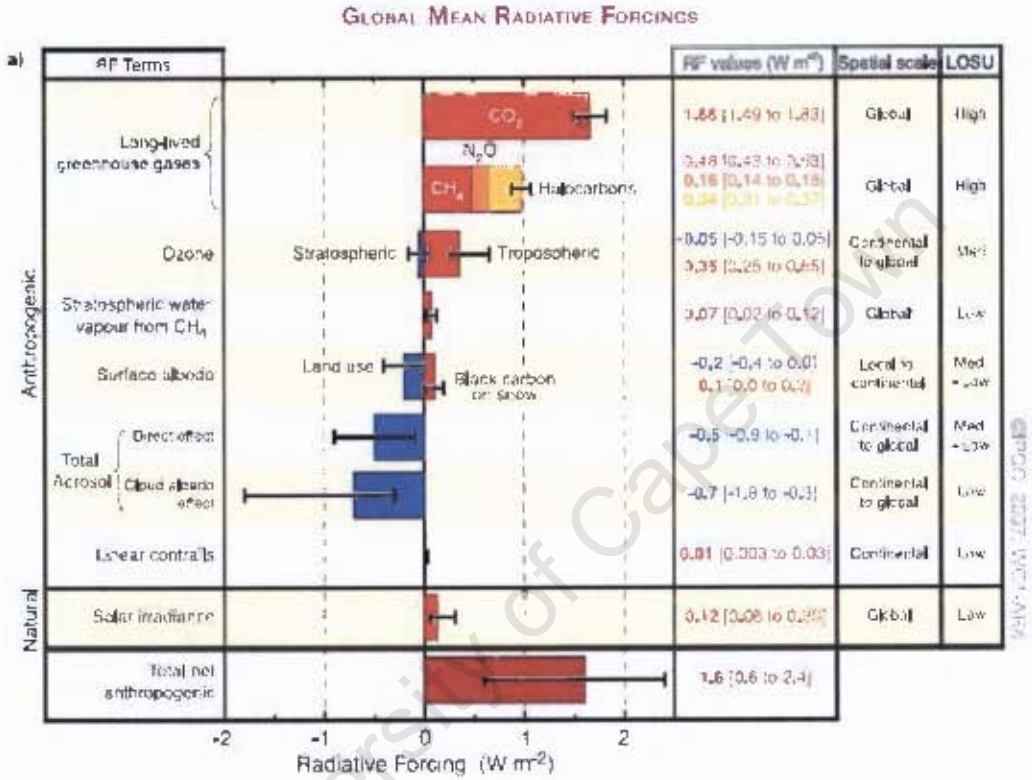

Figure 1.12: Global mean radiative forcings (RF) and their 90% confidence intervals in 2005 for various agents and mechanisms. Columns on the right-hand side specify best estimates and Confidence intervals (RF values); typical geographical extent of the forcing (Spatial scale); and level of scientific understanding (LOSU) indicating the scientific confidence level as explained in Section 2.9. Errors for CH_4, N_2O and halocarbons have been combined. The net anthropogenic radiative forcing and its range are also shown. Best estimates and uncertainty ranges can not be obtained by direct addition of individual terms due to the asymmetric uncertainty ranges for some factors; the values given here were obtained from a Monte Carlo technique. Additional forcing factors not included here are considered to have a very low LOSU. Volcanic aerosols contribute an additional form of natural forcing but are not included due to their episodic nature. The range for linear contrails does not include other possible effects of aviation on cloudiness (from Solomon et al. (2007) Figure T.S.5).

1.2 Components of the modern day carbon cycle

1.2.1 Overview

1.2.1.1 The pre-industrial carbon cycle

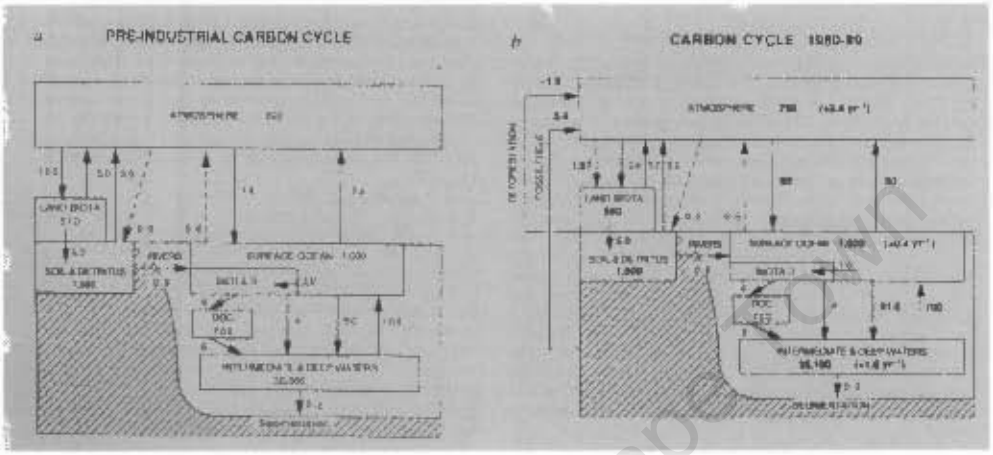

Figure 1.13: The global carbon cycle. Reservoirs and fluxes in Gt C and Gt C.yr^{-1} respectively (1 Gt=10^{15}gC). **a** Reconstructed pre-industrial situation and **b** present day situation. In b bold numbers denote fluxes or reservoir sizes which have changed due to human activities. Note the large size of the deep ocean reservoir, and the DOC pool. Also note that natural ocean-atmosphere exchange is far larger than anthropogenic emissions. The difference between river input and sedimentation has been closed by fluxes from ocean to atmosphere and atmosphere to biota (dashed arrows; from Siegenthaler and Sarmiento (1993) Figure 1).

The global carbon (C) cycle is made up of a series of carbon reservoirs which exchange with each other (Figure 1.13). Naturally the largest carbon reservoir is the lithosphere (Falkowski et al., 2000), however its slow exchanges via weathering and tectonics (millions of years) (Raven and Falkowski, 1999) mean that it is often neglected when referring to recent changes. Of the faster exchanging components (Figure 1.13b) the (deep) ocean is by far the largest reservoir (≈38 000 Gt), containing over 50 times more carbon than the atmosphere (600 Gt) (Siegenthaler and Sarmiento, 1993; Sarmiento and Bender, 1994; Raven and Falkowski, 1999; Falkowski et al., 2000; Schimel et al., 2000; Watson and Orr, 2003). CO_2 is exchanged between the ocean and atmosphere via gas transfer, while photosynthesis and respiration lead to a biologically mediated exchange both in the ocean and on land (see 1.2.2)(Siegenthaler and Sarmiento, 1993).

The pre-industrial atmosphere was in a near steady-state with regards to inputs and outputs of CO_2, requiring that the sum of the air-sea flux and the land-sea flux be zero. However individually these fluxes would not have been in balance because rivers transport around 0.7 - 0.8 Gt C (Siegenthaler and Sarmiento, 1993) from the land into the ocean each year (Toggweiler, 1995; Watson and Orr, 2003). To maintain a steady state, the vast majority of the riverine C must have been outgassed to the atmosphere, making the ocean a net source of carbon in pre-industrial times (Watson and Orr, 2003). Additionally, the disproportionate land mass distribution and ocean circulation led to a pre-industrial inter-hemispheric CO_2 gradient (Siegenthaler and Sarmiento, 1993; Watson and Orr, 2003).

1.2.1.2 The anthropogenic carbon cycle

Recent increases in atmospheric CO_2 concentrations have unbalanced the carbon exchanges of pre-industrial times (Figure 1.13b; Schimel et al., 2000). The natural exchanges between the oceanic and atmospheric reservoirs are far larger than anthropogenic emissions, nonetheless the latter are responsible for the current atmospheric CO_2 spike (see 1.1.1). In brief, the atmosphere has been receiving CO_2 from fossil fuel burning (5.4 Gt) and deforestation (0.6-2.5 Gt), but has only been accumulating 3.4 Gt $C.yr^{-1}$ (Siegenthaler and Sarmiento, 1993). The remaining anthropogenic emissions have been taken up in part by the oceans ($\sim$2.0 Gt $C.yr^{-1}$ or $\approx$50% of fossil fuel emissions) which have become a net sink (Siegenthaler and Sarmiento, 1993; Toggweiler, 1995; Schimel et al., 2000; Watson and Orr, 2003; Keeling et al., 2005). The major discrepancy over the size of the oceanic sink has subsequently been reconciled (Siegenthaler and Sarmiento, 1993), and other differences are mainly a matter of definition (Siegenthaler and Sarmiento, 1993; Schimel et al., 2000).

The above considerations leave a 'missing sink' of $\approx$1.8 Gt $C.yr^{-1}$ (Siegenthaler and Sarmiento, 1993). While there have been occasional claims that this 'missing carbon' could be in the ocean, for example on the continental slopes (Walsh et al., 1981), the consensus opinion places the sink in the terrestrial biosphere (Sarmiento, 1993; Siegenthaler and Sarmiento, 1993; Schimel et al., 2000; Keeling et al., 2005). The magnitude of the terrestrial sink is

however notoriously hard to quantify (Schimel et al., 2000), and it is thus normally calculated indirectly (Keeling et al., 2005) or inferred from changes in atmospheric and oceanic $\delta^{13}C$, albeit with errors (Schimel et al., 2000; Keeling et al., 2005). Nonetheless, the missing global carbon sink can most likely be attributed to NH forest regrowth, together with nitrogen and CO_2 fertilization having enhanced terrestrial carbon fixation (Siegenthaler and Sarmiento, 1993; Schimel et al., 2000; Keeling et al., 2005). On the whole though, the global ocean is clearly the most important player in millennial scale carbon storage and exchange, and deserves further attention here.

1.2.2 The ocean carbon cycle and the biological pump

Carbon dioxide is far more soluble in seawater than ordinary gasses owing mainly to the fact that once dissolved, it dissociates into several different species, which together comprise Dissolved Inorganic Carbon (DIC) (Sarmiento and Bender, 1994; Sigman and Boyle, 2000). The oceanic carbon reservoir is dominated by DIC, which exhibits a critically important vertical gradient, increasing 12% in concentration below ≈1000 m depth (see Figure 1.14;Sarmiento and Bender, 1994). The partial pressure of CO_2 (pCO_2) in seawater is controlled by temperature and ocean chemical composition (Sarmiento and Bender, 1994; Sigman and Boyle, 2000), and it is in turn the pCO_2 difference between the ocean surface and the atmosphere which regulates air-sea exchange (Siegenthaler and Sarmiento, 1993; Watson and Orr, 2003). Thus in cold high latitude regions, where CO_2 is more soluble, the seawater tends to take up atmospheric CO_2, before sinking into the deep ocean due to its high density. In the low latitudes where deep waters upwell to the surface and are subsequently warmed, the solubility of CO_2 decreases, and there tends to be outgassing to the atmosphere. This mechanism of accumulating CO_2 in the cold ocean interior, and dispelling CO_2 from the warm surface waters is known as the solubility pump, and contributes to around one quarter of the observed vertical DIC gradient (Sarmiento and Bender, 1994; Raven and Falkowski, 1999; Watson and Orr, 2003).

Organisms at the surface of the ocean take up inorganic carbon through photosynthesis,

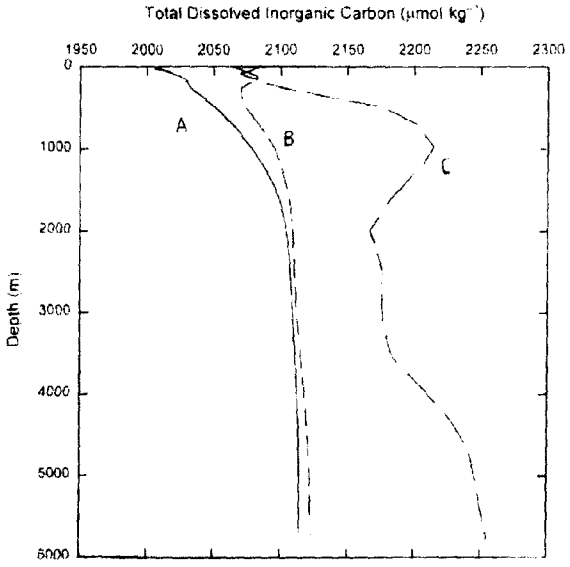

Figure 1.14: Vertical profiles of dissolved inorganic carbon (DIC) in the ocean.
Curve A corresponds to a theoretical profile that would have been obtained prior to the industrial revolution with an atmospheric CO_2 concentration of 280μmol.mol^{-1}. The curve is derived from solubility coefficients for CO_2 in seawater, using a typical thermal and salinity profile from the central Pacific Ocean, and assumes that when surface water cools and sinks to become deep water it has equilibriated with atmospheric CO_2. As such, the calculated profile of TIC reflects the 'solubility pump' and assumes that the 'biological pump' is nil. Curve B corresponds to the same calculated solubility profile of TIC, but in the year 1995, with an atmospheric CO_2 concentration of 360μmol.mol^{-1}. The difference between these two curves is the integrated oceanic uptake of CO_2 from anthropogenic emissions since the beginning of the industrial revolution, with the assumption that biological processes have been in steady state. Curve C is a representative profile of measured TIC from the central Pacific Ocean. The difference between curve C and B is the contribution of biological processes to the uptake of CO_2 in the steady-state (i.e. the contribution of the 'biological pump' to the TIC pool; from Raven and Falkowski (1999) Figure 2).

and subsequently the large organic particles sink, and a fraction of the suspended particles and dissolved organic matter is passively advected to depth by mixing (Sarmiento, 1993; Sarmiento and Bender, 1994; Raven and Falkowski, 1999; Falkowski et al., 2003). In the deep ocean, almost all of the organic matter is respired by bacteria, returning it to the inorganic form, and effectively 'pumping up' the deep ocean DIC reservoir. This transfer of carbon from the surface to the deep ocean, across the barrier of the permanent thermocline, is known as the 'biological pump' (Sarmiento, 1993; Siegenthaler and Sarmiento, 1993; Sarmiento and Bender, 1994; Raven and Falkowski, 1999). The biological pump mechanism is responsible for maintaining around three quarters of the observed DIC gradient between the surface and the deep ocean (see Figure 1.14; Sarmiento and Bender, 1994). More importantly, it exerts a strong influence on the air-sea exchange of carbon dioxide, by decreasing the pCO_2 at the

ocean surface (Sarmiento, 1993; Watson and Orr, 2003). If all life in the ocean were to die, and the biological pump were to cease operating, atmospheric CO_2 concentrations would increase by almost 200 p.p.m. (Siegenthaler and Sarmiento, 1993; Sarmiento and Bender, 1994; Watson and Orr, 2003). Indeed, changes in the efficiency of the biological pump at high southern latitudes is one of the likely explanations for the glacial-interglacial variations in atmospheric CO_2 (Sigman and Boyle, 2000; Watson et al., 2000; Marinov et al., 2006).

The fundamental factors limiting primary production in the ocean are light, nutrient (nitrogen, phosphorous, silicate) supply, and trace element (iron, copper, etc.) availability. Ocean nutrient profiles exhibit significant depletion near the surface and enrichment at depth, because of the biological pump (Raven and Falkowski, 1999) and therefore upwelling or vertical mixing of nutrient rich deep water fuels phytoplankton growth (Raven and Falkowski, 1999). Global primary productivity can be derived from satellite data by using models based on chlorophyll biomass, temperature and Photosynthetically Available Radiation (Figure 1.15)(Behrenfeld and Falkowksi, 1997; Carr, 2002). This satellite derived view tends to show that high biomass and productivity occur in regions of nutrient availability, with particularly outstanding values along eastern boundary currents, the equator and at high latitudes. Conversely, the central ocean gyres are particularly devoid of biomass and productivity (Behrenfeld and Falkowksi, 1997; Falkowski et al., 2003).

The photosynthetic organisms which drive the biological pump, phytoplankton, consist of six light elements and around 54 trace elements. Three of the major light elements C, N, and P occur in the fixed ratios 106:16:1 in phytoplankton, the so called Redfield ratios. Furthermore, in the oceanic dissolved phase these elements are in the same fixed ratios, suggesting that respiration of organic matter in the ocean interior controls the ratios of these elements (Sarmiento and Bender, 1994; Falkowski et al., 2003). The adherence, or possible lack thereof (Toggweiler, 1993; Monteiro, 1996), to the Redfield ratios during organic matter production or oxidation exerts a strong influence on the effectiveness of the biological pump for the following reason: "Nutrient consumption is eventually complete in the modern low-latitude surface ocean, so that inorganic carbon is already stripped to the greatest possible

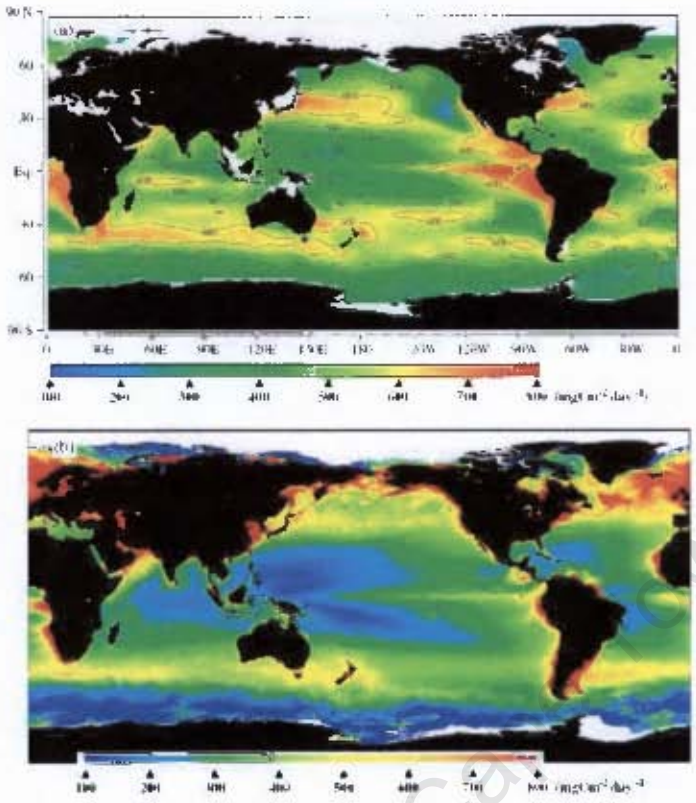

Figure 1.15: Horizontal distributions of the annual mean net primary production (NPP) (a) Coupled Biogeochemical-GCM (b) Satellite observations and model from SeaWifs data in 2000. Note the very high productivity's of the ocean margins compared with the oligotrophic gyres (from Nakata and Doi (2006) Figure 9).

degree, given the oceanic nutrient reservoir and the Redfield ratios. Vertical mixing and upwelling supply excess inorganic carbon to the surface ocean in approximately Redfield proportions with the major nutrients, so that an increase in upwelling would increase the rate of export production from the surface ocean but would not enhance the extraction of DIC from the surface ocean. Increased export production driven by higher rates of vertical mixing or upwelling would only play a role in lowering atmospheric CO_2 if it caused a change in the chemical composition of the exported organic material" (Sigman and Boyle, 2000, p. 864). However, if carbon fixation occurs in excess of the Redfield ratios, or if nitrogen is prefereutially recycled over carbon during oxidation, then an enhanced flux of carbon from the surface ocean to depth becomes possible (e.g. Monteiro, 1996).

Following the production of organic matter during photosynthesis a host of physical and biological forces act upon it, to alter its form and to influence its path through the ocean

system. Freshly produced organic matter may either be channeled through the grazing food chain, respired in the microbial loop (≈50%), stored as Dissolved Organic Matter (DOM), or exported as a sinking flux of senescent autotrophs (Figure 1.16;Azam, 1998; Wollast, 1998; Falkowski et al., 2003; Lochte et al., 2003). DOM is important for biogeochemical cycles because, for example, dissolved organic carbon (DOC) represents the largest biological carbon reservoir in the ocean and is comparable in size to the atmospheric reservoir of inorganic CO_2 (Carlson, 2002).

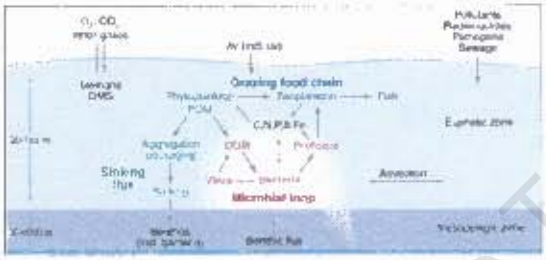

Figure 1.16: Paths of organic matter in the ocean (from Azam (1998) Figure 1).

An important constraint on the biological pump is the efficiency with which particles can sink, or dissolved organic matter can be advected to depth. Several models have been developed to estimate the vertical flux of organic matter, based on the amount of primary production and water depth, so called 'Martin curves' (e.g. Suess (1980); Berelson (2001)). It is estimated from sediment traps that the flux which reaches the aphotic zone is approximately 20-30% of primary production (Falkowski et al., 2003), or perhaps more in the coastal zone (Wollast, 1998; Lochte et al., 2003). This flux is known as export production, and temporally averaged it should correspond the amount of 'new' production (New production is the fraction of total primary production which is fueled by 'new nitrogen' or nitrate, supplied from the deep ocean. The other fraction of production is fueled by *in situ* regeneration of nutrients, mainly ammonium (Falkowski et al., 2003)).

Particle sinking dynamics are determined from the phytoplankton community structure, ballast effects, and the formation of aggregates, marine snow and fecal pellets (De La Rocha and Passow, 2007). Larger particles settle more rapidly than smaller ones proportional to the square of their diameter (Rullkötter, 2000). Particle aggregation and disaggregation is

a complex process, mediated by plankton, bacterial and viral activity, which includes cell lysis on the one hand and the formation of cohesive gels and polymers on the other (Azam, 1998; Verdugo et al., 2004; De La Rocha and Passow, 2007). After passing through the water column, the sinking organic matter is deposited on the seafloor where it is subject to intense degradation by a host of organisms (Rullkötter, 2000; Lochte et al., 2003). It is estimated that around 90% of the organic matter which reaches the ocean floor is respired (Lochte et al., 2003), or that only about 1 to 0.01% of surface primary productivity is permanently preserved in the sea floor sediments (Wollast, 1998; Rullkötter, 2000). Nonetheless organic matter which enters the deep ocean, even if respired, is stored on the timescale of ocean circulation ($\approx$ 500 years; Stuiver et al., 1983).

The biological pump does not affect the oceanic uptake of anthropogenic CO_2, because phytoplankton are not fertilized by rising CO_2 concentrations, nonetheless it is integral in maintaining the natural ocean-atmosphere CO_2 balance (Siegenthaler and Sarmiento, 1993; Raven and Falkowski, 1999). Furthermore, many of the above considerations suggest that organic matter fluxes are likely to be higher near continental margins because of the higher productivity, the community structure in these regions (larger cells and shorter food chains), and due to the more readily available supply of mineral ballasts (Wollast, 1998; Rullkötter, 2000; Falkowski et al., 2003; De La Rocha and Passow, 2007).

1.2.3 The significance of the continental margins

It is a widely held finding that the modest areal extent of the ocean margins account for a disproportionally large fraction of total ocean productivity (Walsh et al., 1981; Wollast, 1998; Rullkötter, 2000; Chen et al., 2003; Falkowski et al., 2003). The observation that a large proportion of this shelf production was fueled by readily available 'new' nitrogen, together with ostensibly low heterotrophic consumption, promoted the hypothesis that shelf carbon budgets of the north-eastern USA were unbalanced (Walsh et al., 1981; Malone et al., 1983). Rather, it was suggested that the large fraction ($\approx$50%) of unconsumed biological matter was laterally exported to the adjacent continental slope and deep ocean (Walsh et al., 1981;

Malone et al., 1983). Thus it was recognised that continental margins could play a significant role in global biogeochemical cycles, despite their limited area (Walsh et al., 1981; Walsh, 1991).

These assertions were tested during the more extensive Shelf Edge Exchange Processes (SEEP) experiments in the Mid-Atlantic Bight (MAB). During SEEP-I in the early 1980s it immediately became clear that the original budgets (Walsh et al., 1981) had neglected seasonality in zooplankton grazing and altogether ignored microbial oxidation, leading to a large overestimation of the off-shelf carbon flux (Rowe et al., 1986). The cross shelf export flux estimates for the margin were subsequently revised down to <20% of Primary Production (PP), although with some disagreement between investigators (Falkowski et al., 1988; Walsh et al., 1988a,b). The second phase of the experiment, SEEP-II, emphatically rejected the original hypothesis and concluded instead that the vast majority of photosynthetically fixed organic matter was oxidized on the shelf with $<<5\%$ exported across the shelf break (Biscaye et al., 1994).

Shortly however, it was recognized that the SEEP experiments had failed to quantify the flux of the most prevalent organic carbon pool, dissolved organic carbon, and the more comprehensive Ocean Margins Program (OMP) was borne (Verity et al., 2002). Using radioisotope ages of DOC, suspended POC and mass balances, Bauer and Druffel (1998) estimated that the carbon input to the deep ocean from continental shelves could be an order of magnitude greater than the vertical sinking flux. While the general conclusions of the OMP for the Cape Hatteras shelf would concur with the results of the two previous SEEP experiments (Verity et al., 2002), two important caveats arose. The first of these was that the DOC pool represented the most significant organic carbon reservoir in the ocean and that the shelf export of DOC could be large (Hopkinson Jr. and Nolin, 2002). Secondly, the MAB was found to be a net annual sink for atmospheric CO_2, although this was achieved through through a solubility, as opposed to a biological pump mechanism (Verity et al., 2002). Nonetheless, the importance of lateral carbon transport on the East coast of the USA has been recognized (Jahnke and Jahnke, 2000).

Such studies of lateral carbon fluxes were by no means limited to the NE USA. Indeed, extensive studies were conducted in the East China Sea (ECS), under the Kuroshio Edge Exchange Processes (KEEP) study amongst others. In-congruent results concerning primary production and heterotrophic carbon requirements prevented the establishment of a closed carbon budget for the region (Wong et al., 2000). Nonetheless it was estimated from water mass exchanges and horizontal gradients, that there were significant exports from the shelf of both POC and DOC (Hung et al., 2000). Here, DOC export was found to be four times larger than POC export (Hung et al., 2000) and the significant shelf-ocean exchange was attributed to the presence of a cyclonic eddy at the shelf edge (Wong et al., 2000). On the whole the ECS has been found to be a net sink for atmospheric CO_2 (Wong et al., 2000), principally through the solubility driven 'continental shelf pump' (Tsunogai et al., 1999).

The other intensively studied region in terms of cross shelf carbon exchange has been the NW European margin. Two phases of the Ocean Margin Exchange project, OMEX I in the northern Gulf of Biscay and OMEX II on the upwelling driven NW Iberian margin produced voluminous results. The OMEX I results showed that the majority of photosynthetically produced organic matter was respired on the shelf, and that no significant sedimentation occurred on the adjacent continental slope. Nevertheless, approximately 15% of primary production was exported to the deep ocean, below the permanent thermocline (Wollast and Chou, 2001a,b). An outstanding result of OMEX I was the importance of bottom and intermediate nepheloid layers in the lateral advection of material across the shelf and into the deep ocean (Thomsen and van Weering, 1998; McCave et al., 2001; van Weering et al., 2001; Wollast and Chou, 2001a,b). Similarly the Iberian margin was found to have well developed nepheloid layers, although transport in these was mainly confined to the alongshore direction, with the very prominent exception that a Strong off shelf flux was found associated with canyons (van Weering et al., 2002). Furthermore, surface export of POC and to a greater extent, DOC, by an upwelling filament highlighted the role of the Iberian shelf in supplying organic matter to the open ocean (Álvarez-Salgado et al., 2001).

Several attempts have been made to collate the diverse set of results on lateral carbon fluxes

obtained from the different continental margins. Wollast (1998), found when considering the SEEP and early OMEX results, together with other data, that the continental margins were a significant source of carbon to the open ocean. Reviewing the work of the Continental Margins Task Team (CMTT), Chen et al. (2003), drew a broad distinction between two types of margins. They defined recycling systems as those with broad shelves and long residence times, while export systems, including all the major coastal upwelling systems, were those with the ability to export material to the open ocean. While on the whole the review concurred with the SEEP-II conclusion, it found that continental shelves are on average net sinks for atmospheric CO_2, and that where export occurs, it is dominated by fluxes in the DOC pool (Chen et al., 2003). In summary, continental margins have recently been estimated to contribute ≈20% of the total biological pump (Liu et al., 2000).

From this broad range of results it is possible to draw several conclusions. While certain shelves with retentive circulation patterns may not be exporters of organic carbon, more dynamic regions with comparatively open boundaries and high productivity should export carbon to the deep ocean (Rowe et al., 1986; Rowe, 1987; Wollast, 1998; Chen et al., 2003). Secondly, in the more recent studies it became evident that the lateral export fluxes of DOC exceed those of POC (Hung et al., 2000; Álvarez-Salgado et al., 2001; Hopkinson Jr. and Nolin, 2002; Chen et al., 2003). Moreover, without fail, all of the major continental margins flux studies identified nepheloid layers, and transport in near bottom layers as pivotal to cross shelf exchange (Falkowski et al., 1988; Walsh et al., 1988a; Walsh, 1991; Biscaye et al., 1994; Thomsen and van Weering, 1998; Thomsen, 1999; Hung et al., 2000; McCave et al., 2001; van Weering et al., 2001; Wollast and Chou, 2001b; van Weering and McCave, 2002; van Weering et al., 2002). Unifying several of these points, Inthorn et al. (2006) have recently shown that the dynamically bounded central Benguela upwelling system exhibits a significant lateral carbon export in bottom nepheloid layers, which is subsequently preserved in a continental slope depocenter. The southern Benguela upwelling system could therefore also be expected to laterally export organic carbon, which is the topic discussed herein.

1.2.4 The southern Benguela upwelling system (BUS)

1.2.4.1 Large scale physical and biogeochemical features

General setting and geomorphology

The Benguela upwelling system is one of the four major wind driven coastal upwelling systems in the world. It stretches in its entirety from Cape Frio in the north ($\approx 18.4°S$), to beyond Cape Point in the south ($\approx 37°S$), although here we are interested only in the southern system, reaching south from Luderitz $\approx 27°S$ (see Figure 1.17; (Shannon, 1985; Shannon and Nelson, 1996; Shillington, 1998). In the southern region the continental shelf is variable in width, being 180 km off the Orange river, but only 40 km off the Cape Peninsula (Shannon, 1985). A double shelf break is common, at depths of 200-380 m and 500 m. The coastline is marked by prominent irregularities, most notably the granitic outcrops of Cape Columbine, the Cape Peninsula, and the embayments of Table Bay and St Helena Bay. The majority of the work reported here is based on cruise data extending offshore of St Helena Bay. The shelf adjacent to the two Capes is cut by deep canyons, the Cape canyon and the Cape Peninsula canyon respectively, which both run approximately N-S (Shannon, 1985; Shannon and Nelson, 1996). The continental margin is bounded on the oceanic edge by the deep Cape Basin, dotted with various seamounts. On the landward edge, a narrow and arid coastal plain gives way to a continental escarpment approximately 200 km inland, which has an important influence on local winds (Shannon and Nelson, 1996).

Meteorological forcing, large scale circulation, upwelling and system boundaries

Physical forcing in the Benguela region is dominated by the winds, which are in turn controlled by the synoptic pressure systems (see Figure 1.18). The flow of the South Atlantic High Pressure (SAHP), is channelled by an inland escarpment and a seasonal heat low, resulting in predominantly southerly, and thus upwelling favourable winds (Nelson and Hutchings, 1983; Shannon, 1985; Shannon and Nelson, 1996). The region of maximum wind stress at Luderitz (see Figure 1.20c;$\approx 27°S$) divides the Benguela into two distinct regimes, one of perennial upwelling in the north, and one of seasonal upwelling in the south (see Figure 1.20;

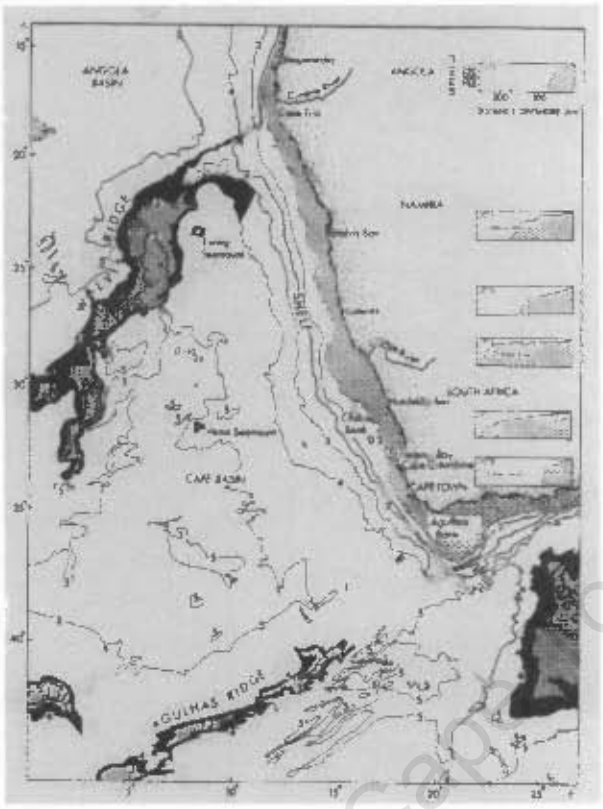

Figure 1.17: Bathymetry of the Benguela (from Shannon and Nelson (1996) Figure 1).

(Shannon, 1985, p. 119). In the southern Benguela system the annual northward shift of the pressure belts in the SH winter, results in the abatement of upwelling favourable winds and the onset of a westerly wind component (Shannon, 1985; Shannon and Nelson, 1996). Upwelling favourable winds in the southern Benguela occur between September and March, with bimodal maxima in spring and late summer (Andrews and Hutchings, 1980).

An important modulating effect on the summer winds in the southern Benguela is exerted by passing mid latitude depressions whose associated cyclonic circulation weakens the southerly winds, and may produce a westerly wind component (Figure 1.18). Therefore, a picture emerges for the SH summer months, where strong southerly winds blow for four to five days, until they are weakened or reversed by a passing depression, thus creating a pulsing system in the southern Benguela (Andrews and Hutchings, 1980; Shannon and Nelson, 1996; Field and Shillington, 2004). This pulsing is associated with the generation of coastal lows in the atmosphere and trapped waves in the ocean, which propagate anticyclonically around the

coast (Nelson and Hutchings, 1983; Shannon and Nelson, 1996).

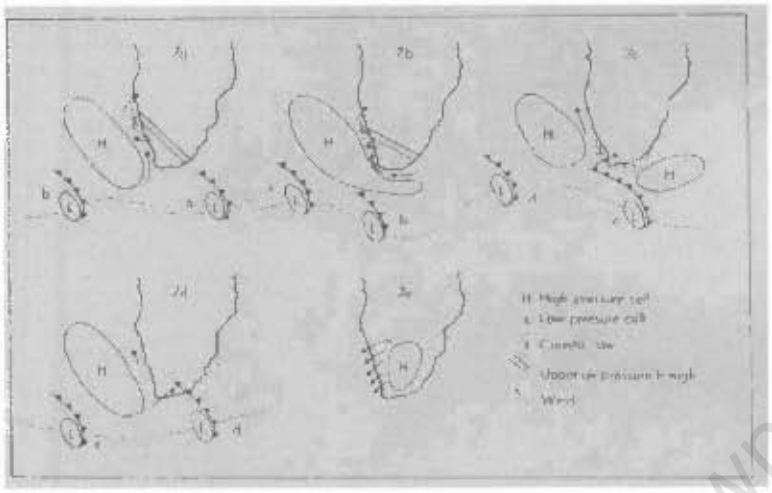

Figure 1.18: Cyclic weather pattern over the Benguela system typical of summer conditions. (a) South Atlantic High established. Coastal low at Luderitz. Southerly winds at Cape Town. (b) South Atlantic high ridging. Gale force winds at Cape Town, Coastal low moves south. (C) South Atlantic high weakens. North-west winds at Cape Town, following passage of coastal low. (d) South Atlantic high strengthens. Southerly winds along west coast. (e) Berg wind conditions (from Nelson and Hutchings (1983), Figure 7).

The Benguela Current may be thought of as the large-scale, wind driven, geostrophically balanced north westward flow which forms the eastern limb of the South Atlantic gyre (Shannon, 1985; Stramma and Peterson, 1989; Shannon and Nelson, 1996; Shillington, 1998). This may be conceptually separated from the coastal upwelling system, driven by the alongshore equatorward winds and Ekman divergence. The coastal upwelling reaches maximum intensity at a number of 'upwelling cells', usually where cyclonic wind-stress curl is greatest (Shannon and Nelson, 1996). These areas are typically coincident with capes, most notably the Cape Peninsula and Cape Columbine in the southern Benguela upwelling system, which also includes the Namaqua upwelling cell to the north (Shannon and Nelson, 1996). While the southerly limit of intense upwelling is often considered to be the Cape Peninsula cell (Andrews and Hutchings, 1980), upwelling can extend to Cape Agulhas, and even further to the east (Shannon and Nelson, 1996; Shillington, 1998). The southern boundary of the Benguela is best taken as the Agulhas retroflection, making it the only region in the world where an eastern and western boundary current interact, with significant implications for shelf-ocean exchange (Shannon and Nelson, 1996; Shillington, 1998).

The oceanic boundary of the upwelling, ≈100-200 km offshore (see Figure 1.20b), is typically marked by a well developed alongshore thermal front and a not necessarily coincident color front (Andrews and Hutchings, 1980; Shannon and Nelson, 1996; Shillington, 1998). The front, termed the Coastal Zone Transition Front (CZTF), is highly convoluted, showing the presence of meanders, eddies, and filaments, which may extend hundreds of kilometers offshore, and are likely to play a significant role in shelf ocean exchange (Lutjeharms and Stockton, 1987; Shillington et al., 1992; Shannon and Nelson, 1996; Shillington, 1998). Furthermore, this cross shelf exchange is enhanced by the periodic interaction of Agulhas rings with the southern Benguela system, which can draw large amount of water off the shelf (Duncombe Rae et al., 1992; Shillington et al., 1992; Shillington, 1998). Inshore, a secondary upwelling front may occur, but in the southern system it is usually merged with the oceanic front (Shannon and Nelson, 1996). The strong temperature gradient associated with the frontal system leads to the formation of a baroclinic equatorward jet current near the surface, particularly offshore of the upwelling cells in the south (see Figure 1.21; (Nelson and Polito, 1987; Shannon and Nelson, 1996; Shillington, 1998).

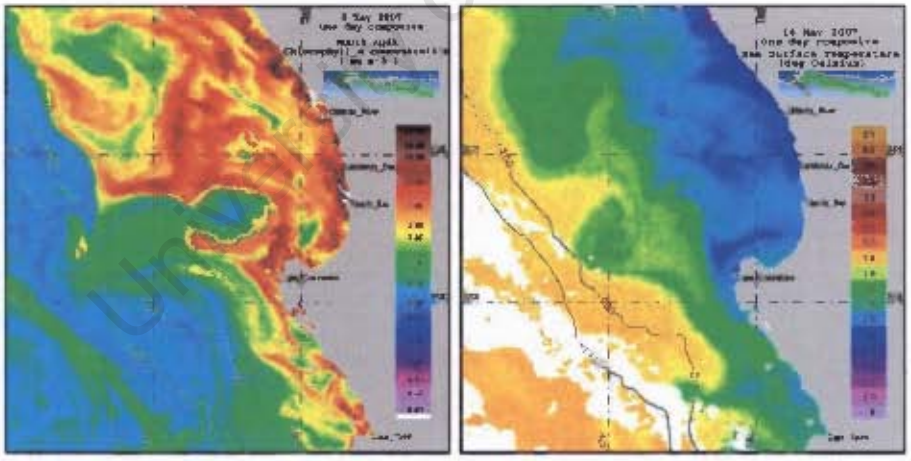

Figure 1.19: Temperature and ocean colour characteristics of the Coastal Zone Transition Front
(Left) One day composite ocean colour image from MODIS AQUA, showing chlorophyll a concentrations in the southern Benguela on 4 May 2007. Intense mesoscale variability is evident in the complex outline of the colour front. (Right) One day SST composite for the 16 May 2007. Note the convoluted nature of the thermal front, and in particular the filament of cold water extending offshore between Cape Town and Cape Columbine.

Beneath the equatorward wind drift at the surface, and the shelf edge jets, the predominant flow in the Benguela is polewards and reaches across the entire shelf and slope (Figure 1.21;

(Nelson and Polito, 1987; Shannon and Nelson, 1996; Shillington, 1998). The generalized poleward flow is seasonal in the north, reversing with the winds, and more permanent in the south. The poleward undercurrent is modulated at a period of 3-10 days by current fluctuations associated with coastal trapped waves, which have been described theoretically and observed in current meter as well as sea-level data (Nelson and Polito, 1987; Shannon and Nelson, 1996; Shillington, 1998; Shillington et al., 2006). Furthermore, water upwelling at the surface is thought to be provided by the rectification of the alongshore poleward flow, rather than by cross shelf advection (Nelson and Hutchings, 1983; Shannon and Nelson, 1996). In summary a three dimensional schematic of the circulation in the Benguela is shown in Figure 1.21.

Biogeochemistry

The major water masses present off South West Africa are ocean surface waters, South Atlantic and South Indian Central Waters (SACW and SICW respectively), Antarctic Intermediate Water (AAIW), North Atlantic Deep Water (NADW) and Antarctic Bottom Water (AABW) all of which are represented in Figure 1.22 (Shannon and Nelson, 1996). The water which upwells in the southern Benguela is a nutrient rich mixture of Indian and Atlantic central waters, originating from 200-300 m depth (Andrews and Hutchings, 1980; Shannon, 1985; Shillington et al., 2006). Several authors have presented 'water types' associated with upwelling, Andrews and Hutchings (1980) identified four water types in the Cape Peninsula upwelling cell: i. Oceanic water, outside the front with T>18°C and S≈35.4psu; ii. Upwelling water with 8° < T < 10°C and S≈34.7psu; iii. Mixed water, found between the coast and the frontal zone with variable properties and iv. Shelf water, underlying upwelled water with T< 8°C. Shannon (1985) suggests that an upper limit of 10°C for upwelled water may be too low in the cases of weaker upwelling events.

The pulsed supply of nutrients through upwelling and subsequent stratification and biological nutrient uptake leads to the development of extensive phytoplankton blooms in the southern Benguela (Andrews and Hutchings, 1980). Figure 1.20e shows the seasonal distribution of

chlorophyll a with latitude, and concentrated peaks are evident near St Helena Bay at 32°S. This corresponds to region 5 in Figure 1.23, which shows a time series of biomass with latitude, again with the highest values in the southern Benguela occurring near St Helena Bay (Demarcq et al., in prep.). Standing stocks in the southern Benguela are found to be higher during the Austral summer (upwelling season), with maxima occurring during quiescent phases of upwelling (Andrews and Hutchings, 1980). Chlorophyll a concentrations vary greatly during the summer upwelling season although typical values for the southern Benguela are ≈ 2 mg.m^{-3}, but have been measured at >130 mg.m^{-3} during blooms (Andrews and Hutchings, 1980; Shannon and Pillar, 1986; Brown and Hutchings, 1987; Brown et al., 1991; Walker and Pitcher, 1991). Integrated phytoplankton biomass has been found as $\approx$11 g.C.m^{-2} on average (Andrews and Hutchings, 1980), or about 300 mg.C.m^{-3} in St Helena Bay (Walker and Pitcher, 1991). Andrews and Hutchings (1980, p. 48) found that diatoms formed the 'overwhelming bulk of the phytoplankton' in the Cape Peninsula upwelling cell, a sentiment echoed by Shannon and Pillar (1986). Sun warming and the development of a stable water column typically sees the succession from diatoms to dinoflagellates, whose motility allows them to balance the requirements of light and nutrients (Pitcher et al., 1998). Under such conditions nutrient limitation can be expected, usually where saturated oxygen levels exist (typically > 4ml/l) (Andrews and Hutchings, 1980). Nitrate is generally considered to be the limiting nutrient in the ocean, however, evidence exists of silicate limitation in the northern Benguela (Shannon, 1985). Andrews and Hutchings (1980) found that both nitrate and silicate were used in greater quantities than they occur, and could therefore become limiting, although they concluded that nitrate was in fact the limiting nutrient in the Benguela (Chapman and Shannon, 1985).

Primary production in St Helena Bay has been estimated at 5.1 $\pm$ 2.6 g C.m^{-2}.d^{-1} (Shannon and Pillar, 1986), average southern Benguela measured (^{14}C) values are 3.5 g C.m^{-2}.d^{-1} (Brown et al., 1991), but during intense blooms values of nearly 40 g C.m^{-2}.d^{-1} have been measured (Andrews and Hutchings, 1980). From satellite data Carr (2002) has recently estimated the Benguela to be the most productive eastern boundary current of all, turning

over 0.37 Gt C.yr^{-1} (corresponding to 2.5 g.C.m^{-2}.d^{-1}). Since the northern and southern subsystems have a similar productivity, this can be scaled to ≈0.16 Gt C.yr^{-1} for the southern Benguela, which is considerably higher than previous estimates from *in situ* data (0.077 Gt C.yr^{-1}, Brown et al. (1991)). The f-ratio is the ratio of new production to total production; New Production is the fraction of primary production driven by newly available nitrogen. This is principally the nitrate and nitrite which becomes available when deep ocean waters are brought up into the euphotic zone, but could include sources from the atmosphere (deposition; fixation) or riverine inputs (Falkowski et al., 2003). Nitrogen is recycled in the water column through the excretions of zooplankton and oxidation by bacteria, making it available again in dissolved form for use by primary producers - the fraction of production fuelled through these 'recycled' forms of nutrients (urea, ammonium) is termed recycled production. The f-ratio in the southern Benguela has a wide quoted range (0.2-0.7), with typical values of around 0.3, but higher values are achieved by rapidly sedimenting diatom blooms (Probyn, 1992; Waldron et al., 1997; Touratier et al., 2003; Kóne et al., 2005).

Numerous attempts have been made to follow the flow of carbon through the trophic foodweb of the southern Benguela (e.g. Moloney, 1992; Painting et al., 1992; Touratier et al., 2003). Typically it appears that due to the delayed response of the zooplankton community following a phytoplankton bloom, only a small fraction of primary production (≈25%) is channeled through the grazing foodweb (Brown and Hutchings, 1987; Hutchings et al., 1991; Verheye, 1991; Field and Shillington, 2004). A far larger proportion is likely excreted as DOC, perhaps as much as 40% (Monteiro, 1996; Carlson, 2002; Touratier et al., 2003), and this pool may exhibit non-Redfield stoichiometry, because phytoplankton tend to exude carbon rich carbohydrates whilst under nutrient stress (Carlson, 2002). The remaining fraction of primary productivity is channelled into the sinking detritus pool, which may either be respired in the water column or delivered to the sediment interface. Local nutrient regeneration in the southern Benguela sediments enriches the central waters by up to 30% in nitrate (Waldron et al., 1998) and other nutrients as they cross the shelf prior to upwelling to the surface (Chapman and Shannon, 1985; Bailey, 1987). At the end of the productive season,

the accumulated heterotrophic removal of oxygen from the water column may lead to oxygen deficiency (Chapman and Shannon, 1985). Following an intense bloom, bacterial respiration can lead to anoxic conditions, particularly in retentive circulation regions such as St Helena Bay. Low oxygen waters may also be advected southwards from the northern and central Benguela via the prevailing poleward undercurrent (Andrews and Hutchings, 1980; Chapman and Shannon, 1985; Shannon and Nelson, 1996). Such conditions can have dramatic effects on the local ecosystem, causing fish and shellfish mass mortalities or walkouts (Chapman and Shannon, 1985; Pitcher and Calder, 2000). Under such anoxic conditions certain bacteria may switch to using nitrate or ammonium for their metabolism, reducing it to elemental nitrogen which is subsequently lost to the atmosphere (Jørgensen, 2000). The Benguela has been observed to lose nitrogen through denitrification (Calvert and Price, 1971; Chapman and Shannon, 1985; Bailey, 1987; Bailey and Chapman, 1991) and recently anaerobic ammonium oxidation (anammox; anammox is the anaerobic oxidation of ammonium with nitrate to yield N_2; Kuypers et al., 2005) has been shown to account for massive nitrogen losses of up to 1.4×10^{12}g.N.yr^{-1} from the system (Kuypers et al., 2005), severely influencing Redfield stoichiometry in the inorganic pool. Estimates of bacterial production remain sparse in the southern Benguela, although available data that were collated for a modeling synthesis suggested that up to 86-147% of PP could potentially be consumed by the heterotrophs, with an absolute minimum consumption of 9% of PP (Brown et al., 1991; Painting et al., 1992; Touratier et al., 2003).

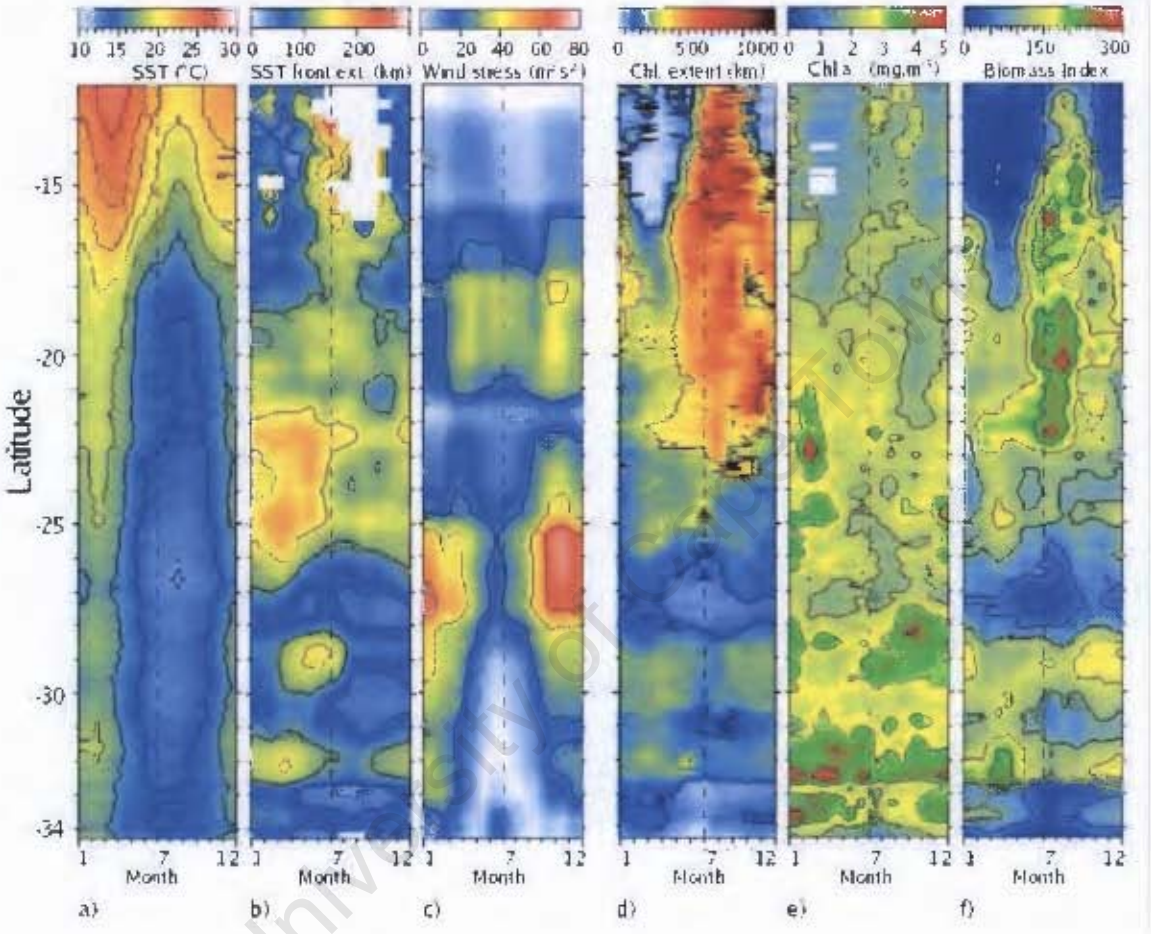

Figure 1.20: Hovmöller plots of the annual variation in physical and biological parameters for the west coast (12°S-34°S) averaged for 1997-2004:

(a) coastal SST; (b) offshore extent of the SST front marking the transition to oceanic waters; (c) pseudo wind-stress; (d) offshore extent of the average 1 $mg.m^{-3}$ chlorophyll a isopleth; (e) average chlorophyll a concentration within this area; (f) Chl Index representing chl integrated from the coast to the 1 $mg.m^{-3}$ chlorophyll a isopleth. Note the maximum windstress and biomass minimum near Luderitz (≈27°S), which separates the perennial upwelling of the northern Benguela, from the seasonal southern Benguela (after Demarcq et al. (in prep)).

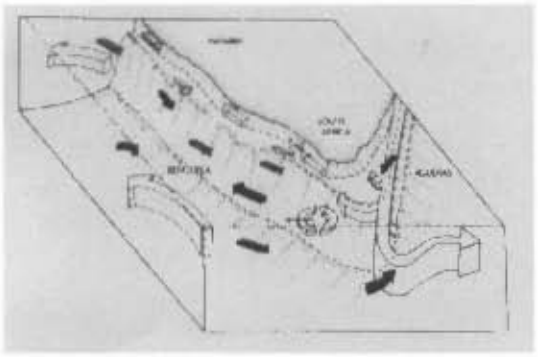

Figure 1.21: Conceptualized 3-D flow field in the Benguela system.

Features to note are the offshore, geostrophic Benguela current, the shelf edge jet current off the Southern Cape, the well developed poleward undercurrent on the shelf and slope, and the Agulhas ring entering the South Atlantic, potentially influencing the BUS (Shannon and Nelson (1996) Figure 28).

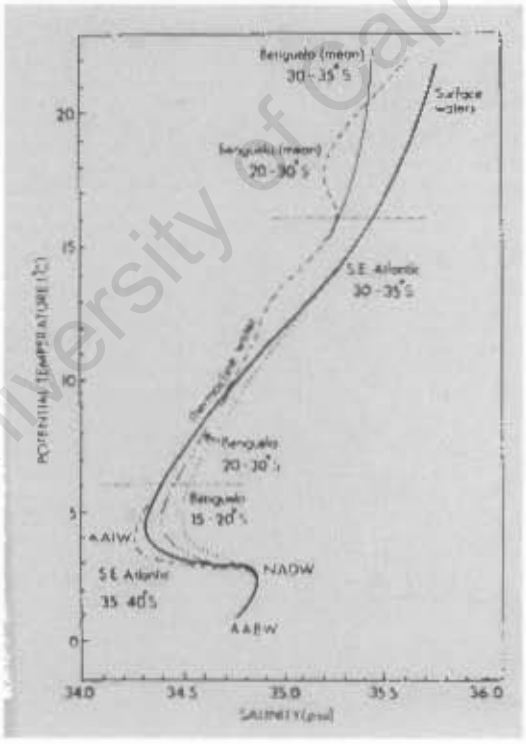

Figure 1.22: Principal Water Masses of the SE Atlantic.

Slight differences are apparent between coastal waters marked 'Benguela' and true South Atlantic waters. Shown are surface waters, the linear part of the curve representing central waters, Antarctic Intermediate Water (AAIW), North Atlantic Deep Water (NADW) and Antarctic Bottom Water (AABW; Shannon and Nelson (1996), Figure 14)

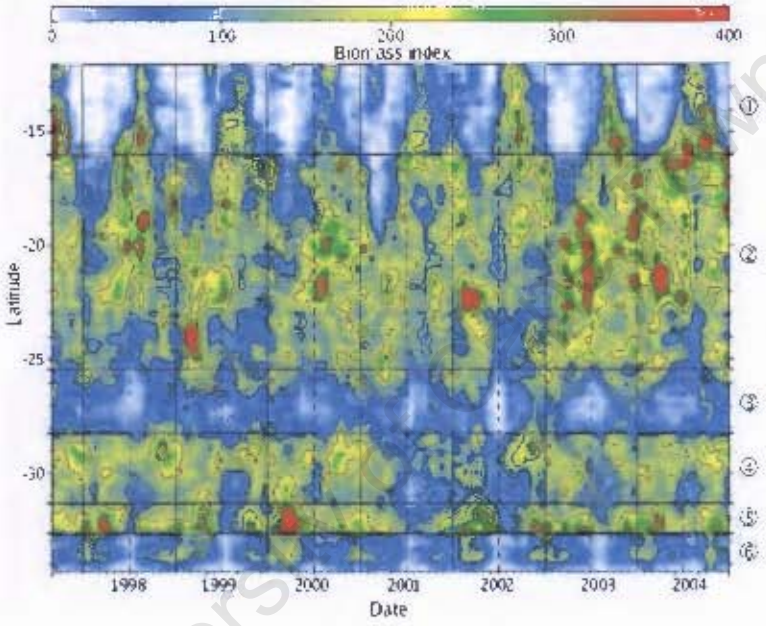

Figure 1.23: Hovmöller plot of the chlorophyll index (Chl Index) for the west coast (12°S-34°S) from September 1997 to December 2004.

Six sub-provinces are delineated on the plot; (1) the Angola-Benguela front (12°S-16°S); (2) the central northern Benguela (16°S-25.5°S); (3) the Luderitz cell (25.5°S-28°S); (4) the Orange River-Namaqua cell (28°S-31°S); (5) Cape Columbine-St Helena Bay (31°S-33°S); (6) southern Cape (33°S-34°S); (After Demarcq et al. (in prep.)).

1.2.4.2 Previous lateral carbon flux studies

Waldron et al. (1992) identified six carbon flux pathways, and constructed a nitrate budget for the Benguela system, which was later re-appraised for the southern Benguela (Waldron et al., 1998). New production, remineralization, and carbon export in the surface layer were taken from the literature or estimated. Nitrate was converted to carbon assuming Redfield stoichiometry and complete nutrient utilization. From this the authors calculated that ≈70% of southern Benguela new production was not consumed on the shelf, but was available for sequestration or lateral export in the sub-surface layers. This result was supported to some degree by observations of zooplankton grazing (Verheye, 1991) and the sedimentation rate of senescent phytoplankton (Pitcher et al., 1991) in the southern Benguela, which suggested that over 60% of primary production could not be accounted for by these mechanisms. Verheye (1991) suggested however, that consumption by other classes of heterotrophs was the likely missing 'sink'.

In a detailed research project on carbon fluxes in the Benguela system, Monteiro (1996) found based on observed non-Redfield uptake and remineralization ratios, that the southern Benguela was likely to be a region of carbon export. However, quantification of carbon fluxes in a box model showed the converse, and suggested that nearly 100% of southern Benguela new production was consumed by heterotrophs. Thus, a small fraction of primary production was exported to the shelf sediments as fecal pellets, and a larger, yet less well constrained proportion was available for export as DOC (subsequently estimated at ≈40% of PP; Touratier et al., 2003). This alternate view gains support from the observed low f-ratios (∼0.2) prevalent in the southern Benguela, which suggest that it is predominantly a recycling system (Probyn, 1992).

Inspired by the budgetary calculations of Waldron et al. (1998), and the possible existence of a SEEP type lateral export from the more dynamic and productive Benguela as had been suggested (Rowe et al., 1986; Rowe, 1987), Swart, Waldron, and Hutchings (2007) undertook an observational study to search for near bottom lateral carbon transport. Finding elevated levels of POC and PON in the BNL near the shelf break, the authors concluded that lateral

export of particulate matter was occurring in the Benguela, and repeated the budgetary exercise of the earlier study (Waldron et al., 1998). However, the presence of locally elevated concentrations of PM near the shelf break does not necessarily imply any lateral export - it could simply represent enhanced resuspension. Furthermore, it seems that in terms of the later studies (Monteiro, 1996), and data syntheses (Chen et al., 2003), that the budget derived export of >60% of PP (Waldron et al., 1992, 1998; Swart et al., 2007) represents a large overestimate. Possible reasons being that no account was taken for a flux of primary production into DOM, or for non-Redfield stoichiometry. Secondly, the calculations assumed that the nitrate net flux would be balanced, neglecting the possibility of a net import of nitrate to the system, and a net export of recycled forms of nitrogen, which were not considered. Most significantly however, no allowance was made for nitrogen loss through denitrification or anammox, which is now known to be highly prevalent in the Benguela system (Tyrrell and Lucas, 2002; Kuypers et al., 2005). This point is further reinforced by the fact that bacterial consumption in the Benguela has been estimated at over 80% of total primary production, leaving little for lateral export (Brown et al., 1991).

On the other extreme, the box model of Monteiro (1996), does not agree at all with observed (Brown and Hutchings, 1987; Hutchings et al., 1991; Verheye, 1991), or modelled (Touratier et al., 2003) zooplankton consumption, which is closer to 25% of primary production than 100% as suggested. Furthermore, several observational (Waldron et al., 1997) and modelling studies (Touratier et al., 2003) have suggested higher f-ratio's in the southern Benguela of around 0.6, at least periodically during intense plankton blooms (Probyn, 1992). Thus on the whole, the potential for a lateral carbon flux from the southern Benguela appears unresolved. What has become clear, is that elucidating the until now unknown DOM fluxes is crucial to understanding the overall behaviour of the system (Monteiro, 1996; Touratier et al., 2003).

1.3 Key questions

The key questions to be addressed by this thesis have been derived with careful consideration of the progress made during the continental margins studies around the world and specifically in the Benguela. They are as follows:

- What are the principal physical mechanisms responsible for cross-shelf advection and particle resuspension in the southern Benguela?
- What are the organic matter (particulate and dissolved) characteristics and important biogeochemical processes in the system?
- Is there a lateral export of organic carbon from the southern Benguela continental shelf to the deep ocean, and can it be quantified?

These questions are addressed systematically in the following three Chapters.

Chapter 2

Internal waves, the bottom boundary layer and lateral advection in the southern Benguela

2.1 Introduction

2.1.1 General

The exchange of biogeochemical constituents such as carbon, between the continental shelf and the open ocean is inextricably dependent on the physical mechanisms which mediate the cross shelf advection of fluid. The aim of this Chapter is to provide a basis for understanding some of the principal physical mechanisms of shelf-ocean exchange. Previous continental margin flux studies have identified the bottom boundary layer as a potential conduit for shelf-ocean exchange (Falkowski et al., 1988; Walsh et al., 1988a; Walsh, 1991; Biscaye et al., 1994; Thomsen and van Weering, 1998; Thomsen, 1999; Hung et al., 2000; McCave et al., 2001; van Weering et al., 2001; Wollast and Chou, 2001b; van Weering and McCave, 2002; van Weering et al., 2002). Preliminary investigations (Swart et al., 2007), and budget flux studies (Waldron et al., 1998) have also suggested that a near bottom path may dominate lateral carbon export

in the southern Benguela. The approach here is to consider cross shelf fluxes in general, with a specific focus on the bottom boundary layer and the turbulent mechanisms which generate bottom mixing, such as internal waves. This is done firstly by considering the theoretical requirements for cross shelf flow and the observed circulation in the southern Benguela, which was also dealt with in Chapter 1. Some specific observational results pertaining to internal tide generation, the bottom boundary layer, and lateral advection are then presented.

2.1.2 Cross shelf flows and shelf-ocean exchanges

2.1.2.1 General

In general, along shelf flows are considered to dominate coastal dynamics, with cross shelf flows, the mechanism of shelf-ocean exchange, often neglected. This is because the steeply sloping topography of the continental margin forms a physical barrier to exchange and because of the constraint of the *Taylor-Proudman* theorem which states that laminar geostrophic flow cannot cross the isobaths (Gill, 1982; Brink, 1998). If this is the case ($\delta w/\delta z = 0$), then the continuity equation simplifies to:

$\frac{\delta u}{\delta x} + \frac{\delta v}{\delta y} = 0$

If U and V are the cross shelf and along-shelf velocity scales, and L_x and L_y the across and along shelf length scales respectively, then:

$U = V.\frac{L_x}{L_y} = V\delta$, where $\delta = L_x/L_y$

It is clear that if $L_x << L_y$, as is generally the case, then the cross shelf velocity will be far smaller than the along-shelf velocity (Trowbridge et al., 1998).

The assumption of the Taylor-Proudman theorem is that the geostrophic flow is linear, inviscid (non-turbulent) and steady. By breaking anyone of these assumptions, as discussed below, cross-shelf flows can be induced, and shelf-ocean exchange initiated (Brink, 1998). In particular, in regions where cross shelf length scales become comparable or greater than along shelf length scales, such as near capes and topographic features such as canyons, escarpment

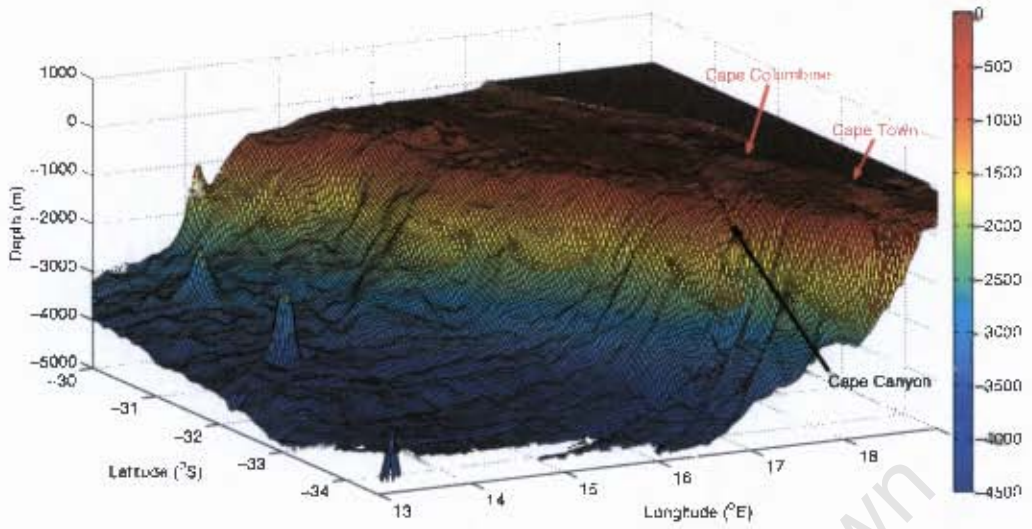

Figure 2.1: The Bathymetry of the southern Benguela

or banks, δ becomes > 1. In these regions cross shelf flow may rival or exceed the along-shelf flow, leading to enhanced shelf ocean exchanges (Trowbridge et al., 1998).

Figure 2.1 shows a 3-D representation of the bathymetry in the southern Benguela. The shelf is broadest in the north (~180 km), and narrows considerably south of Cape Columbine to only 40 km in the region of the Cape Peninsula. The shelf break is deep, lying at approximately 400 m, although in places an inner shelf break exists at around 140 m depth. Seaward of the shelf break, the continental slopes descends rapidly to abyssal depths of 5000 m in the Cape Basin. There are certain major bathymetric features which are of potential relevance for cross shelf flows and shelf-ocean exchange. These include the two large capes, the Cape Peninsula in the south, and Cape Columbine to the north, which affect both the wind stress and ocean dynamics in the region. Transecting the shelf in a nearly N-S orientation are the Cape Canyon, off Cape Columbine, and the Cape Peninsula Canyon further south. These river cut canyons reach the shelf break, and have previously been implicated as conduits of shelf-ocean exchange (Shannon, 1985). The influences of these features in breaking the constraint of the Taylor-Proudman theorem, and initiation cross shelf flows are discussed below.

2.1.2.2 Non-linearities

The Rossby number is a scaling of the non-linear terms to the rotational terms in the momentum equations, and when it starts to become important then the geostrophic constraint can be broken (Brink, 1998). Western boundary currents have large Rossby numbers and are highly non-linear, as are the baroclinic eddies which these currents shed. Such baroclinic eddies impinging on the slope can draw large amounts of water off the continental shelf (Brink, 1998). The southern Benguela is the only eastern boundary current which is bounded by, and interacts with a western boundary current (Shillington, 1998). The large anticyclonic rings which are spawned by the Agulhas Retroflection propagate into the south east Atlantic, and on occasion they interact with the Benguela system (Lutjeharms and Stockton, 1987; Duncombe Rae et al., 1992; Shillington et al., 1992; Brink, 1998). Indeed, Agulhas rings have been shown to draw large amounts of water off the southern Benguela shelf in cool filaments (Lutjeharms and Stockton, 1987; Duncombe Rae et al., 1992; Shillington et al., 1992). In one such event surface speeds reached 50 $cm.s^{-1}$, drawing over 5×10^{12} m^3 of Benguela shelf water into the deep South Atlantic, highlighting the potential of the rings to induce shelf-ocean exchange (Duncombe Rae et al., 1992).

Large shears in an alongshore flow can also lead to instabilities and the development of eddies, which if in proximity to the shelf break can lead to shelf-ocean exchanges. Such instabilities can be found in upwelling fronts, particularly associated with the jet features (Brink, 1987, 1998; Hill et al., 1998). An along-shelf current flowing past an irregularity in the coastline may separate from the coast and form meanders and eddies downstream (Hill et al., 1998; Trowbridge et al., 1998). In particular, downstream of a cape, flow decelerates, and frictional effects close to the coast lead to a reversal of the flow inshore in order to balance the pressure gradient. This flow pattern forms large semi-permanent eddies adjacent to the coast, which periodically propagate offshore, advecting with them large amounts of mass and momentum, inducing drag on the mean flow and enhancing lateral exchange (Trowbridge et al., 1998). Meanwhile, the detached alongshore flow circumvents the eddy, and reattaches to the coast downstream. Instabilities in the separated alongshore flow can result in the formation of

mesoscale eddies, squirts and filaments (Trowbridge et al., 1998). In the southern Benguela, shelf edge jets and a convoluted, eddying upwelling front are well documented features (Nelson and Hutchings, 1983; Lutjeharms and Stockton, 1987; Shillington, 1998; Shillington et al., 2006). Furthermore in the lee of Cape Columbine, a well developed cyclonic eddy is the predominant feature of the circulation (Shannon, 1985; Bailey and Chapman, 1991). Intense filaments and squirts have been observed extending offshore of the Benguela, leading to significant exchanges of mass and biogeochemical properties with the open ocean (Lutjeharms and Stockton, 1987; Shillington et al., 1992).

2.1.2.3 Turbulent processes

In the surface and bottom boundary layers, turbulence causes the shear stress terms to become large enough that they rival the Coriolis term in the momentum equations, and break the geostrophic constraint (Brink, 1998). Including friction in the momentum equations leads to the formulation of Ekman layers at the surface and at the bottom. Balance between the frictional and Coriolis forces dictates that net transport in a surface Ekman layer is rotated 90° anticyclonically relative to the surface (wind) stress, while in a bottom Ekman layer the flow veers cyclonically as the bed is approached (Pond and Pickard, 1983). The role of the bottom boundary layer is considered in more detail in Section 2.1.2.5. In the presence of boundaries, such as the coast, divergence in the surface Ekman layer leads to upwelling, while conversely, convergence at the boundary leads to downwelling. Both of these scenarios involve lateral transport of water across the shelf, and are instrumental in shelf-ocean exchange (for a detailed discussion of Ekman dynamics see Gill, 1982; Pond and Pickard, 1983). Furthermore in the presence of short along shelf scales, such as a cape, cyclonic curl in the equatorward wind-stress can lead to enhanced upwelling. Being one of the four major wind driven coastal upwelling systems, a major constituent of shelf-ocean exchange in the Benguela is modulated though upwelling, the details of which were discussed in Chapter 1 (Andrews and Hutchings, 1980; Nelson and Hutchings, 1983; Shannon and Nelson, 1996; Shillington, 1998; Shillington et al., 2006).

2.1.2.4 Time dependence

Time dependent flows with high frequency, such as waves, again lead to the breakdown of the geostrophic approximation. In the coastal zone, tides, internal waves and coastal trapped waves may all result in significant cross shelf velocities. Tides tend to be a major energy source for the coastal ocean where they are often amplified relative to the open ocean, and their turbulent dissipation at the sea floor leads to enhanced mixing. Tidal flows on sloping topography (slopes/shelves) can be asymmetric, and lead to considerable net transport across the shelf. Furthermore, the barotropic surface tide can generated large amplitude internal tides in regions of critical topography, which themselves can lead to significant current speeds and bottom shear stresses (Brink, 1998; see Section 2.1.3). Coastal trapped waves are generated when there is an along shelf variation in the pressure gradient, caused for example by enhanced upwelling near a cape (Trowbridge et al., 1998). These features propagate cyclonically around the coast, and may be scattered into shorter wavelengths upon experiencing significant changes in topography or coastline (Trowbridge et al., 1998). The end result is the production of intense mesoscale features or eddies on the shelf, capable of inducing an exchange with the open ocean. While the barotropic tidal range is generally modest in the southern Benguela region (<2 m) (Shillington, 1998), the generation and importance of large amplitude internal tides has been recognized and is discussed in detail below (Chapman and Shannon, 1985; Shannon, 1985; Bailey and Chapman, 1991; Monteiro et al., 2005). Furthermore, coastal trapped waves are prominent features of the circulation in the southern Benguela (Shannon and Nelson, 1996; Shillington, 1998), modulating the upwelling process, and leaving a clear signal in current meter records (Nelson and Polito, 1987; Nelson, 1989).

2.1.2.5 Flow in the Bottom Boundary layer

The benthic boundary layer, or bottom boundary layer (BBL), is that part of the water column which is directly influenced in its characteristics by bottom drag (Trowbridge et al., 1998). This layer is the principal site of energy dissipation from currents, waves and turbulence and is a region of enhanced lateral and vertical transport of particulates and solutes. It

provides the habitat for a wide range of benthic organisms, plants and microorganisms and it is a region of enhanced diagenesis and biological reactivity (Thomsen and van Weering, 1998; Thomsen, 1999, 2002). The BBL is typically metres to tens of meters thick, but can extend to hundred of meters in particular cases (Gill, 1982; Soulsby, 1983; Lentz and Trowbridge, 1991; Trowbridge et al., 1998; Dade et al., 2001). It typically has temperatures and salinities which are well mixed, and elevated levels of suspended material, due to turbulent mixing (Lentz and Trowbridge, 1991; Trowbridge et al., 1998). Horizontal currents experience cyclonic Ekman veering in the BBL, which makes it a region of cross-shelf transport, and a vital conduit for shelf-ocean exchanges (Gill, 1982; Pond and Pickard, 1983; Trowbridge et al., 1998; Dade et al., 2001; Thomsen, 2002).

Flow in the BBL may be partitioned into mean flow, steady over a period of hours or longer and turbulence, which refers to high frequency irregular motions (eddies; Soulsby, 1983; Dade et al., 2001). The BBL has a well defined vertical structure, based on stress dominance. The full vertical extent of the BBL, at least in the open ocean, is the depth over which friction operates and is known as the Ekman layer, a type of planetary boundary layer. The Ekman layer is overlain by the interior geostrophic flow with the 'free stream velocity' (Gill, 1982; Pond and Pickard, 1983; Soulsby, 1983; Dade et al., 2001). As noted, the flow in the BBL is veered cyclonically relative to the free stream velocity, and for a theoretical Ekman layer, flow would veer by 45° by the bottom of the layer where u becomes zero. However in reality the angle is more likely to be between 10°-30°, and can be given by $\cos(\theta) = U/U_\infty$, where U_∞ is the free stream velocity (Gill, 1982; Pond and Pickard, 1983; Dade et al., 2001). Qualitatively the veering occurs because as the BBL is entered, friction slows the flow, and Coriolis force decreases, while the pressure gradient force (PGF) remains the same (barotropic case). Thus the flow rotates cyclonically until the sum of the frictional force and Coriolis force balance the PGF (Pond and Pickard, 1983). It is worth noting that under certain circumstances, buoyancy arrest of the BBL can slow down the speed of the flow, thus reducing, but not eliminating, the cross-shelf exchange. Specifically, during upwelling conditions, the upslope Ekman flux transports denser water up the slope, beneath lighter water, which enhances the

stratification and hinders the growth of the BBL. By contrast, during downwelling conditions, associated with poleward flow, Ekman transport moves lighter water downslope, beneath heavier water. This reduces the stratification and allows for the growth of the BBL.

Turbulence in the BBL essentially consists of eddies, generated because of shear stresses, which are advected downstream in the general flow (Thomsen, 2002), and possesses the ability to mix momentum, energy and contaminants at a rate far higher than molecular diffusion (Dade et al., 2001). Turbulence in the BBL is not necessarily completely random, and certain large scale features can persist. A cycle known as the 'bursting phenomenon' has been observed, whereby an 'ejection' (or burst) of low velocity fluid moves up into the overlying flow from the bottom, followed by a compensating high-speed down rush or 'sweep'. The bursting phenomenon is thought to dominate BBL turbulent stress, and is therefore mostly responsible for the observed mixing and elevated particle concentrations in the BBL (Soulsby, 1983; Dade et al., 2001). Turbulence and bottom mixing may also be induced by the breaking of internal waves, which in certain instances are non-symmetrical, and lead to cross-shelf flows. These mechanisms are considered in detail below.

2.1.3 Internal waves

Internal waves are, as the name implies, gravity waves which are manifest in the interior of the ocean and not on the surface. In the simplest case the waves occur at the interface between two water parcels of differing densities, such as above and below the thermocline. Although the water motion would extend above and below this interface. The density differences between the two internal water parcels are much smaller than the density differences at the surface between the ocean and the atmosphere. This has two implications, firstly, internal waves propagate considerably more slowly than surface waves, and secondly, the small density difference allows internal waves to have large amplitudes, even for modest energy contents. Also, since internal waves cause pressure and velocity to vary with depth, they are termed as baroclinic modes (Gill, 1982; Pond and Pickard, 1983).

Internal waves may be generated through several mechanisms, however one of the most common is through transfer of energy from the barotropic surface tide in the presence of steep topography, such as continental slopes and sills. For example, when the barotropic surface tide flows off the continental shelf, vertical motion will result which depresses the pycnocline (Pond and Pickard, 1983; Gerkema and Zimmerman, 1995; Johnson et al., 2001). When the tide weakens or reverses, the depression propagates onto the shelf (Holloway, 1987; Johnson et al., 2001). Such vertical water displacements by the barotropic tide are the driving force behind internal tides, which are simply internal waves with a tidal frequency, and are commonly observed in the ocean (Pond and Pickard, 1983; Sandstrom and Elliot, 1984; Holloway, 1987; Johnson et al., 2001; Cacchione et al., 2002; McPhee-Shaw et al., 2004).

In the more complex case, internal waves can occur under conditions of continuous stratification. The dispersive nature of the internal waves under such conditions leads to the peculiar property that the group velocity travels perpendicularly to the phase velocity (i.e. parallel to the wave crests; see Figure 2.2). Thus, the wave energy travels in beams at an angle to the horizontal, perpendicular to the wave crests (see Figure 2.2) (Pond and Pickard, 1983). This angle is determined by the frequency of the internal waves, the vertical density structure and the latitude and is given by:

$$c = \left[\frac{\sigma^2 - f^2}{N^2 - \sigma^2}\right]^{1/2} \quad (1)$$

where σ is the internal wave frequency (cph); f=(sinϕ)/12 (cph), where ϕ is latitude; and N is the buoyancy frequency given by

$$N \simeq 573\,[(g/\rho)(\delta\rho/\delta z)]^{1/2}\,\text{(cph)} \quad (2)$$

where ρ is the density, z is the depth, and g is gravity (Cacchione et al., 2002).

When interacting with the bottom, the surface, or the base of the pycnocline, the waves are reflected with an angle equal to the angle of incidence, relative to the local gravity vector (not normal to the surface; Cacchione et al., 2002). In the case of a sloping bottom, the waves may either be reflected, or transmitted, depending on the ratio of the bottom slope to the incident ray slope (Cacchione and Drake, 1986; Cacchione et al., 2002; McPhee-Shaw et al.,

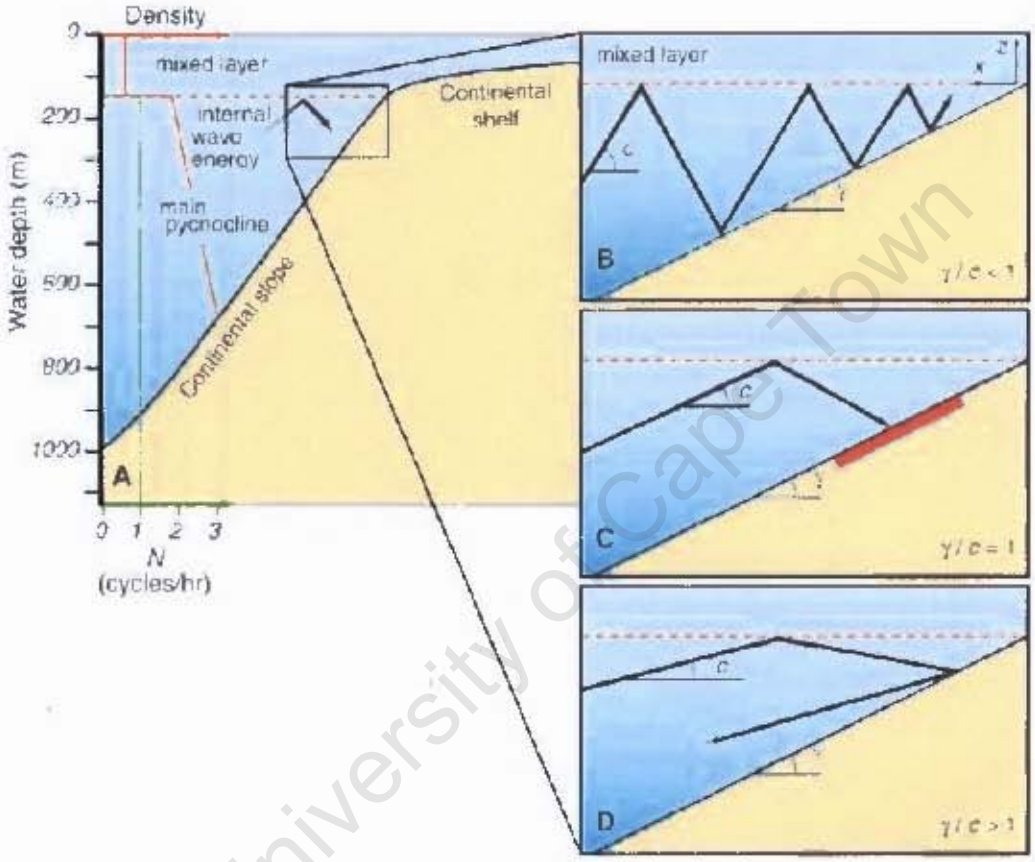

Figure 2.2: Reflection of internal wave characteristics (black lines) from the bottom: (A) simplified density profile (red) and Brunt-Vaisala frequency profile N (green), transmissive [(B), $\gamma/c<1$], critical [(C), $\gamma/c=1$], and reflective [(D), $\gamma/c>1$]. Energy is trapped along the bottom, and bottom velocities are intensified in (C) (maroon bar indicates velocity intensification); bottom velocities also increase up-slope in (B). From Cacchione et al. (2002) Figure 1.

2004). Transmitted rays will be reflected from the bottom at an angle equal to the angle of incidence about the local gravity vector, whereas reflected rays are reflected at the incident angle relative to the horizontal. To determine the behaviour of internal waves on a sloping environment, the angle of the slope γ, may be compared to the incident wave angle c (see Figure 2.2). Where $\gamma/c < 1$, the waves will be transmitted, where $\gamma/c > 1$, the angle is said to be super-critical, and the internal waves will be reflected from the slope. In the special case where $\gamma/c = 1$, the so called critical angle, the energy of the internal wave is trapped near the bottom, leading to maximum bottom velocities and shear stresses (Cacchione and Drake, 1986; Cacchione et al., 2002; McPhee-Shaw et al., 2004).

For the transmissive case ($\gamma/c < 1$), wave velocities and bottom stresses increase up-slope, and eventually may steepen and break, resulting in turbulent mixing (Cacchione and Drake, 1986). The resulting mixed layer may then collapse into an intrusion and spread seaward, forming a potentially important lateral transport mechanism on the shelf (Cacchione and Drake, 1986; McPhee-Shaw and Kunze, 2002). In near critical regions, where γ/c remains just less than unity, nonlinear steepening of the internal wave can occur, leading to the on-shelf propagation of internal tidal bores, or hydraulic jumps, associated with large amplitude temperature and current fluctuations (Cacchione and Drake, 1986; Holloway, 1987; Johnson et al., 2001; McPhee-Shaw et al., 2004). Such nonlinear internal tides have been shown to disintegrate into high frequency solitary waves, or solitons, which propagate behind the internal tide in a rank ordered fashion, dissipating significant amounts of energy (Sandstrom and Elliot, 1984; Holloway, 1987; Gerkema and Zimmerman, 1995). These non-linear internal tides and solitons are also frequently asymmetrical with respect to current structure, and thus can lead to significant cross-shelf transports of water and suspended particulates (Cacchione and Drake, 1986; Johnson et al., 2001; McPhee-Shaw et al., 2004; Monteiro et al., 2005). Internal waves are of great significance in the ocean, because the bottom turbulence associated with their up-slope intensification and breaking has been shown in many instances to generate and maintain bottom nepheloid layers (Cacchione and Drake, 1986; Johnson et al., 2001; McPhee-Shaw et al., 2004), which are important biologically (Monteiro et al., 2005), and

particularly as cross-shelf conduits for sediment and tracer transport. Separation and offshore advection can also lead to the formation of intermediate nepheloid layers (McPhee-Shaw and Kunze, 2002; McPhee-Shaw et al., 2004). Furthermore, the vertical propagation of internal wave energy has been proposed as important for ocean mixing (Pond and Pickard, 1983; McPhee-Shaw and Kunze, 2002), and for the supply of nutrients to the continental shelf and the euphotic zone (Cullen et al., 1983; Sandstrom and Elliot, 1984). The presence of internal tides, and the characteristics of their propagation in the southern Benguela are considered below using density, temperature and current meter data.

2.2 Data

2.2.1 Hydrographic and bathymetric data

Hydrographic data were collected on the approximately monthly repeat St Helena Bay Monitoring Line (SHBML) off the west coast of South Africa (Figure 3.1). The line stretched from Station 3 near the coast, in approximately 75 m of water, to Station 12 on the upper continental slope, around 90 Nautical miles (Nm) offshore, in a water depth of around 1400 m. At each Station hydrographic data were collected with a Seabird electronics CTD system, to within 5 m of the bottom. Hydrographic data collected since the inception of the SHBML in 2000, to the most recently available processed data (2004) was obtained from Marine and Coastal Management in Cape Town, South Africa. In this study, after certain data were excluded for quality purposes, a total of 24 SHBML cruises were used, which are detailed in the appendix. The determination of the Brunt-Vaisala Buoyancy frequency, and the calculation of bottom boundary layer thickness was done using σ_t profiles, calculated from the temperature and salinity data using the UNESCO 1983 polynomial (Fofonoff and Millard, 1983). The bathymetric database used in this study was the ETOPO2 version 1 data set, provided by NOAA (http://www.ngdc.noaa.gov/mgg/fliers/01mgg04.html). The quality of the ETOPO2 data set was qualitatively deemed as superior over the GEBCO 1 minute grid, for the study region.

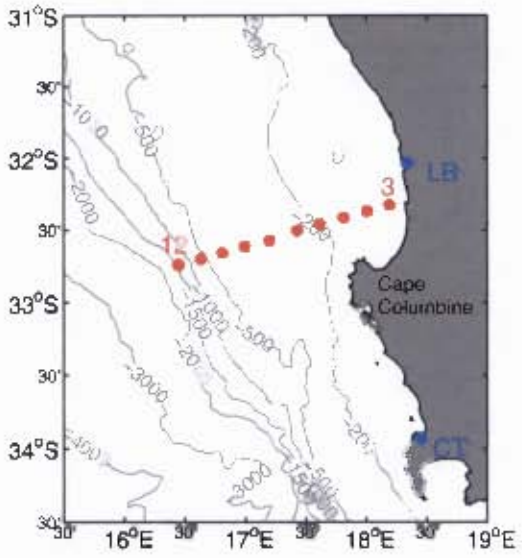

Figure 2.3: The positions of the SHBML Stations 3-12 in the southern Benguela.
Station 3 is in 75 m of water. Station 12 is approximately 90 NM offshore on the upper slope, in a water depth of 1400 m. The positions of Lambert's Bay (LB) and Cape Town (CT) are marked in blue. The local bathymetry is shown for reference.

2.2.2 Current meter data

In an attempt to directly observe cross shelf fluxes and high frequency fluctuations in the bottom boundary layer, an upward facing ADCP was deployed in 380 m of water, near the shelf break on the SHBML in June 2006. Unfortunately, the mooring was not recovered. Subsequently, the data for nearly 60 Recording Current Meter (RCM) records, obtained at sporadic intervals since the 1980s, at multiple locations on the southern Benguela shelf and slope, was downloaded from the South African Data Centre for Oceanography (SADCO; http://sadco.csir.co.za/). Seven of these records were selected for their merit in displaying lateral advection, and are analysed and discussed in Section 2.3.2.2. The records have sampling intervals ranging between 15 minutes and 1 hour, and they have been rotated so that the y axis is parallel to the local bathymetry (see Table 2.1 for details).

2.3 Results and discussion

2.3.1 Internal waves

In order to assess the relationship γ/c, the angle of the bathymetry in the southern Benguela, in degrees from the horizontal, was calculated and is presented in Figure 2.4. The angle was determined from ETOPO2 bathymetry by finding, at each point, the maximum change in depth (in m) which occurred in any direction, over a 2 minute interval (in m). That is, at every point, the change in depth was calculated perpendicular to the local bathymetry, over an interval which extended from 1 minute up-slope of the point to 1 minute down-slope of the point. The distance of the interval was calculated based on a great circle path, with an earth radius of 6367.442 km, and the angle calculated trigonometrically. The angle of propagation of the internal tide characteristic, c, was calculated for semi-diurnal frequencies (0.081 cph) according to equation 1, using average density profiles from the SHBML. Average summer and winter buoyancy frequency profiles were calculated according to equation 2 from the historical SHBML data set (see appendix for details), and were then extrapolated in the alongshore direction to cover the entire southern Benguela.

The resulting seasonal distribution of γ/c in the southern Benguela is presented in Figure 2.5. It is a first approximation because the bathymetry used is fairly coarse, and it has been assumed that there is no alongshore variation in vertical density structure. Nonetheless, the result provides a broad scale view of the important features, and is a valuable first step. The continental shelf is transmissive ($\gamma/c<1$) for internal tides during both summer and winter, however the steep bathymetry of the continental slope, and certain seamounts may be near critical ($\gamma/c \sim 1$) or reflective ($\gamma/c>1$). The very steep continental slope bathymetry offshore of the Cape Peninsula, reaching nearly 5°(Figure 2.4), is in general more reflective or near critical than the more gentle bathymetry of the continental slope to the north. Careful examination also reveals that the steep sides of the Cape Canyon tend to have a higher γ/c than the surrounding area. Temporally it is evident that the continental slope exhibits higher values of γ/c during winter than during summer. In winter the slope off the Cape

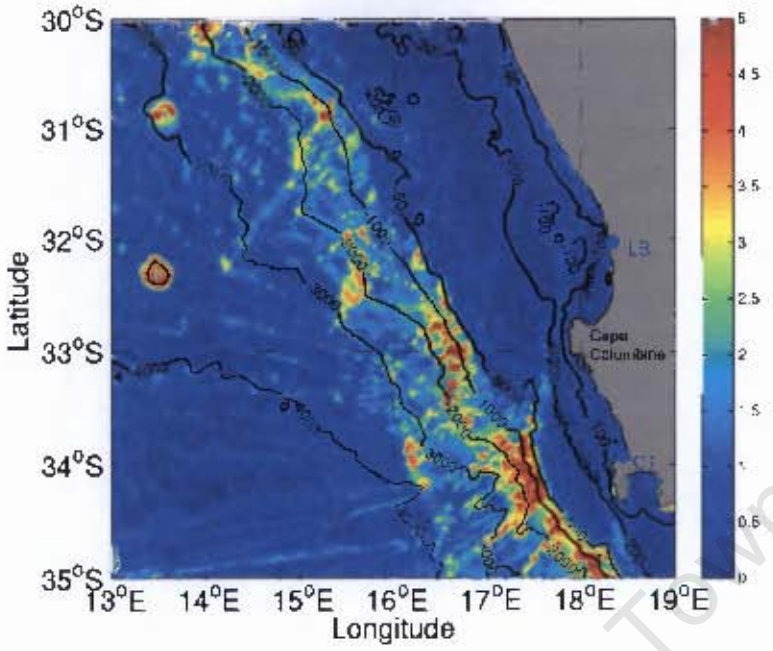

Figure 2.4: The angle, in degrees from the horizontal, of the bathymetry in the southern Benguela. See text for details on the calculation of the slope angle

Peninsula is almost entirely reflective, whereas in summer it is closer to critical. Further north, the continental slope is largely transmissive in summer, but becomes close to critical during winter, a particular hot spot being the upper slope region offshore of Cape Columbine.

The γ/c distribution implies that semi-diurnal internal tides may become bottom trapped on the near critical upper continental slope, where they would dissipate their energy and enhance bottom velocities and turbulent mixing (Cacchione and Drake, 1986; Cacchione et al., 2002; McPhee-Shaw and Kunze, 2002). Such internal tidal energy dissipation could be important for the generation of bottom nepheloid layers, as well as for the distribution and transport of organic and lithogenic particles (McPhee-Shaw and Kunze, 2002; McPhee-Shaw et al., 2004). Furthermore, it appears that internal tides would be more likely be transmitted onto the continental shelf during summer, than during winter, when they would be dissipated on or reflected from the continental slope. Internal tides which manage to propagate onto the shelf may steepen and eventually break as they move into shallower water, inducing enhanced mixing, particle resuspension and BNL formation (Cacchione et al., 2002). Indeed, the presence of internal tides have previously been identified in the southern (Chapman and

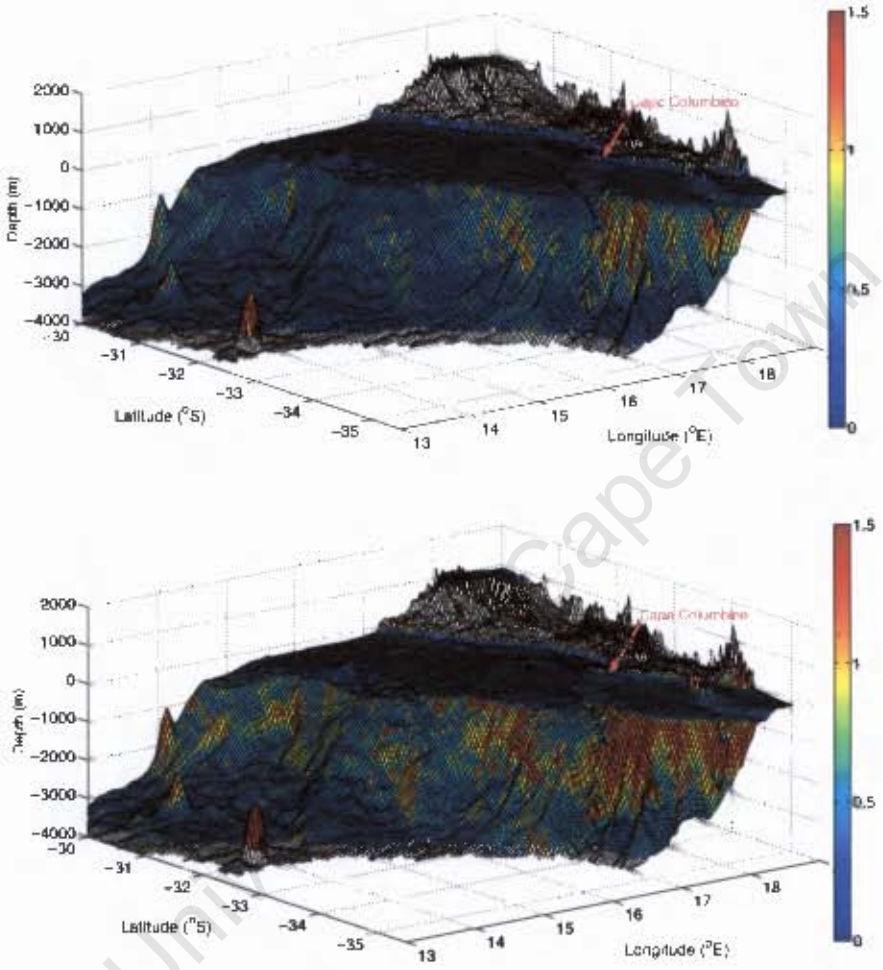

Figure 2.5: γ/c for the southern Benguela in summer (top) and winter (bottom). The bathymetry slope of the bathymetry, γ, was taken from 2.4 and calculated from the ETOPO2 data set. The angle of the internal tide characteristic propagation, c, was calculated using typical summer and winter density profiles from the SHOML, see text for details. The entire continental shelf is transmissive ($\gamma/c<1$), but regions of the slope, particularly off the Cape Peninsula, are near critical or even reflective for semi-diurnal internal tides. The slope is generally more reflective ($\gamma/c>1$) in winter, owing to a more stratified water column, and higher N.

Shannon, 1985; Bailey and Chapman, 1991) and central Benguela (Monteiro et al., 2005), and their implications for vertical mixing and biogeochemical processes as well as particulate matter advection has been recognized.

A mooring in 457 m of water (g, Figure 2.16) with recording current meters at 77, 118, 199 and 380 m furnishes us with information on internal tide dynamics in the southern Benguela. In general, the synchronous 12 day records show a southwestwards flow, with a distinct anticyclonic veering evident with depth. Since the records were exactly synchronous, it was possible to calculate a baroclinic component of the velocity field, by subtracting velocities at the bottom record from those at 77 m. Thus, for the u component of the flow, the baroclinic velocity $\delta u = u_{77\,m} - u_{380\,m}$, and is shown in Figure 2.7. Typical maximum baroclinic velocities in the u direction were 0.15 $m.s^{-1}$, and exhibited strong reversals approximately twice a day. A low frequency oscillation in the mean velocity was also evident, but on the whole, the semi-diurnal fluctuations were asymmetrical, and the mean baroclinic velocity was negative.

A Fourier analysis of the u component of the baroclinic velocity reveals a marked peak at semi-diurnal frequencies (2 cpd), with an additional lower frequency component (Figure 2.7). Readers are referred to the appendix entitled Statistical methods, where the statistical techniques employed here, and in the remainder of the dissertation are fully defined. Since the surface tide is barotropic, the only feasible mechanism which is able to explain the large amount of baroclinic energy observed at semi-diurnal frequencies is an internal tide. Thus, at this mooring position within the Cape Canyon, internal tides were responsible for generating baroclinic velocities of $\sim$0.15 $m.s^{-1}$. Since the region is known to be near critical for internal tide propagation, bottom velocities might well be elevated beyond this (Cacchione et al., 2002). Furthermore, since the baroclinic velocity fluctuations were asymmetrical and the resulting mean velocity negative, it appears that internal tides here may play a role in seaward lateral advection (Cacchione and Drake, 1986; McPhee-Shaw and Kunze, 2002). Indeed, internal tides may help to explain the sediment size distribution on the southern Benguela shelf, something which has previously been proposed for the central part of the system (Monteiro et al., 2005; Inthorn, 2006a). Figure 2.8 shows that the lower slope and

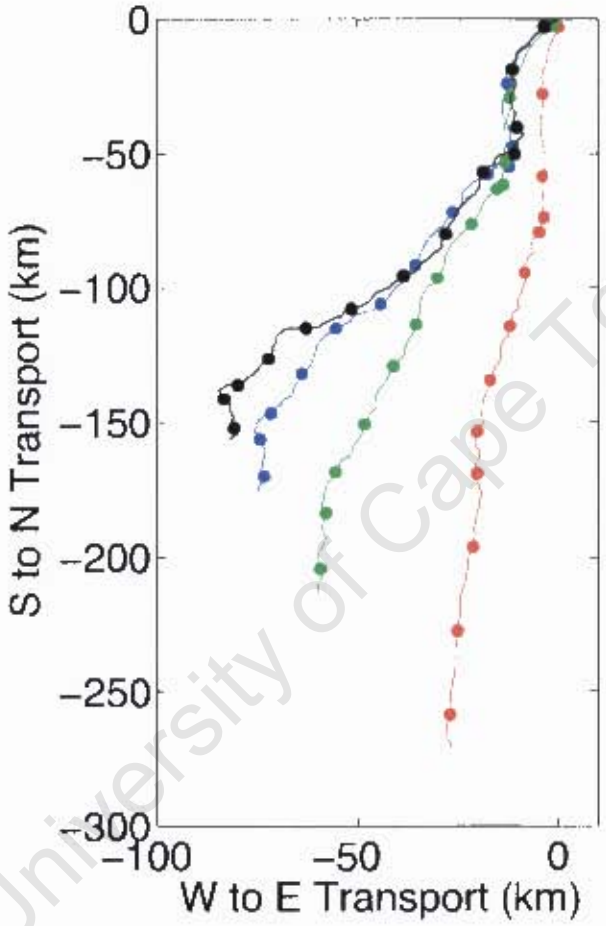

Figure 2.6: Progressive vector diagrams of current meters at depths of 77 (black), 118 (blue), 199 (green) and 380 m (red), on a mooring in 457 m off water. The dots are day markers, and all the records are simultaneous, running from 18:00 on 12 February 1991 -10:00 on 25 February 1991, sampling every 30 minutes. The position of the mooring within the Cape Canyon is marked as **g** in Figure 2.16. At all depths the current is to the south. There is a significant anticyclonic veering of the current with increasing depth, the surface currents having more of a westerly component than those at depth.

inner shelf are both characterized by fine, muddy sediments. The outer continental shelf and upper slope, by contrast, contain coarser sandy sediments. If, as has been shown, internal tidal energy were bottom focused over the outer continental shelf and upper slope region, then the enhanced velocities and turbulent mixing would prohibit the deposition of fine grained sediments, and could in fact actively erode material from the region (Dade et al., 2001; Cacchione et al., 2002; Thomsen, 2002). Asymmetry in the internal tide velocities, or the presence of a low frequency off-shelf current could then transport the material into the abyssal ocean. Thus it appears that internal tides must play a vital role in turbulence generation, particle suspension, and lateral advection in the Benguela system, making them highly relevant to biogeochemical flux studies.

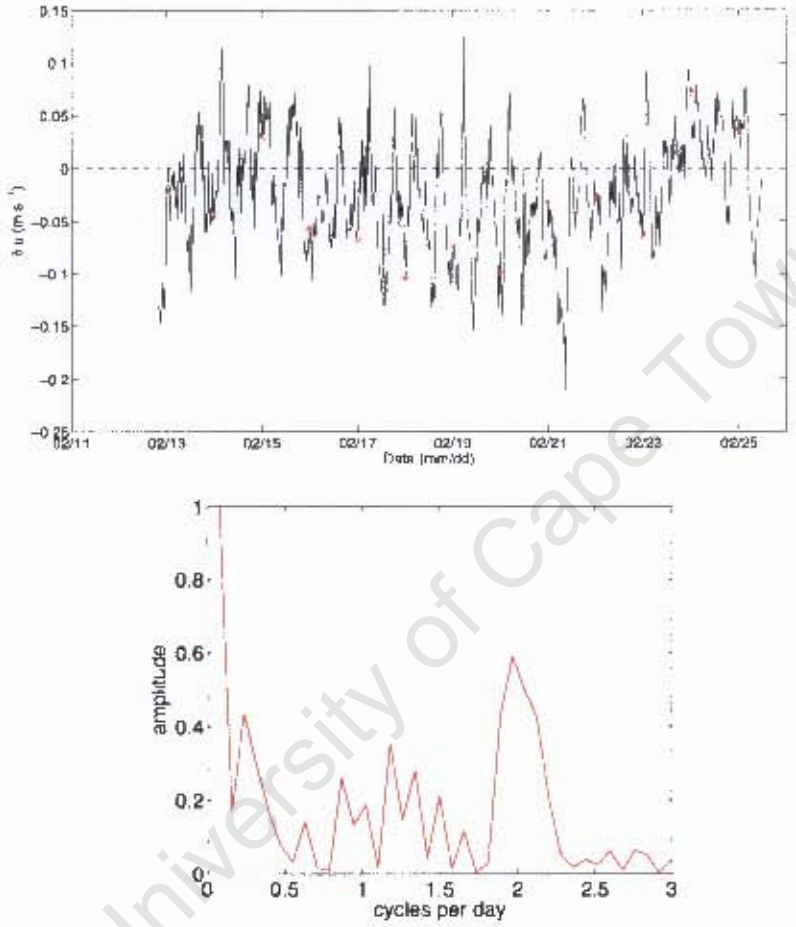

Figure 2.7: The baroclinic component of the current in the u direction at mooring g (top) and its spectral analysis (bottom) . The baroclinic component was calculated as $\delta u = u_{77\,m} - u_{380\,m}$. The red dots are day markers, corresponding to the dots in 2.6. The baroclinic component of the current can be seen to oscillate approximately twice a day, and to also exhibit a lower frequency fluctuation. The energy spectrum of the Fourier analysis confirms this, showing a distinct peak a semi-diurnal frequencies (2 cpd), with an additional lower frequency component. The surface tide is barotropic, and therefore cannot account for the energy at semi-diurnal frequencies in this baroclinic record. However, internal tides are baroclinic, and thus the large amount of baroclinic energy at tidal frequencies highlights the existence of strong internal tides in the study region.

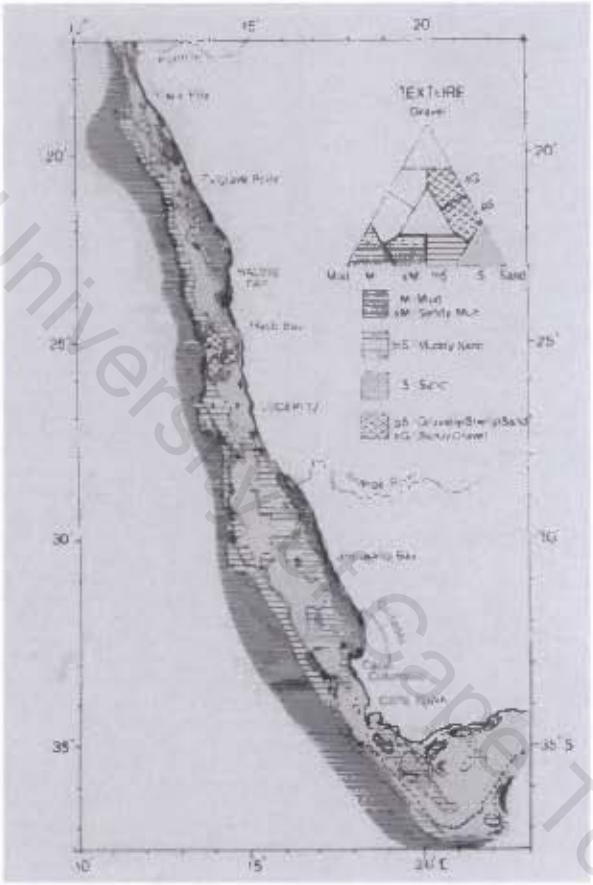

Figure 2.8: Sediment size distribution in the Benguela

In the southern Benguela, the mud-belt can be seen extending south from the Orange River south, close inshore. The lower continental slope is also dominated by fine, muddy sediments. The outer continental shelf and upper slope are characterized by coarser, sandy sediments. These coarser sediments are evidence of a high energy environment, preventing fine particle deposition. Considering that the upper continental slope becomes near critical for internal tide propagation, particularly in winter, bottom energy dissipation from internal tides may help to explain the sediment size distribution (from Rogers and Bremner, 1991).

2.3.2 The bottom boundary layer

2.3.2.1 Distribution and characteristics of the BBL

While the bottom boundary layer is correctly defined as the region over which the flow is affected by the influence of bottom friction (Trowbridge et al., 1998), its existence maybe approximated by the presence of a bottom mixed layer (Lentz and Trowbridge, 1991). Defined in this way, the distribution and vertical extent of the the BBL maybe characterized using vertical CTD profiles. Here, an automated algorithm was used to estimate the bottom mixed layer height from density profiles collected on 24 SHBML cruises conducted since 2000 (see appendix for details). Station 12 (16.4°E) was excluded because the CTD was often not deployed to the full depth at that Station. The height of the bottom mixed layer, h_m was defined as the point where the change in density per meter, $\delta\rho/\delta z$, exceeded 0.002 $kg.m^{-3}.m^{-1}$. If $\delta\rho/\delta z$ exceeded this value over the bottom meter then $h_m$was defined as zero. Since the CTD typically only reached to within 5 m of the bottom, BBLs thinner than 5 m would not be detected, and would be defined here as zero. The $\delta\rho/\delta z$ limit of 0.002 $kg.m^{-3}.m^{-1}$ was subjectively chosen and can be adjusted to improve the performance of the algorithm. Figure 2.9 shows four examples of density profiles, with red dots which mark h_m as defined by the algorithm and a $\delta\rho/\delta z$ limit of 0.002 $kg.m^{-3}.m^{-1}$. From these it can be seen that the algorithm is successful in determining the vertical extent of the bottom mixed layer, and we may use it to define the characteristics of the BBL in the southern Benguela.

The 209 density profiles analysed exhibit an exponential distribution of BBL thickness (Figure 2.10). A BBL was present on over 90% of occasions, with a mean thickness of 19 m and a median thickness of 21 m. Thicker BBLs were less likely, and the maximum recorded bottom mixed layer height was 93 m. These observations are in line with previous estimates, which describe the BBL in the Benguela as typically 10-20 m thick and as being modulated by bottom velocity (Shannon and Nelson, 1996). Similarly a study on the California shelf showed a near exponential distribution and a typical BBL thickness of 5-15 m (Lentz and Trowbridge, 1991).

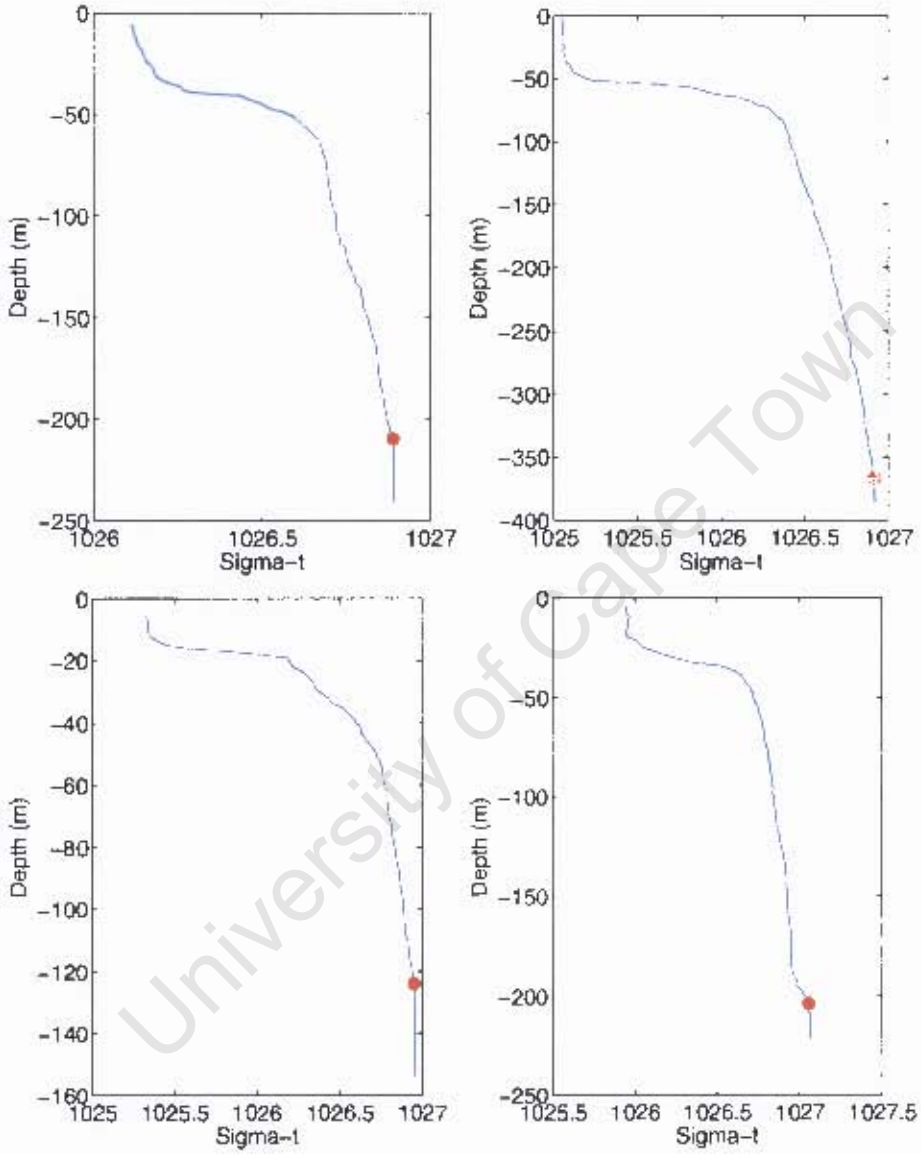

Figure 2.9: Performance of the algorithm for determining bottom boundary layer thickness. Four example profiles of σ_t, from top left, Station 7 (06/2001), Station 10 (01/2003), Station 5 (02/2002) and Station 6 (04/2004). The red dot marks the position of the top of the BBL, as determined by the algorithm used to derive BBL thickness. For these four Stations, and on the whole, the algorithm appears effective at determining the vertical extent of the BBL.

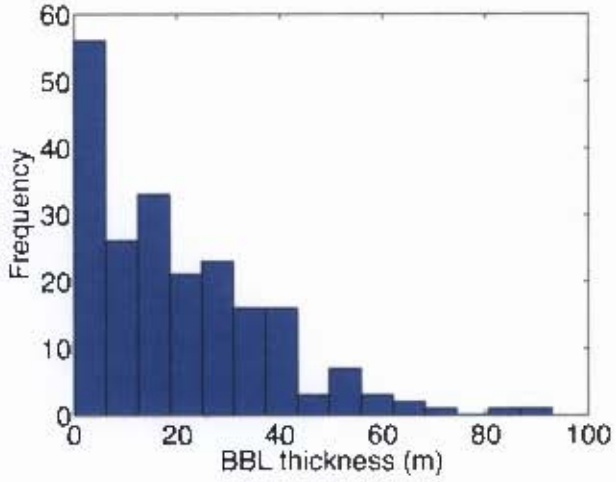

Figure 2.10: Frequency distribution of BBL thickness.
The bins are approximately 6 m wide. Station 12 was excluded because the CTD was often did not reach the bottom of the water column there.

The cross shelf distribution of mean BBL thickness is shown in Figure 2.11. The BBL is on average thinnest near the coast, and tends in general to increase in thickness across the shelf until Station 8 (17.2°E), after which is decreases again to just over 20 m on the upper slope at Station 11. The distribution of BBL thickness against water depth exhibits a large amount of scatter, and renders little information, and has thus not been included here. The cross shelf Mean Absolute Deviation (MAD; a measure of variability for non-Gaussian distributions, see Statistical methods appendix for details) in BBL thickness, on the other hand shows an interesting pattern (Figure 2.12). The MAD in BBL thickness is low, and constant at about 12 m over the entire continental shelf, but then rapidly increases to over 21 m at Station 11 on the upper continental slope (16.6°E). This suggests a mechanism of episodic enhanced bottom mixing on the upper continental slope, which tends to increase the variability in bottom mixed layer height.

The density profiles may also be used to determine the cross shelf distribution of buoyancy frequency, calculated using equation 2. Figure 2.13 shows two cross shelf distributions of buoyancy frequency, the upper distribution is an average value for N over the bottom 20 m of the water column, corresponding to the mean BBL thickness. While there is not a clear pattern, N tends on average to decrease across the shelf, and then rise again on the upper

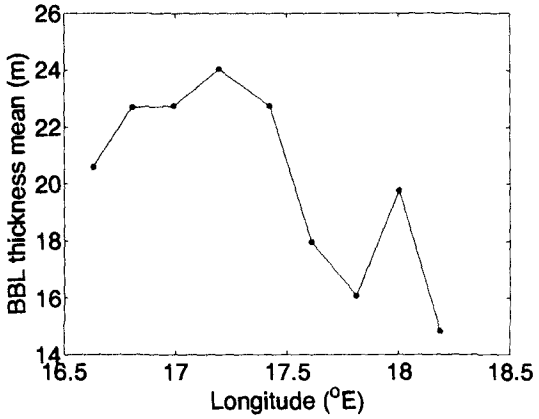

Figure 2.11: Cross shelf distribution of mean BBL thickness.
The dots mark Station positions on the SHBML, and only Station 3 (18.2°E) to 11 (16.6°E) are shown. Data from Station 12 were excluded. The coast is on the right.

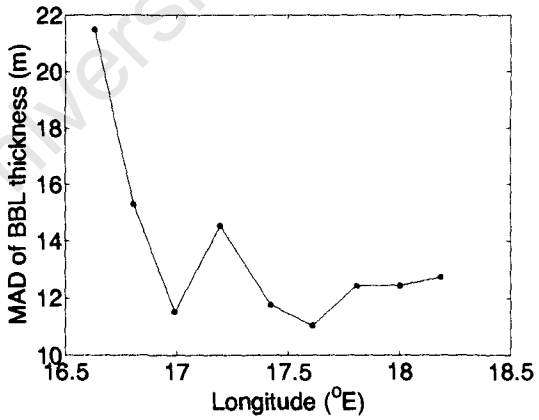

Figure 2.12: Cross shelf distribution of the Mean Absolute Deviation (MAD) in BBL thickness.
The dots mark Station positions on the SHBML, and only Station 3 (18.2°E) to 11 (16.6°E) are shown. The MAD in BBL thickness is a maximum at Station 11.

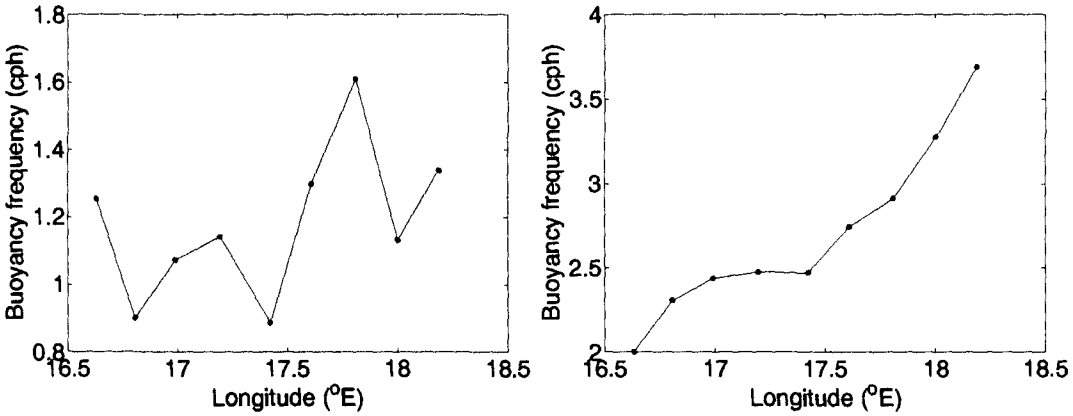

Figure 2.13: The cross shelf distribution of buoyancy frequency, averaged over the bottom 20 m of the water column (left) and averaged over the whole water column (right). The dots mark Station positions on the SHBML, and only Station 3 (18.2°E) to 11 (16.6°E) are shown. The coast is on the right.

slope at Station 11. The bottom distribution is a average of N over the entire water column, and it shows a distinct decrease in buoyancy frequency with increasing distance from the coast. Thus on average, the water column of the inner shelf is more stably stratified than the water column over the outer shelf and continental slope. Furthermore, the water column is more stratified at all Stations during winter, than during summer (not shown), possibly because of increased wind stress and upwelling during the latter.

The thickness of the BBL may also be compared to the buoyancy frequency (Figure 2.14), calculated from each density profile from equation 2, and averaged over the water column. It is immediately clear that the maximum BBL thickness is strongly modulated by the density stratification. High values of N, and therefore strong stratification suppress mixing and result in low or absent BBLs. On the other hand, when values of N are low, and stratification is weak, the BBL reaches its maximum thicknesses. However, weak stratification does not dictate the presence of a BBL, with low or zero mixed layer heights often associated with low values of N. Evidently then, while the strength of stratification may limit the vertical extend of the bottom mixed layer, it is not the only modulating factor, and a turbulence generating mechanism must also play a role (Dade et al., 2001).

It is possible to extract from the calculations in Section 2.3.1, the annual mean distribution of γ/c on the SHBML (Figure 2.15). γ/c is very low over the entire continental shelf, and

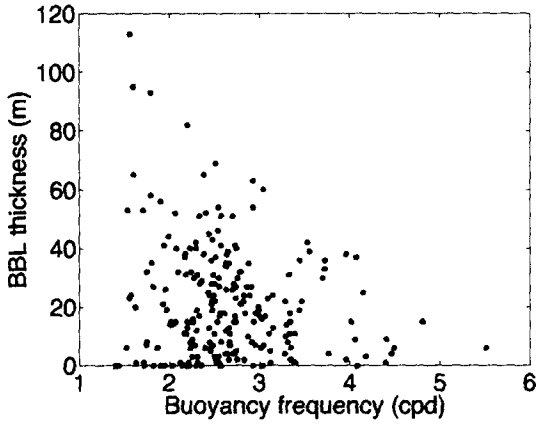

Figure 2.14: BBL thickness vs buoyancy frequency averaged over the water column. Data from Station 12 were not included.

then leaps to 0.6 at Station 11 (16.6°E) on the upper continental slope. Considering that it is a mean, this value is close to the critical angle which would bottom trap semi-diurnal internal tide energy and enhance bottom velocities and turbulent mixing, as discussed. Thus it seems that internal tides maybe the sought turbulence generating mechanism which is responsible for the increased variability of BBL thickness over the upper continental slope. Certainly, the internal tide mechanism has been identified previously as an agent of bottom mixing, and bottom nepheloid layer generation (Cacchione and Drake, 1986; Johnson et al., 2001; McPhee-Shaw and Kunze, 2002). Internal waves which propagate onto the shelf may likewise help to sustain a bottom mixed layer there, although near bottom currents, which are considered next, would certainly also play a role (Dade et al., 2001; Thomsen, 2002).

2.3.2.2 Lateral advection in the BBL

It was shown in the preceding Section that the BBL is a nearly perennial feature of the southern Benguela continental shelf and slope. Also, it has been considered that approaching the bottom, flow tends to veer cyclonically in the bottom Ekman layer due to the rotation of the earth (Gill, 1982; Pond and Pickard, 1983; Trowbridge et al., 1998; Dade et al., 2001; Thomsen, 2002). Thus in the southern Benguela, where the near bottom flow over much of the shelf and slope is characterized by the poleward undercurrent (Nelson and Polito, 1987; Nelson, 1989; Shannon and Nelson, 1996; Shillington, 1998), cyclonic veering would lead to

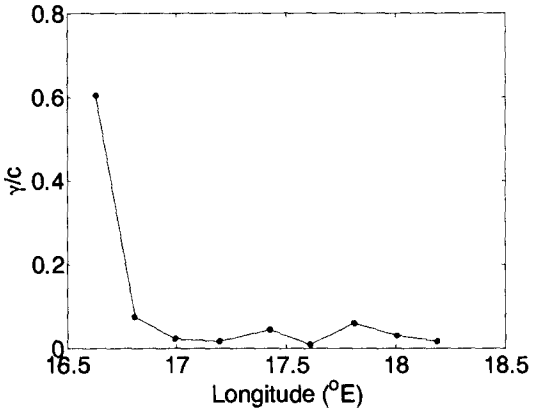

Figure 2.15: Cross shelf distribution of mean for all available data γ/c for semi-diurnal tidal frequencies The dots mark Station positions on the SHBML, and only Station 3 (18.2°E) to 11 (16.6°E) are shown. The γ/c is very low over the entire continental shelf, and then jumps to close to the critical angle over the upper continental slope (16.6°E; Station 11). This suggests that internal tides may become bottom trapped on the upper slope, which would lead to enhanced bottom velocities and energy dissipation.

off-shelf lateral transport in the bottom Ekman layer. The nature of the flow in the BBL can be directly considered by examining Recording Current Meter records collected near the bottom of the water column. The progressive vector diagrams (p.v.ds) for the records, and the Fourier analyses of the u components of the flow are provided in Figure 2.17. The positions of the seven records considered here are shown in Figure 2.16, and the sampling details are given in Table 2.1. While some of the p.v.ds have been rotated to align with the local isobaths, the positive alongshore direction is very roughly north, and the positive cross shelf direction is roughly east (onshore). It should be noted, that the bottom depths quoted were not available directly from the RCM data, but were extracted from the ETOPO2 data set based on mooring location, and maybe incorrect by tens of meters. Nonetheless, the quoted depths provide the best estimate available.

The RCM at mooring a, near mid-shelf, was positioned approximately 20 meters off the bottom (m.o.b.) and sampled for almost 2 months during winter. The beginning of the record (position 0,0 on the progressive vector diagram) exhibits low velocities and oscillatory motions. Subsequently, the flow was solely northwards, with a distinctly onshore component, as would be expected from cyclonic Ekman veering near the bottom. The Fourier analysis reveals that energy was concentrated at tidal (1 and 2 cpd) and inertial (1.07 cpd) frequencies,

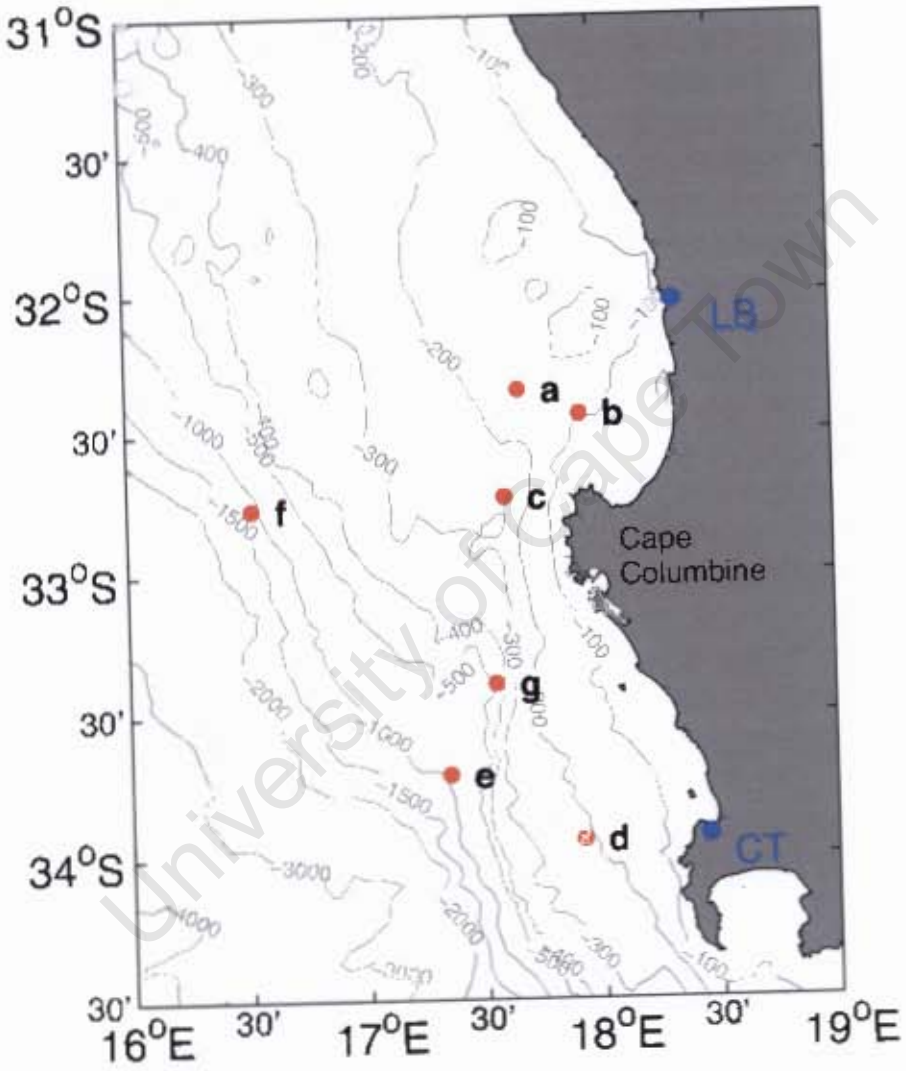

Figure 2.16: Recording current meter positions

with a prominent low frequency component (<0.3 cpd), corresponding to a period of 3-5 days. The latter is the time period associated with reversals caused by the passage of coastal trapped waves (CTWs) (Nelson and Polito, 1987; Nelson, 1989). The RCM 20 m.o.b. at mooring position b, collected during spring/summer, shows a remarkably different flow pattern, despite its proximity to mooring a. The vast majority of the 67 day record is dominated by a strong south westward flow, with several periods of clear acceleration in the velocities. Small reversals are also evident at the very start and end of the record. While the energy spectrum is dominated by very low frequencies (0.04 cpd ~17 day period), coastal trapped waves (0.17 -0.3 cpd, corresponding to periods 5-3 days) and tidal (1 and 2 cpd) signals were still marked in the record. The off-shelf component to the flow is exactly what would be expected for a poleward current, and this record highlights the potential for lateral advection in the BBL. Indeed, in this particular case, cross shelf flow exceeded along-shelf flow, covering a distance of 558 km in 67 days, at an average cross shelf velocity of 0.09 $m.s^{-1}$.

Moving south, directly off Cape Columbine, we examine the RCM about 20 m.o.b. at mooring location c. The nearly three month summer record begins with a period of low velocities and evident reversals. There is a subsequent period of pronounced north-easterly flow (rotation is 0 for this record), followed by a stagnation in the current. Once velocities increase again, movement is almost exclusively due south. The Fourier analysis shows that the majority of energy is concentrated in the very low frequency band, corresponding to a period of weeks, followed by a ~6 day period (0.15 cpd), likely linked to CTWs, and a fairly evident semi-diurnal signal. The isobaths in this region (Figure 2.16) certainly those to the south, are orientated nearly N-S, and are perhaps constraining the flow to the along-shelf direction. Being summer, it is also tempting to speculate that the ~4 period of onshore flow near the beginning of the record corresponds to an upwelling event. This is not unlikely given that upwelling typically occurs from between 200-300 m, and the fact that Cape Columbine is an upwelling cell (Shannon, 1985). It should be noted that this record comes from a long-term mooring position off Cape Columbine, and that in fact, many of the other records, at

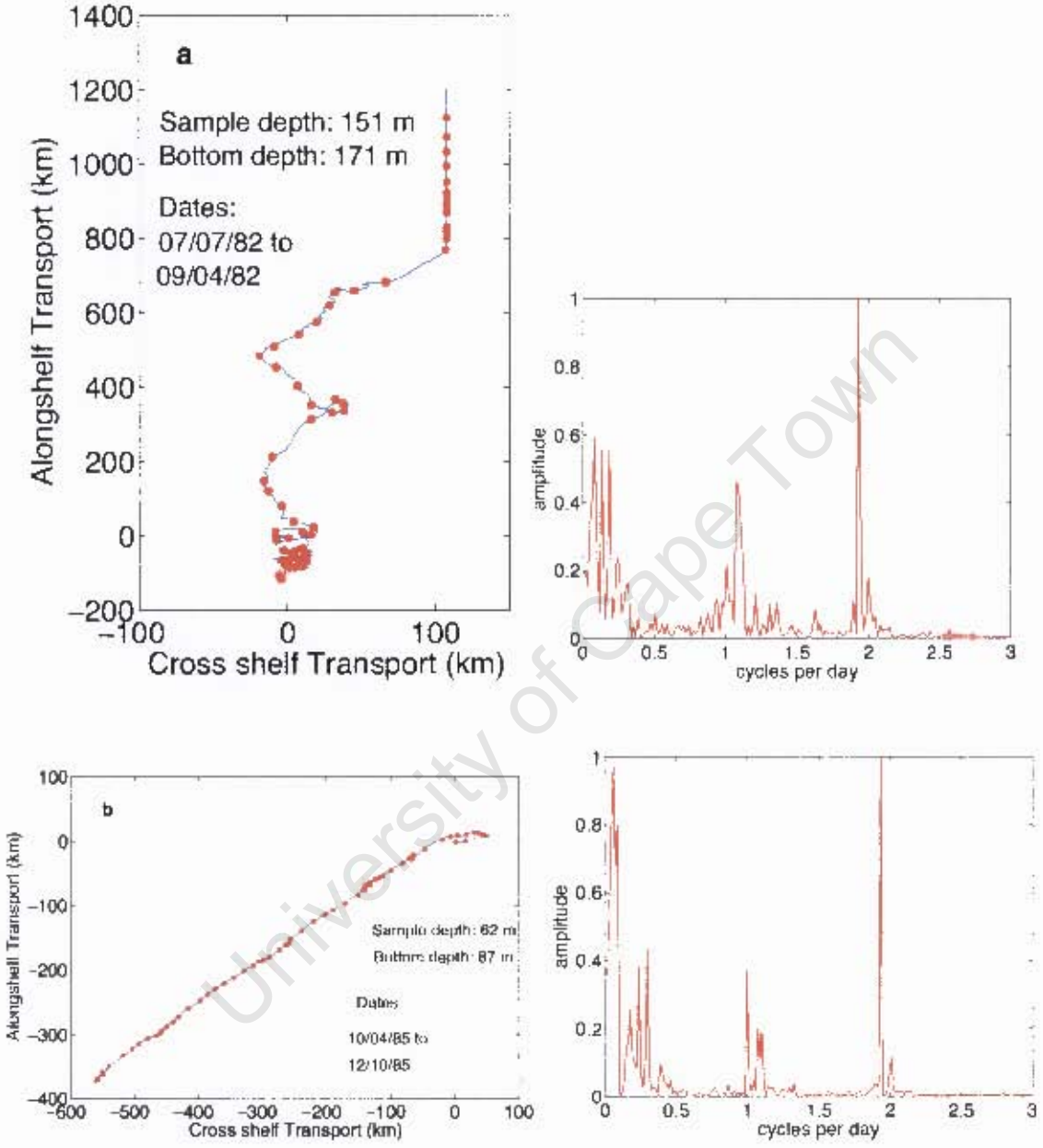

Figure 2.17: Progressive vector diagrams and Fourier analyses of Recording Current Meters at various positions in the southern Benguela.

Fourier transformations were performed on the v component of the flow only. Certain of the RCM records were rotated by up to 35° to align with the local isobaths. Roughly speaking though, the positive alongshore direction is north, and the positive cross-shore direction is east (onshore). See Table 2.1 for details. The locations of the RCMs is given in Figure 2.16.

shallower depths, exhibit a marked off-shelf flow component.

The short, 22 day current record at location d, produced an interesting result. For the first 16 days of the record, flow is predominantly directed in the negative alongshore direction with an off-shelf component, with the exception of the first 4 days. The off-shelf component is an expected consequence of Ekman veering under poleward flow regimes, but this does not explain why the current continues to move offshore after the reversal to equatorward flow on the 19th day. The lower frequency component of the flow seems to be dominated by a typical CTW frequency range of 3-6 days (0.35 and 0.17 cpd), but the overwhelming signal in the Fourier analysis appears near the semi-diurnal frequency. Perhaps at this location, a large amount of energy is contained in semi-diurnal baroclinic internal tides, as was seen earlier at location g. In the absence of a second RCM on the mooring, this is however impossible to quantify.

The final two RCMs of interest come from moorings on the upper continental slope, near the 1000 m isobath. Mooring e was positioned directly within the Cape Canyon, and the RCM collected a 5 month record over winter, perhaps as much as 100 m.o.b.. The progressive vector diagram shows a continuous flow, which is directed down the axis of the canyon. Due to the length of the record, brief periodic reversals which did occur are hidden. Nonetheless, water seems to barrel down the canyon, leading to a significant off-shelf transport, with a corresponding average off-shelf velocity of 0.04 $m.s^{-1}$. There is little to no tidal signal in the RCM record, whose energy is centered almost normally around a frequency of 0.3 cpd or a 3 day period. This corresponds to previous observations that the poleward undercurrent in the region is modulated by CTW activity (Nelson and Polito, 1987; Nelson, 1989). Furthermore it can be noted that the record shown in Section 2.3.1 for mooring g, also in the Cape Canyon, but collected during summer, showed a pronounced down canyon flow near the bottom.

Thus it appears on the basis of these records, and others not shown, that flow is perennially directed down the axis of the Cape Canyon. This nullifies the hypothesis that the Cape Canyon enhances upwelling at Cape Columbine, by making central waters available close to the coast (Shannon, 1985). More significantly however, it highlights the potential role of the

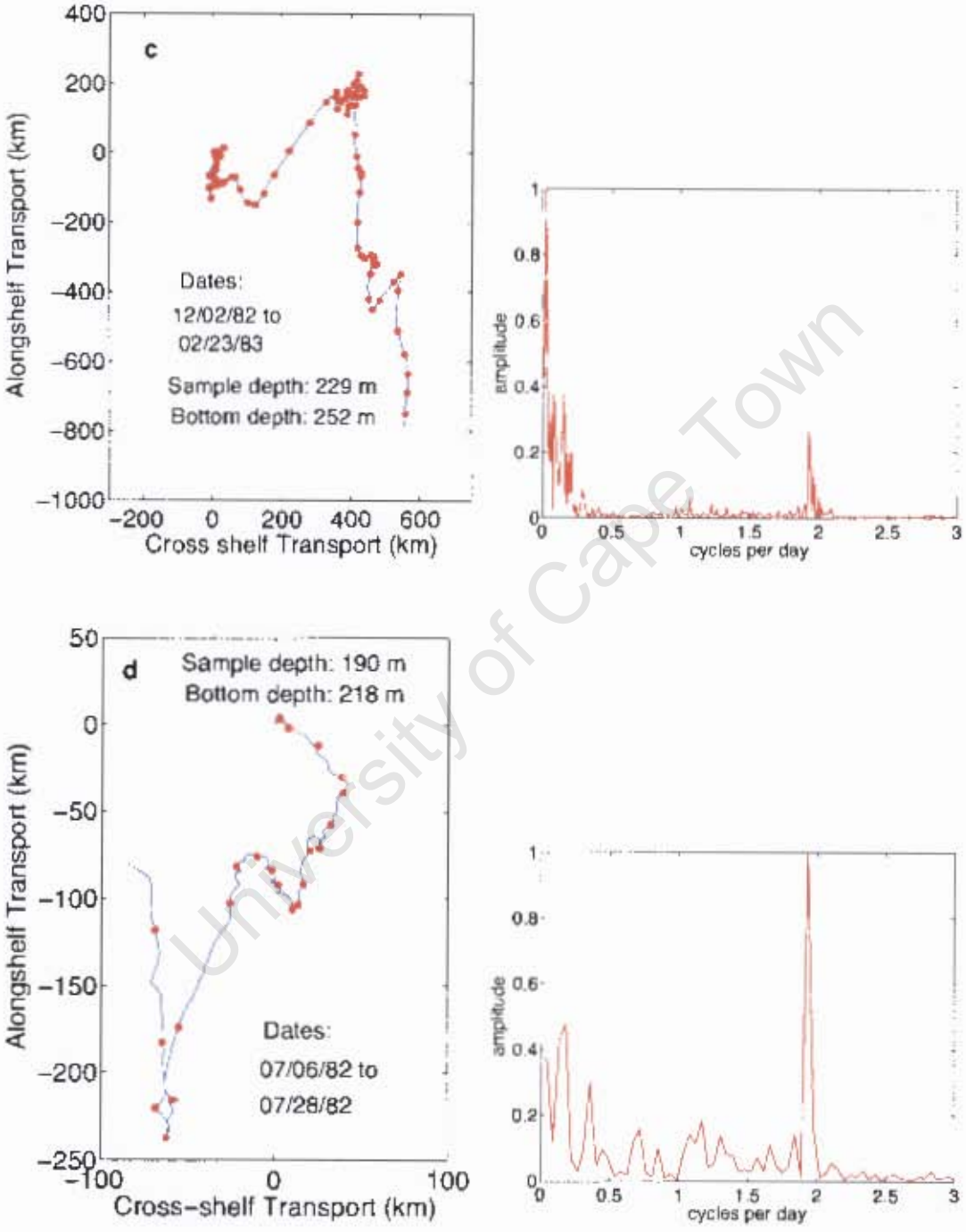

Figure 2.17 continued

canyon as a conduit for shelf-ocean exchange, and a potential site for the seaward export of biogeochemical constituents from the highly productive St Helena Bay region (Brown et al., 1991). The elevated importance of canyons for such types of lateral exchanges is expected both as a consequence of theory (Brink, 1998; Trowbridge et al., 1998), and previous observations (Thomsen and van Weering, 1998; van Weering et al., 2002).

The upper slope site at mooring f, to the north, provided a RCM record over nearly three months during spring, which fits neatly into expectations of a bottom Ekman layer. Flow in the first third of the record was in the negative alongshore direction, and off shelf, with relatively high velocities. The flow reversal and subsequent on-shelf component to the flow in the second third of the record also fits the paradigm of bottom Ekman veering. The final third of the record, when flow is in the negative alongshore direction, and onshore, is somewhat of a mystery. It can be noted though that during this final period, propagation was much slower, perhaps reducing the influence of bottom friction (Dade et al., 2001). The flow here appears to have been modulated almost exclusively by very low frequency forcing, with only a hint of tidal activity at semi-diurnal frequencies and marginal energy at diurnal and inertial periods. While along-shore propagation dominated this record, the interesting feature is the off-shelf component of the flow which occurred during the accelerated poleward motion during the first 24 days.

Several of the records presented here show that cross shelf advection is as important as along-shelf advection in the BBL, demonstrating that the constraint of the Taylor-Proudman theorem can be broken in the presence of bottom friction (Brink, 1998; Trowbridge et al., 1998). On the whole then, despite some noted exceptions, the BBL appears to be a conduit for cross-shelf exchange in the southern Benguela, owing to the cyclonic Ekman veering of the poleward undercurrent. Similar conclusions have also been reached on other continental margins (e.g. Lentz and Trowbridge, 1991), where lateral advection in the BBL has been identified as a mechanism capable of transporting organic carbon and other biogeochemically important tracers into the deep ocean (Thomsen and van Weering, 1998; Thomsen, 1999; van Weering et al., 2001; Thomsen, 2002; van Weering et al., 2002).

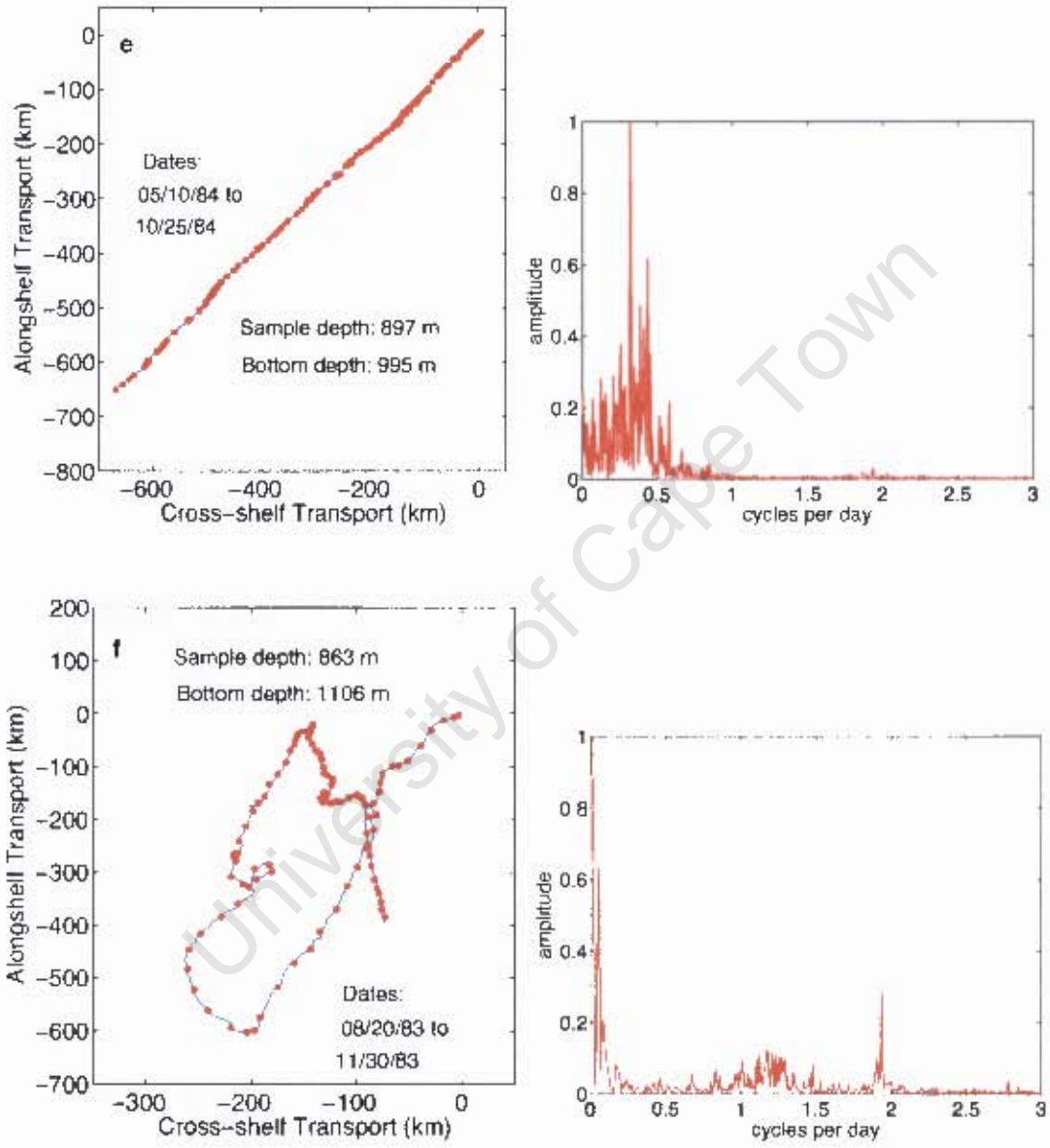

Figure 2.17 continued

2.4 Summary and conclusions

In most coastal systems, along-shelf length scales dominate cross-shelf length scales, and consideration of the equations of motion suggests that along-shelf flows should be prevalent, and shelf-ocean exchange minimal. However under certain specific conditions, the geostrophic approximation breaks down, and cross-shelf flows can become important. This happens particularly when bathymetric features such as canyons create dominant along shelf length scales, under the influence of strong shears and baroclinicity, in regions near the surface and bottom of the water column where frictional effects become important, and when time-dependent flows such as tides and coastal trapped waves are important. In the southern Benguela it was recognized that the bottom boundary layer may play an enhanced role in cross-shelf exchanges through the cyclonic Ekman veering of the flow under the influence of bottom friction. Density profiles from historic CTD data revealed that BBLs were perennial features of the southern Benguela shelf, with a typical thickness of 20 m, and an enhanced variability over the continental slope. The thickness of the BBL was modulated by the stability of the water column, together with the presence of turbulence generating mechanisms. As expected, flow within the BBL was found to have a significant off-shelf component during poleward flow regimes, although exceptions did occur. The forcing mechanisms controlling the off-shelf advection in the BBL varied with location, but many of the records contained noticeable signals at frequencies associated with coastal trapped waves.

This was particularly the case in the Cape Canyon, where the flow was found to propagate down the canyon axis at all times of the year, leading to a significant shelf-ocean exchange. At least one portion of the canyon also exhibited pronounced flows associated with baroclinic internal tides. The internal tides there were asymmetric and lead to a net off-shelf advection. Indeed, internal tides were also shown to occur on the inner Benguela shelf, where they are thought to be important for bottom mixing. Calculating the angle of semi-diurnal internal tide propagation and comparing it to the bathymetry of the southern Benguela revealed that internal tide energy would be preferentially dissipated on the upper continental slope. In this region, the internal tide may become bottom trapped, and dissipate its energy through

Record	Longitude ($°E$)	Latitude ($°S$)	Bottom Depth* (m)	Sample Depth (m)	Sampling frequency (min)	Record length (days)	Rotation (°)
a	17.670	32.350	171	151	15	59	0
b	17.928	32.438	87	62	30	67	0
c	17.603	32.730	252	229	15	82	0
d	17.913	33.945	218	190	15	22	30
e	17.350	33.712	995	897	60	167	35
f	16.528	32.767	1106	863	15	102	35
g	17.552	33.392	457	380	30	12	0
g	17.552	33.392	457	199	30	12	0
g	17.552	33.392	457	118	30	12	0
g	17.552	33.392	457	77	30	12	0

Table 2.1: Details of the Recording Current Meters used in this study.

*Bottom depths were not available with the RCM records, and have therefore been taken here as the bathymetry value in the ETOPO2 data set for the RCM position. They are thus crude estimates.

turbulent mixing, with large implications for the generation of bottom nepheloid layers and off-shelf advection of particulate matter. On the whole, what this Chapter has demonstrated is that physical mechanisms exist in the dynamic southern Benguela which have the ability to form bottom nepheloid layers, and to advect material seaward near the bottom of the water column. Thus, the potential exists for a near bottom lateral carbon flux from the shelf to the open ocean. The biogeochemical setting of the southern Benguela continental shelf and slope is considered next, and is followed by a consideration of bottom nepheloid layers and a quantification of the lateral carbon flux in Chapter 4.

Chapter 3

Biogeochemical characteristics of the water column in the southern Benguela

3.1 Introduction

Continental margins play a significant role in global biogeochemical cycles (see chapter 1 for a full discussion Walsh et al., 1981; Walsh, 1991; Bauer and Druffel, 1998; Wollast, 1998; Verity et al., 2002). They are responsible for a disproportionally large fraction of total primary production, organic matter burial, fish production, and are associated with prominent oxygen minimum zones where denitrification, anammox and other important alterations of biogeochemical constituents can occur (Walsh et al., 1981; Walsh, 1991; Wollast, 1998; Rullkötter, 2000; Chen et al., 2003; Falkowski et al., 2003). Eastern boundary currents in particular are known to have intense biogeochemical processes. Of these, the Benguela upwelling system sticks out as having one of the highest productivity's (Brown et al., 1991; Carr, 2002), rates of biogeochemical alteration (Tyrrell and Lucas, 2002; Kuypers et al., 2005), and as being the only eastern boundary current directly influenced by a warm water western boundary current on its poleward edge (see chapter 1 for a full review; Shillington, 1998). The high new production (Waldron et al., 1997), and ostensibly low heterotrophic consumption (Brown and Hutchings, 1987; Verheye, 1991; Field and Shillington, 2004) in the southern Benguela have

furthermore led to the proposition that it could be a significant source of organic carbon to the deep ocean (Rowe, 1987; Waldron et al., 1997; Swart et al., 2007). Here, hydrographic variables, organic matter, oxygen and nutrient concentrations are reported for three cruises on the southern Benguela continental shelf and slope. The seasonality, distribution and significance of organic matter and biogeochemical processes in the system is then considered with reference to global biogeochemical cycles. In particular, we provide to the best of our knowledge the first reliable HTC DOC measurements in the southern Benguela, in an attempt to address this identified gap in our understanding of the system (Monteiro, 1996; Touratier et al., 2003).

3.2 Data and methods

Hydrographic and biogeochemical data were collected during 3 cruises of the *RV Africana* on the St Helena Bay Monitoring Line off the west coast of South Africa (Figure 3.1). The line stretched from Station 3 near the coast, in approximately 75 m of water, to Station 12 on the upper continental slope, around 90 Nautical miles (Nm) offshore, in a water depth of around 1400 m. Station spacing was nominally 10 Nm, and the line was completed within 24 hours on all three occasions. The cruises were conducted in late austral summer (14 March), and winter (28 June, 2 August) of 2006. At each Station the Seabird electronics CTD was lowered to within 5 m of the bottom. Fluorescence and turbidity (optical backscatter) data were collected with a Chelsea Instruments fluorometer onboard the CTD. One Niskin bottle was fired at the maximum depth, and the remaining bottle samples were spaced throughout the water column, with a bias in density towards the surface. Water samples were collected from each bottle, frozen, and taken ashore for SiO_2, NO_3, NO_2 and PO_4 determinations on an auto-analyser at Marine and Coastal Management, South Africa. Between 0.5 and 3 l of sample water were drawn from selected Niskin bottles into acid washed and Milli-q rinsed glass Schott bottles, depending on the Station and depth. Predominantly following JGOFS protocols (JGOFS, 1994), the samples were vacuum filtered, at less than 10 inches mercury,

through pre-combusted 47 mm Whatmann GFFs. The filter papers were then folded in half, foil wrapped, and frozen at -80°C until later analysis in the lab ashore. Once ashore, the GFFs were thawed, oven dried and fumed overnight with HCl to remove any inorganic carbon and then re-dried. The filters were subsequently divided into quarters using stainless steel scissors, and packed into tin capsules. Prepared samples were then combusted in a Carlo-Erba CHN analyser, and fed directly into a isotope ratio mass spectrometer (IRMS) for $\delta^{13}C$ and $\delta^{15}N$ determination. The $\delta^{13}C$ and $\delta^{15}N$ ratios were determined from the instrument response to the sample, and they were subsequently blank corrected through mass balance (Hayes, 1982). POC and PON were determined from the blank corrected instrument response to the sample, in relation to a known standard, divided by one quarter of the filtered volume (Zimmerman et al., 1997).

During the winter cruises, additional samples were drawn from selected depths into pre-combusted borosillicate vials (with acid washed lids) for DOC and total nitrogen (TN) determination. Immediately after collection DOC samples were acidified with 2 drops of trace metal grade HCl, and stored at room temperature until analysis. The samples were run against deep water and recognized laboratory standards on a Shimadzu DOC analyser with attached TN determination, according to the methods of (Sharp et al., 1995, 2002). For comparative purposes, DOC and TN data from the central South Atlantic (32-34°S, 25°W), collected on the A16 line in February 2005, and analysed by the Hansell lab at RSMAS, were obtained (http://www.rsmas.miami.edu/groups/biogeochem/index.html).

Wind data for the periods surrounding the cruises were obtained for the Lambert's Bay Nortier Station, about 3 km directly inland of the coast, courtesy of the South African Weather Service. Predicted hourly tidal heights for the same periods were obtained from the tide Tables published by the Hydrographer of the South African navy, for Saldanha Bay, just south of the SHBML.

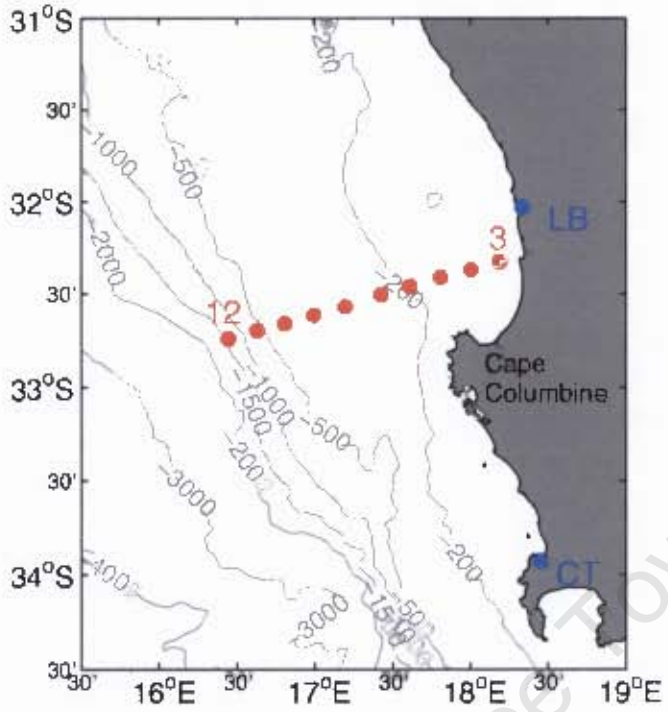

Figure 3.1: The positions of St Helena Bay Monitoring Line Stations 3-12 off the west coast of South Africa. Station 3 is in 75 m of water, Station 12 is approximately 90 NM offshore on the upper slope, in a water depth of 1400 m. The positions of Lambert's Bay (LB) and Cape Town (CT) are marked in blue. The local bathymetry is shown for reference.

3.3 Results

3.3.1 March 2006

3.3.1.1 Physical setting and continuous CTD data

The two weeks preceding the March SHBML were dominated by northerly winds of between 4 and 6 $m.s^{-1}$ (Figure 3.2), besides for a weak south westerly excursion on the day before the cruise. During the cruise, winds were NW at about 5 $m.s^{-1}$. Thus predominantly downwelling conditions would be expected in the water column. At the time of the cruise, which took place just two days before the spring tide, the predominantly semi-diurnal tidal range was $\approx$1.3 m.

The water column was stably stratified in mid-March, with the isopycnals sloping up towards the coastline (Figure 3.3). Temperatures were warm offshore near the surface, where salinities

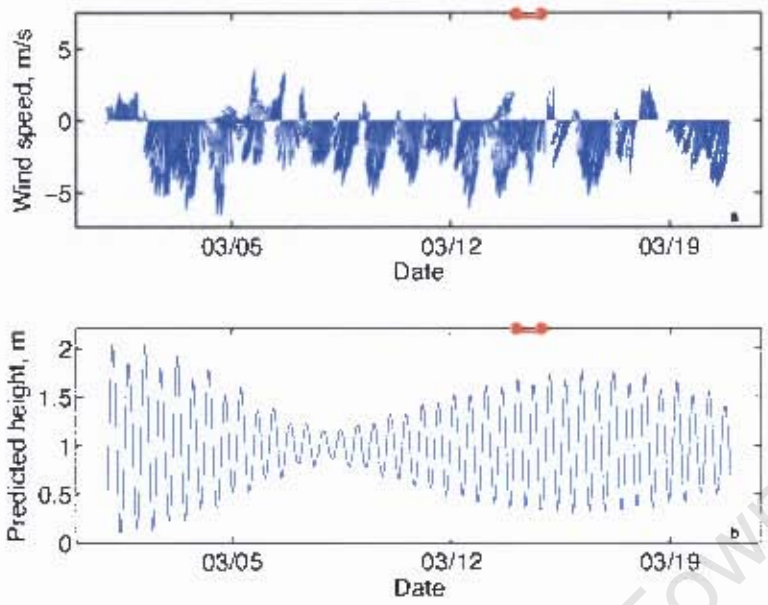

Figure 3.2: **a** Wind velocity at Lambert's Bay (+ve velocities are northwards) and **b** Predicted hourly tidal heights for Saldanha Bay for February/March 2006. The red dots mark the date of the SHIML cruise on 14 March.

were also highest. Isotherms and isohalines sloped upwards towards the coast, confining cold, fresh waters to the bottom over the shelf. Oxygen concentrations were super-saturated (>5.5 $ml.l^{-1}$) close to the surface over much of the shelf, while low oxygen conditions (<2 $ml.l^{-1}$) were present inshore near the bottom. Chlorophyll fluorescence was high (>1) in the upper 50 m over the whole shelf, and decreased over the slope, reflecting the distribution of phytoplankton. Below 50 m, fluorescence values were very close to zero everywhere, besides for very close to the coast, where high values extended to the bottom. In general, fluorescence was higher on the shelf, and decreased over the continental slope, throughout the water column. The cross shelf turbidity distribution displayed an interesting pattern (Figure 3.3). Highest values ($\approx$1) were found in a surface nepheloid layer (SNL), confined to the upper 50 m, and corresponding to the phytoplankton standing stocks reflected in the fluorescence signal. The middle of the water column showed the lowest turbidity values, decreasing with distance across the shelf, with lowest values (<0.02) found over the upper continental slope throughout the upper and middle water column. A very clearly defined bottom nepheloid layer formed a secondary turbidity maximum, and stretched over the entire shelf and upper

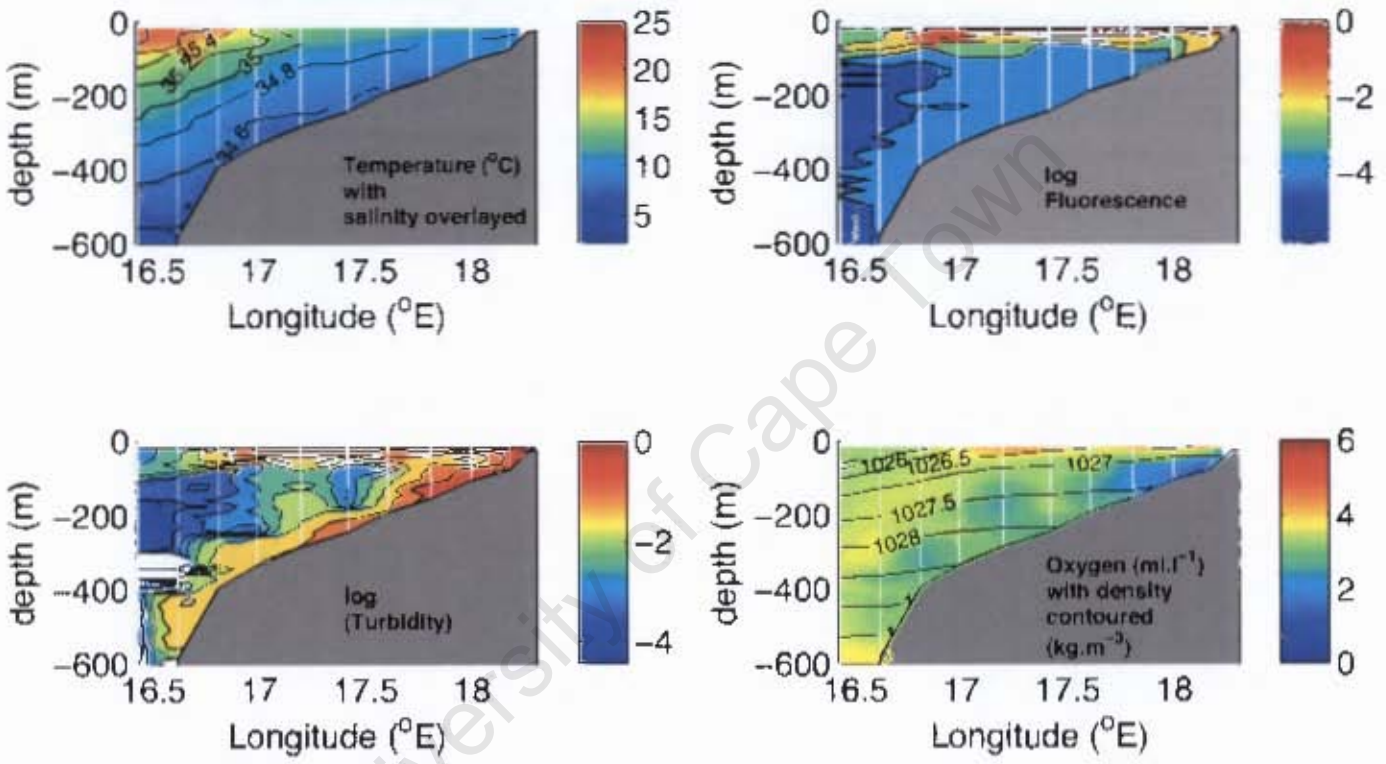

Figure 3.3: Continuous CTD data of Oxygen, overlayed with density, fluorescence and turbidity on the SHBML for March 2006.

Fluorescence and turbidity data are contoured on a log scale. Vertical white lines are Station positions. Features to note are the low oxygen conditions developing inshore, near the bottom; the surface fluorescence maximum and the turbidity maxima clearly demarcating a surface nepheloid layer and a bottom nepheloid layer which extend of the entire shelf and upper slope.

slope, decreasing in intensity with distance from the coast. The BNL was over 100 m thick, and was more pronounced than the SNL over the outer shelf and slope.

3.3.1.2 Nutrient distributions and processes

The silicate, phosphate and nitrate distributions all exhibited a general minimum at the surface due to biological utilization, although surface concentrations were not fully depleted. The highest values occurred near the bottom over the shelf (Figure 3.4). Highest silicate (>30 μM) and phosphate (>2 μM) concentrations were found inshore near the bottom, presumably corresponding to *in situ* nutrient regeneration, while nitrate concentrations were consistently high in the lower water column (>20 μM) across the shelf. Nitrite concentrations were highest near the surface, but showed secondary maxima inner and mid shelf near the bottom.

The parameter N* is a quasi-conservative tracer which linearly combines nitrogen and phosphate, and whose variability reflects the processes of denitrification and nitrogen fixation (Gruber and Sarmiento, 1997). It is defined here as N*= $N - 16P$, where N is nitrogen ($NO_3 + NO_2$), P is phosphate, and 16 represents the Redfield ratio of N:P (Gruber and Sarmiento, 1997). Since organic matter synthesis and remineralization occur according to Redfield stoichiometry, they do not influence the variability of N*. On the other hand, denitrification proceeds with a N:P of ≈-104:1, and thus produces negative departures in the values of N* (Gruber and Sarmiento, 1997). The bottom panel of Figure 3.4 shows that N* is negative everywhere in the water column over the SHBML, but that the lowest values (<-20) occur inshore near the bottom. Comparison with Figure 3.3 shows that the lowest values of N* correspond to the region of greatest oxygen depletion. The relationship between NO_3 and PO_4 (Figure 3.5) for the March data reveals that at high PO_4 concentrations (>2 μM) there is less nitrogen present than would be expected from Redfield stoichiometry, as shown by the dashed line. This ≈10-45 μM nitrogen deficit, as represented by N*, can also be seen to be negatively correlated with nitrite concentrations, with highest NO_2 values corresponding to the lowest values of N* (Figure3.5). This correlation is statistically significant at the 1% level (R^2=0.52).

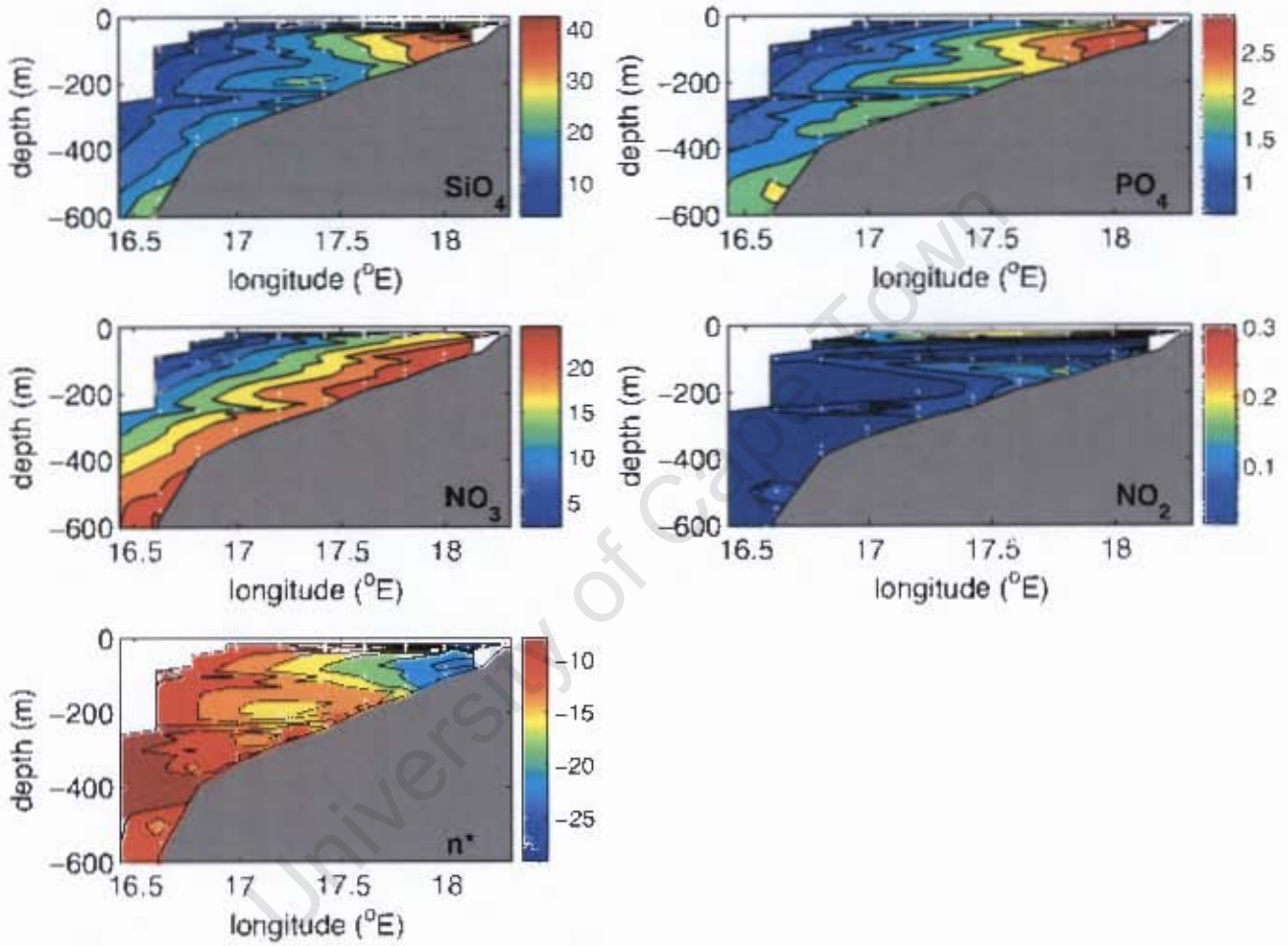

Figure 3.4: Nutrients concentrations in μM on the SHBML in March 2006.

White dots mark the positions of bottle samples. N* is calculated a $NO_3 + NO_2 - 16PO_4$ and is an indicator of denitrification (see text for details).

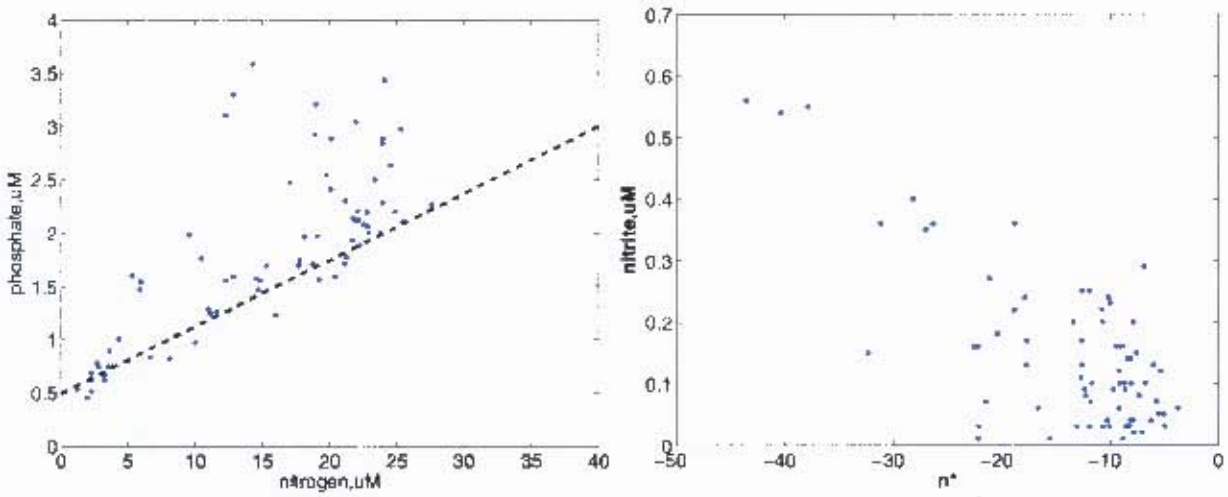

Figure 3.5: Indicators of denitrification during March 2006.

PO_4 vs. Nitrogen (NO_3+NO_2) (left). The dashed line indicates the theoretical 'Redfield ratio' of N:P=16:1, with a non-zero intercept. At high PO_4 concentrations (>2.5 μM), less nitrogen is present than expected, indicating that denitrification maybe occurring in the system. The right panel shows nitrate against the quasi-conservative tracer N*. Low values of N* are associated with high concentrations of nitrite, which suggests that denitrification is occurring. The negative correlation between NO_2 and N* during March 2006 is statistically significant (R^2=0.52; p<0.01).

3.3.1.3 Particulate Organic Matter characteristics

Particulate organic carbon was concentrated in the 50 m thick surface nepheloid layer where concentrations exceeded 650 $\mu g.l^{-1}$ over the inner and middle shelf (Figure 3.6). This confirms that the fluorescence signal was reflecting biological matter in the water column. POC exhibited another maximum near the bottom in the region around the shelf-slope break, where concentrations were in excess of 200 $\mu g.l^{-1}$. In the remainder of the water column concentrations were generally $<<100$ $\mu g.l^{-1}$, except in an intermediate layer near 120 m, which stretched across the shelf. The minima POC concentrations (<60 $\mu g.l^{-1}$) occurred in the subsurface waters offshore at Station 12.

The range of $\delta^{13}C$ values for POM during the March SHBML are consistent with those for marine phytoplankton (Rullkötter, 2000). Values were enriched (>-22‰) in a surface layer <100 m thick, stretching across most of the shelf. This corresponds to the layer of high POC, and thus likely reflects the decreasing discrimination of the plankton against the heavy isotope during vigorous photosynthesis and resulting DIC uptake. Enriched $\delta^{13}C$ values in the 100-150 m thick bottom layer are likely on the other-hand to represent the preferential

oxidation of the light carbon fraction by bacteria. The central water column, and region offshore of the shelf break are comparatively depleted in $\delta^{13}C$, reaching values as low as -26‰ offshore at depth in the region of low POC. The C:N ratio is very close to the expected 6.6 in the surface high POC layer. In other regions, particularly mid-shelf near the bottom, and offshore of the shelf break, the ratio increases to over 10. This could reflect an enhanced state of degradation of the POM in these regions, since N is recycled more rapidly than C. However, it should be noted that in the regions of extremely low POM, particularly offshore, the concentrations of PON were approaching the instrument detection limit, and are therefore unreliable.

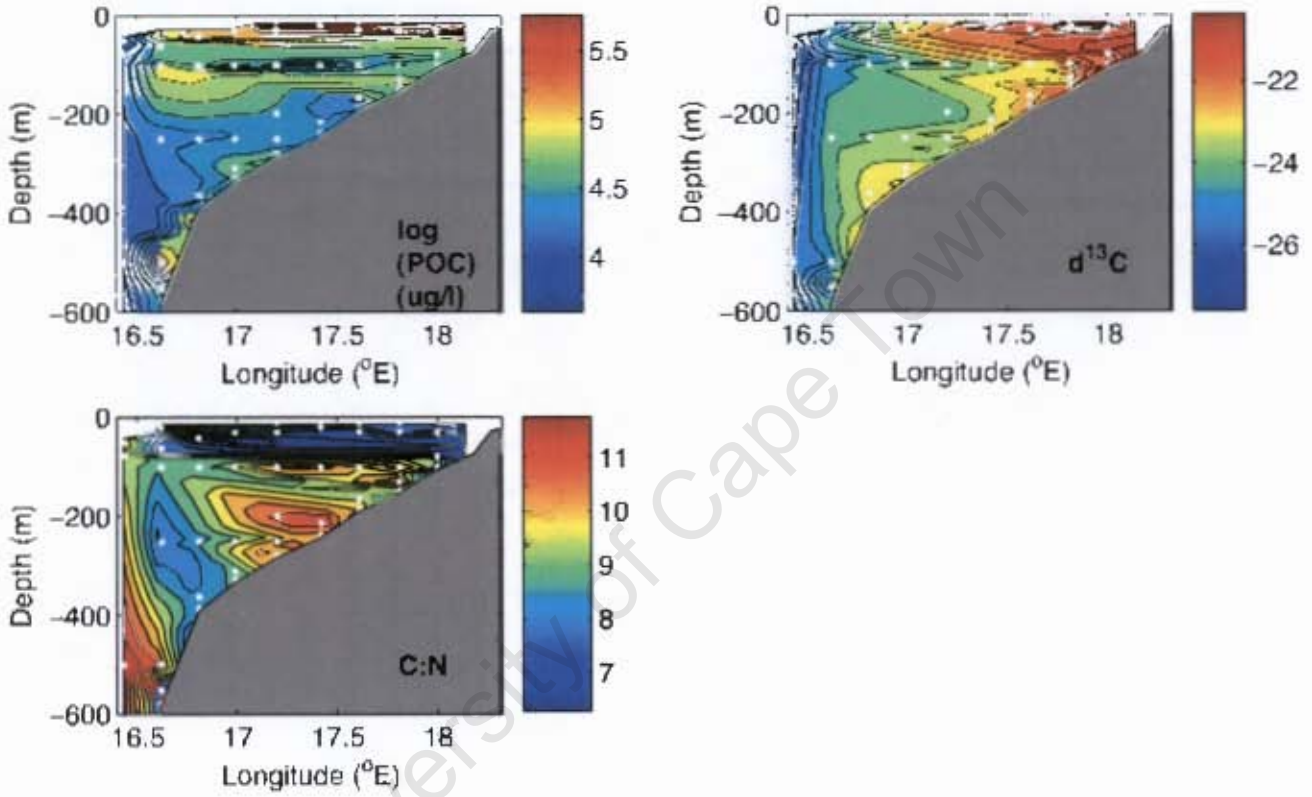

Figure 3.6: Characteristics of POM in the water column during the SHBML in March 2006.

POC is contoured on a log scale. White dots mark the positions of bottle samples. High POC concentrations are found near the surface, in a layer near 100 m, and at the bottom. Note the elevated POC concentrations near the bottom at the shelf break. $\delta^{13}C$ of POM showed enriched values near the surface, corresponding the high POC values, and primary production. Enriched values were also evident near the bottom, in a layer stretching across the shelf, and likely representative of decaying organic matter. Mid water column values were more negative, and all samples offshore of Station 11 were <26 ‰. C:N ratios were close to the expected Redfield ratio of 6.6 near the surface, but higher ratios were evident mid-shelf near the bottom, and offshore, although these could be biased.

3.3.2 June 2006

3.3.2.1 Physical setting and continuous CTD data

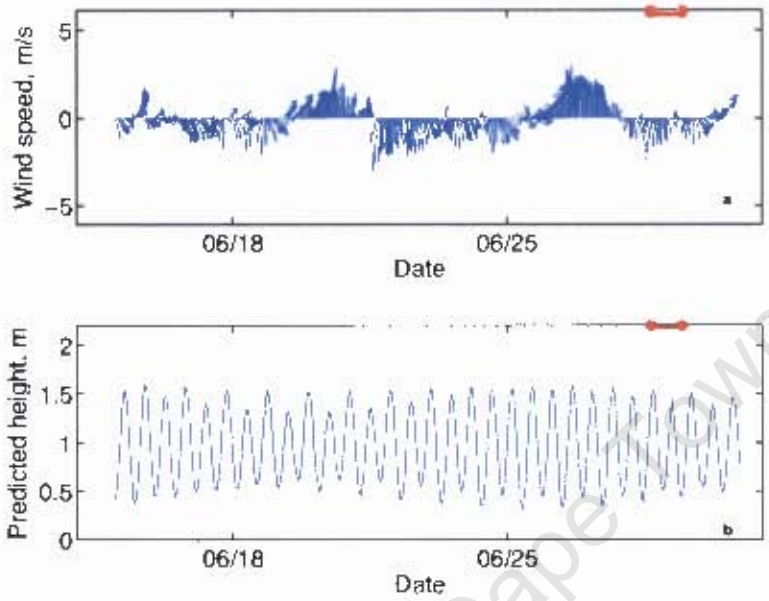

Figure 3.7: a Wind speed and direction at Lambert's Bay and b Predicted hourly tidal heights for Saldanha Bay for June 2006. The red dots mark the date of the SHBML cruise on 28 June.

For several days preceding the June SHBML, the winds blew from a southerly direction at about 3 $m.s^{-1}$. The cruise itself took place during light winds (2 $m.s^{-1}$), which had just switched to a northerly direction. Thus, despite being mid-winter, an upwelling type circulation pattern could have been set up by the preceding days southerlies, although its unlikely that any large scale upwelling would have occurred considering the low wind strength. The tidal cycle was advancing towards neap, and the tidal range at the time of the cruise was $\approx$1.0 m.

The isopycnals were generally fairly flat during the June 2006 SHBML (Figure 3.8), although a slight upturn of the 1027.5 surface near the bottom maybe indicative of the upwelling favourable windstress. An isolated patch of cold, fresh water was also evident inshore, at the bottom, perhaps a relict of the recent upwelling. Although on the whole the isohalines were nearly horizontal, they separated the cooler, fresher shelf water from the warmer, more saline surface water offshore. Oxygen concentrations were saturated everywhere in the upper 50

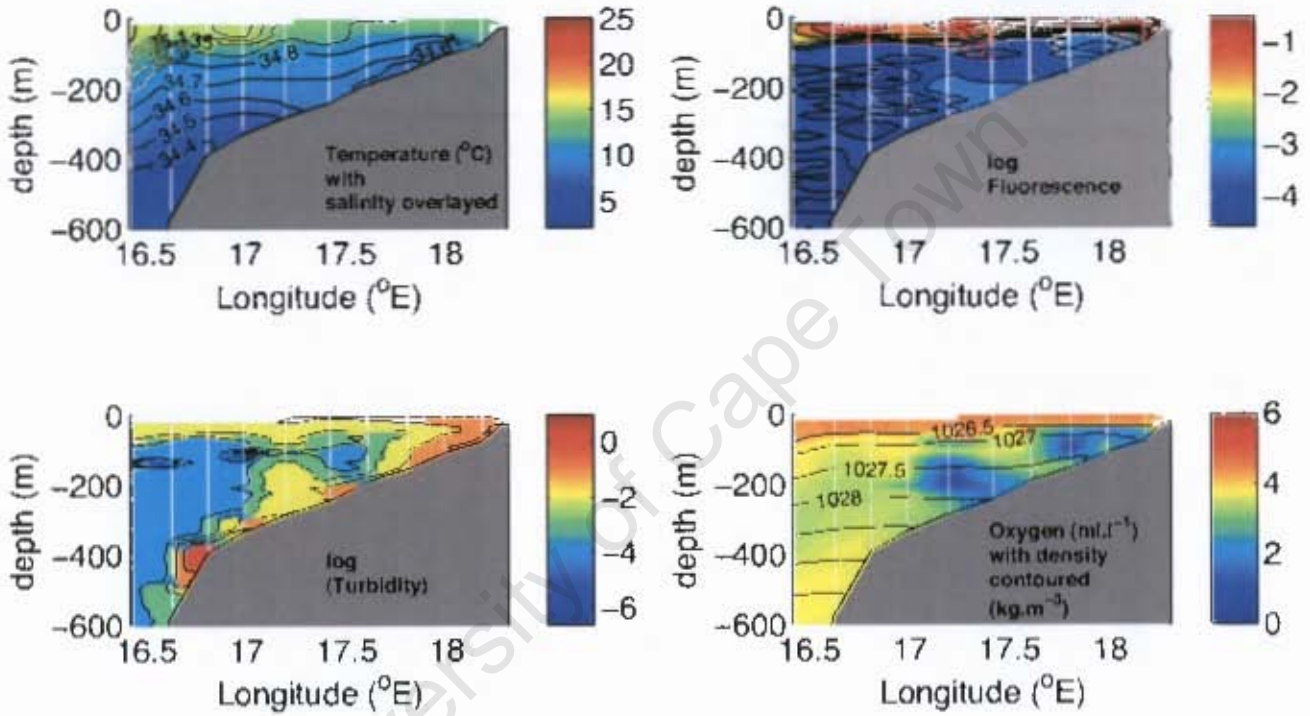

Figure 3.8: Continuous CTD data of Oxygen, overlayed with density; fluorescence and turbidity on the SHBML during June 2006. Fluorescence and turbidity data are contoured on a log scale. Vertical white lines are Station positions. Low oxygen waters are evident near the bottom mid-shelf, and close to the coast. Fluorescence is high in a ≈50 m thick layer near the surface, and very low throughout the rest of the water column. The turbidity data showed a mid-depth minimum separating a surface, and very well defined bottom nepheloid layers.

m, but displayed marked minima (<2 ml.l^{-1}) near the coast and mid-shelf, which extended up off the bottom. Fluorescence values were highest near the coast, in a surface layer 50 m thick, which extended across the shelf. Everywhere below this, fluorescence was nearly nil, besides for a slight local maximum, mid-shelf, in the region of the oxygen minimum. Lowest values occurred offshore, below 400 m. The turbidity distribution mirrored the fluorescence signal near the surface, but showed greatest values in a well developed BNL of approximately 50 m thick. Within the BNL, the maximum values (>2) occurred over the shelf break. On the outer-shelf ($\approx$ 17.2°E), a plume of high turbidity extended over 120 m upwards from the bottom - a feature also evident in the March distribution.

3.3.2.2 Nutrient distributions and processes

Nitrate, silicate and phosphate were all depleted to near zero in the surface layer during the June SHBML (Figure 3.9). All three nutrient distributions also exhibit tongues of high concentration extending from the ocean onto the shelf across the bottom - perhaps a reflection of the prevailing upwelling circulation pattern. Despite this, nutrient concentrations in the lower part of the water column were in all cases lower than in March. A region of elevated PO_4 concentrations is evident at the shelf break, overlying the turbidity maximum. A layer of elevated SiO_4 and PO_4 was also evident, extending seaward from the shelf at $\approx$ 18°E. Nitrite on the other hand was highest near the surface, and in a small region inshore near the bottom. The N* parameter was negative everywhere (Figure 3.9), but did not display a marked minimum as in March, although the lowest values occurred at the shelf break, mirroring the PO_4 distribution. The relation between PO_4 and nitrogen (Figure 3.10), did not reveal a significant deviation from expected Redfield stoichiometry, and nitrite showed no significant relation to N* or oxygen (not shown).

3.3.2.3 Particulate Organic Matter characteristics

There was significantly less POC in the water column during the June SHBML than in March. The 50 m thick surface layer, reached a maximum of 140 μg.l^{-1}, but more typically had a

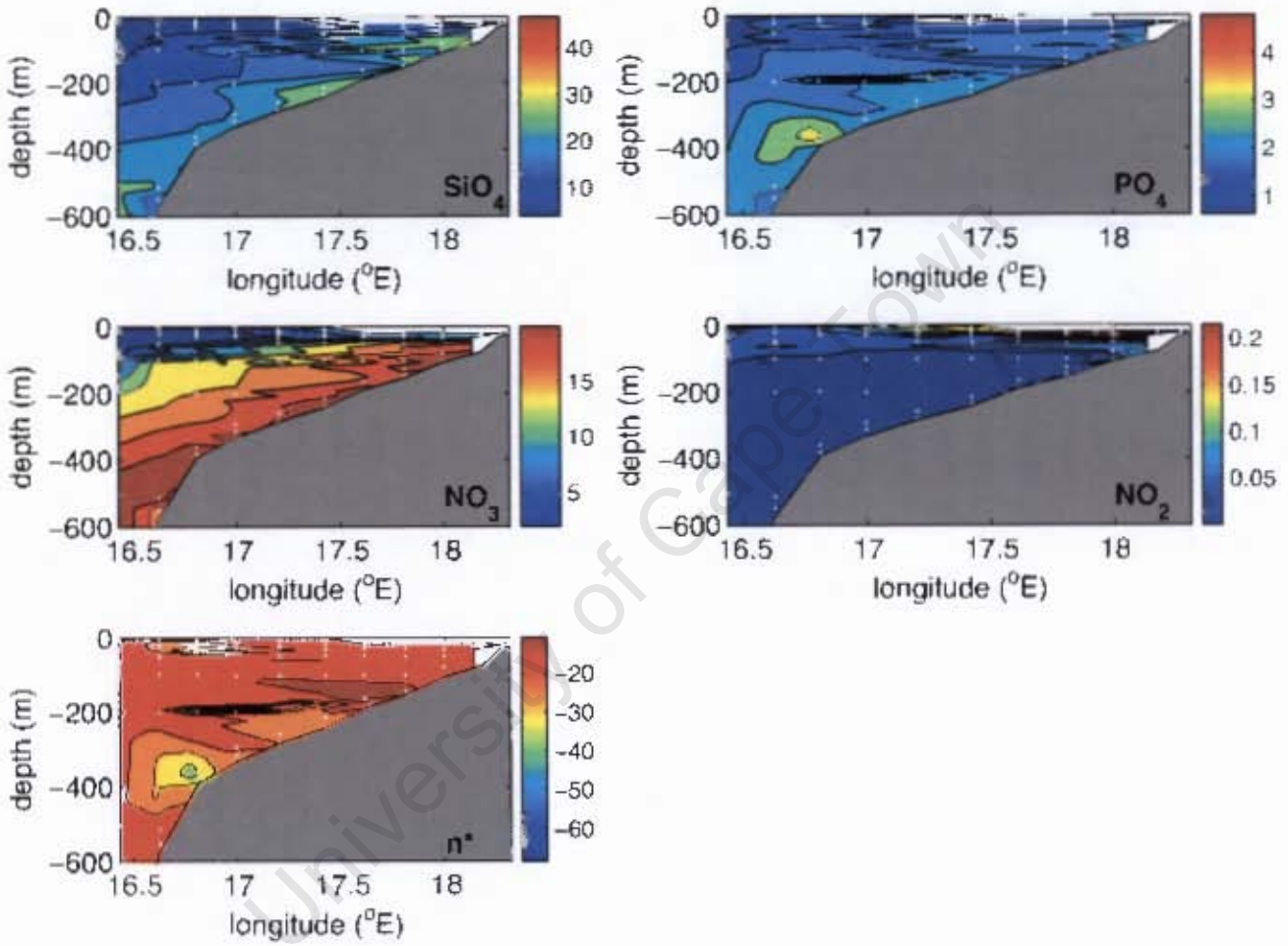

Figure 3.9: Nutrients concentrations in μM on the SHBML in June 2006.

White dots mark the position of bottle samples. N* is calculated a $NO_3 + NO_2 - 16PO_4$ and is an indicator of denitrification (see text for details).

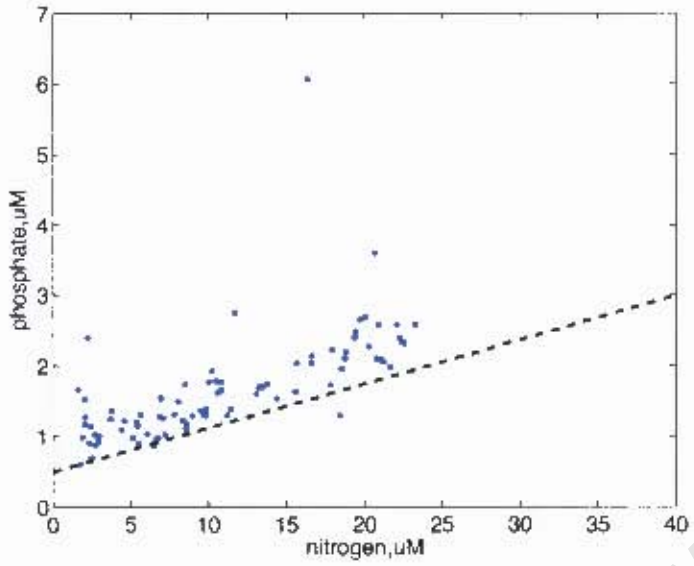

Figure 3.10: Indicators of denitrification during June 2006.
PO_4 vs. $nitrogen(NO_3 + NO_2)$(top). The dashed line indicates the theoretical 'Redfield ratio' of N:P=16:1, with a non-zero intercept.

concentration of 100 $\mu g.l^{-1}$. The bottom nepheloid layer evident in the turbidity data was also present in the POC distribution, with the highest concentrations of 40 $\mu g.l^{-1}$ occurring near the shelf break. Two lateral intermediate layers of high POC are evident, one, similarly to the nutrient distributions, extending seaward from the sloping shelf at $\approx$ 18°E and the other originating further down the shelf at $\approx$ 18.6°E. The central water column and region offshore was devoid of POC, with concentrations <20 $\mu g.l^{-1}$. The $\delta^{13}C$ distribution showed that the most enriched material (>-21 ‰) was present inshore near the surface, and in a >>150 m thick bottom layer which extended across the shelf. The water column overlying the slope again had the most depleted $\delta^{13}C$ material reaching as low as -26‰, nonetheless, the values are in line with a marine origin. The C:N ratios are anomalously low through much of the water column, and as before, such values are attributed to inaccurate PON determinations. Nonetheless, the regions of high POC, at the bottom near the shelf break, and in the intermediate layer extending seaward of $\approx$ 18°E, show up as marked maxima of $\approx$6.5 in the C:N field.

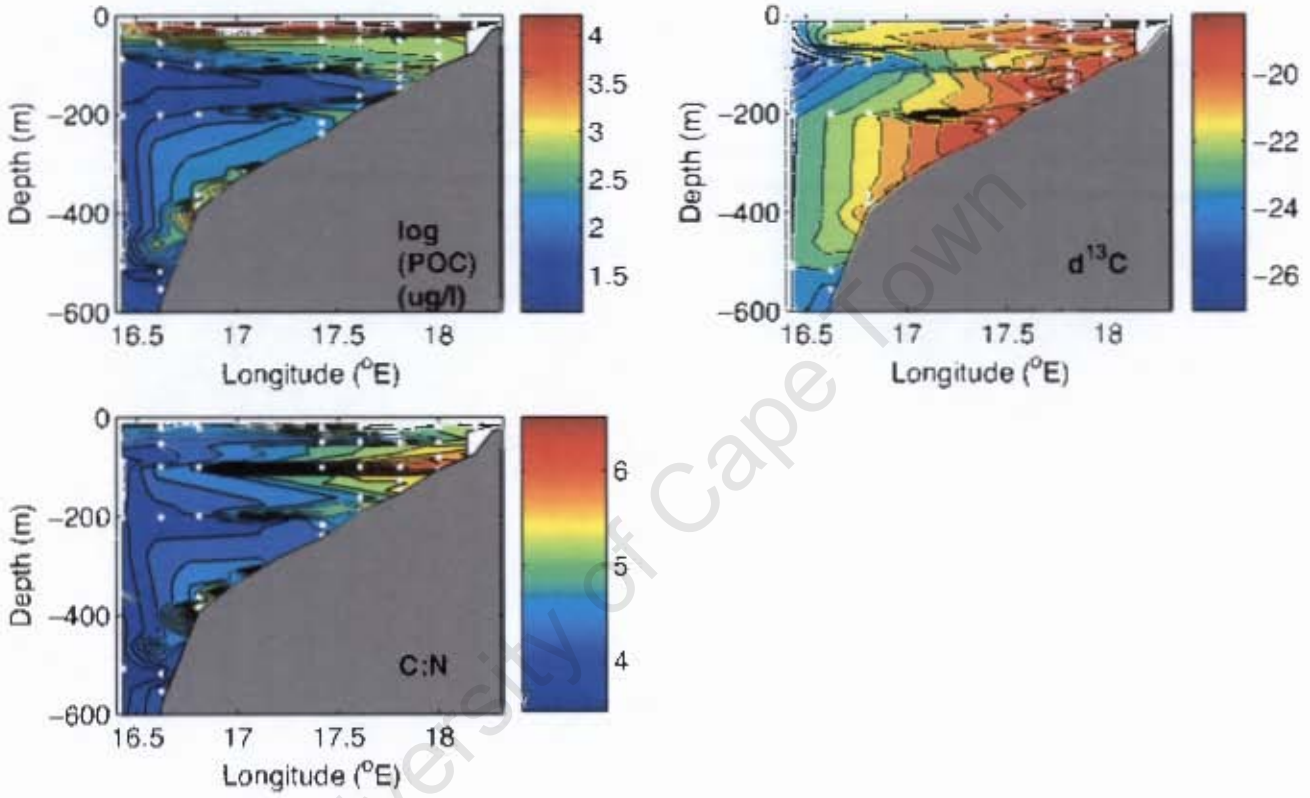

Figure 3.11: Characteristics of POM in the water column during the SHBML in June 2006.

POC is contoured on a log scale. White dots mark bottle sample positions. Concentrations are highest near the surface, in the euphotic zone, and decrease to a minimum mid-water column. POC can be seen to have been accumulating in a bottom layer, with particularly high concentrations near the shelf break. $\delta^{13}C$ values are most enriched in a thin surface layer, and a thick bottom layer, and depleted offshore. C:N ratios are anomalously low offshore and in the middle of the water column representing measurement bias, with near Redfield values in the regions of POC maxima near the shelf break and inshore.

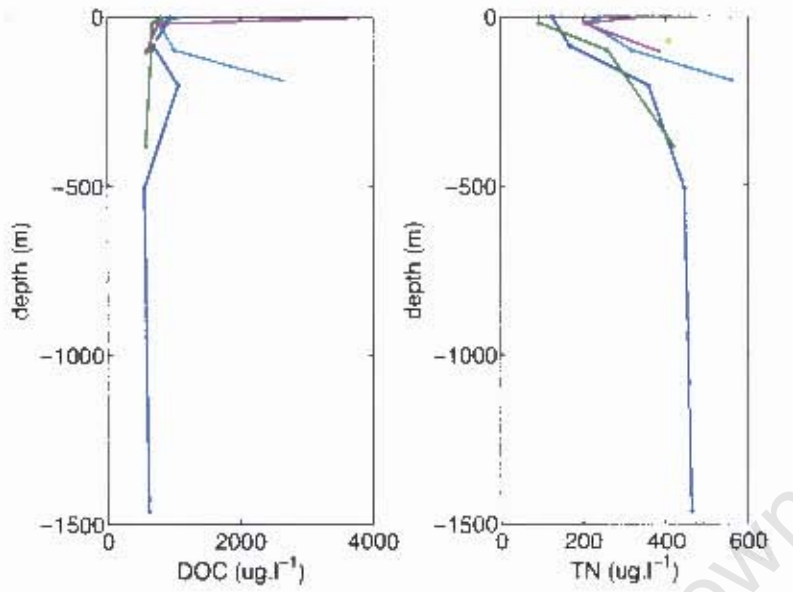

Figure 3.12: DOC and Total nitrogen (TN) at four Stations (12 (blue); 10 (green); 6 (turquoise); 4 (purple)) on the June 2006 SHEML. DOC concentrations are highest at the surface inshore (>3700 $\mu g.l^{-1}$), corresponding to high primary production. A bottom accumulation (2600 $\mu g.l^{-1}$) of DOC is evident at Station 6. Further offshore values range between 500-1000 $\mu g.l^{-1}$. Total nitrogen is everywhere more enriched near the bottom, and depleted near the surface, owing to biological consumption of inorganic nitrogen and subsequent export to depth. Concentrations near the bottom are higher inshore, perhaps owing to enrichment from the shelf sediments and overlying production.

3.3.2.4 Dissolved Organic Matter

Extremely high DOC concentrations (>3700 $\mu g.l^{-1}$) were measured in June at the surface of Station 4 and are likely to be associated with exudation from phytoplankton (Figure 3.12). At all the other Stations, surface values ranged from 800 -1100 $\mu g.l^{-1}$ and generally decreased with depth. The exception was Station 6, where a bottom maximum of >2600 $\mu g.l^{-1}$ of DOC occurred. The total nitrogen profiles show the opposite trend (Figure 3.12), with highest values occurring near the bottom and the surface waters being depleted. This pattern was presumably maintained through the biologically mediated inorganic nitrogen depletion at the surface. Total nitrogen concentrations also underwent a marked increase towards the coast, perhaps in response to inorganic nutrient regeneration from the sediments or elevated biological activity.

3.3.3 August 2006

3.3.3.1 Physical setting and continuous CTD data

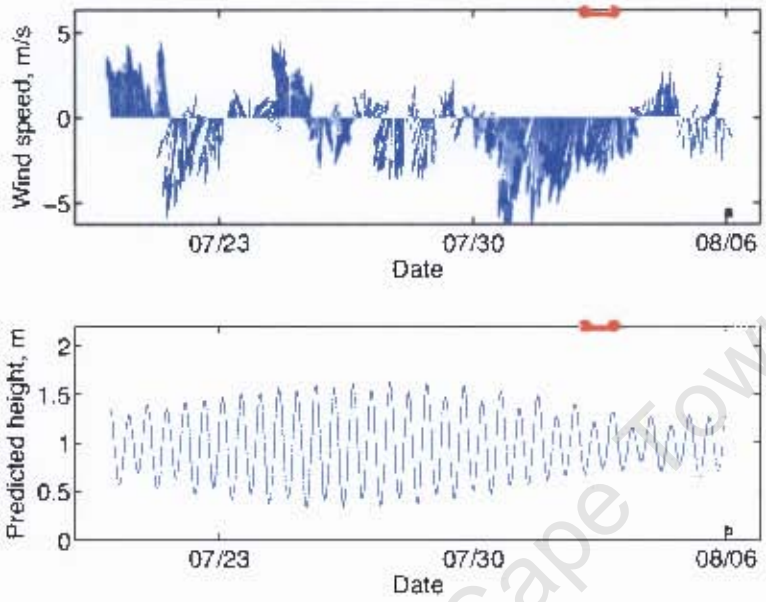

Figure 3.13: a Wind speed and direction at Lambert's Bay and b Predicted hourly tidal heights for Saldanha Bay for July/August 2006. The red dots mark the date of the SHBML cruise on 2 August.

The August SHBML occurred during a period of sustained northerly winds, with velocities of > 6 m.s^{-1}, and therefore a strong downwelling circulation pattern would be expected for this period. The sampling of the SHBML took place on the day before the neap tide, when the tidal range was <0.8 m.

Despite the downwelling favourable winds, the isopycnals sloped gently upwards towards the coast in August. A tongue of cool fresh water was evident protruding onto the shelf near the bottom, and was separated from warmer, more saline surface waters by a distinct gradient near 100 m. Low oxygen waters were present along the bottom of the entire shelf, particularly close to the coast where concentrations dipped below 1 ml.l^{-1}. Surface oxygen concentrations were generally saturated, and the effect of deep winter mixing was evident over the slope, where high concentrations (>4 ml.l^{-1}) extended to below 200 m. High fluorescence values were confined to a small region at the surface near the coast. Below 100 m fluorescence values

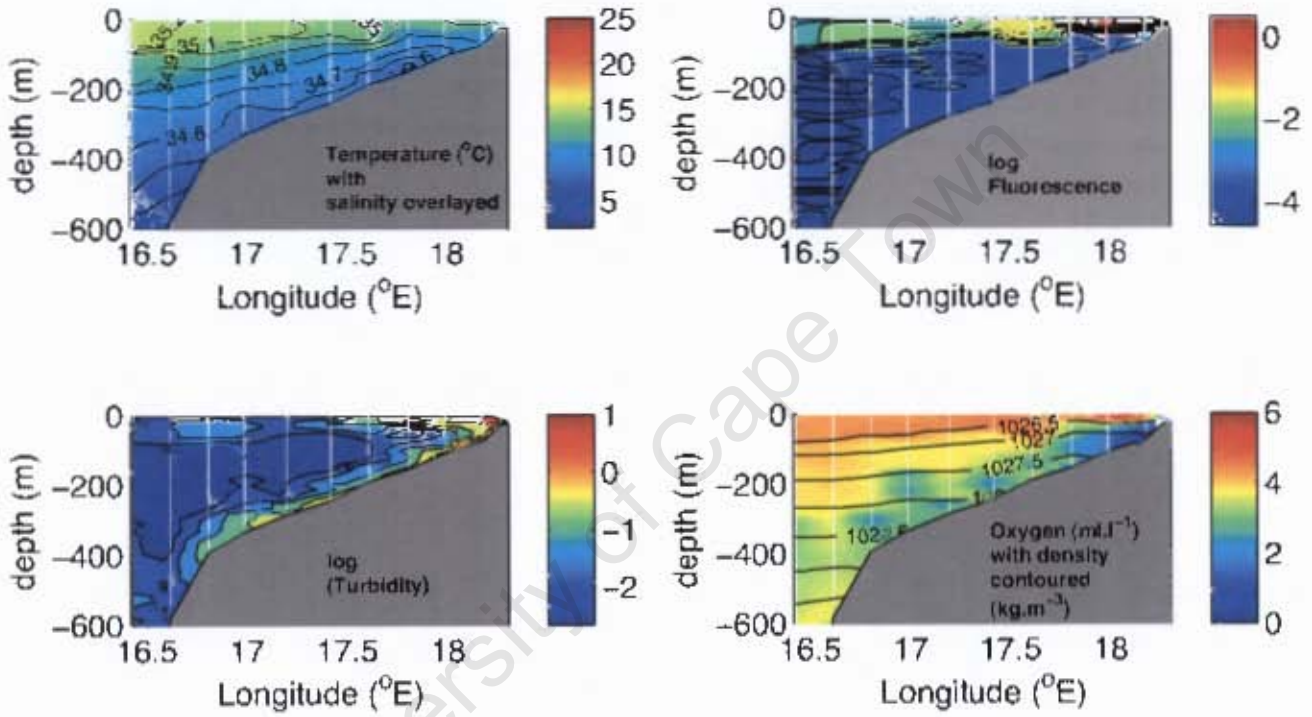

Figure 3.14: Continuous CTD data of Oxygen, overlayed with density; fluorescence and turbidity on the S11BML during June 2006.

Fluorescence and turbidity data are contoured on a log scale. Vertical white lines represent Station positions. A region of low oxygen is evident inshore at the bottom. High fluorescence value are confined to a small region at the surface close to the coast, with very low values below 100 m. The turbidity signal reflects the high fluorescence values found inshore near the surface, and exhibits a marked bottom nepheloid layer stretching across the shelf.

were low, and decreased offshore, being minimal over the slope. The turbidity distribution again echoed the high fluorescence values in the near shore surface region. However the dominant pattern in the turbidity data was the well developed, 50 m thick BNL which extended across the entire continental shelf, decreasing in amplitude offshore. A slight turbidity plume extending up from the bottom was evident over the shelf break, but the outer shelf plume seen in the previous two cruises was absent.

3.3.3.2 Particulate Organic Matter characteristics

The POC concentrations during the August 2006 SHBML were higher at the surface than in June, reaching a maximum of 270 $\mu g.l^{-1}$ (Figure 3.15). The highest concentrations were confined to the surface nepheloid layer which extended all the way across the shelf, and decreased rapidly over the slope. POC concentrations were elevated (15 -20 $\mu g.l^{-1}$) in the consistent cross shelf BNL, but very low in the centre of the water column and offshore (<10 $\mu g.l^{-1}$). The surface layer of high POC again had the most enriched $\delta^{13}C$ values, being >-19‰, while similarly enriched values were also found inshore near the bottom (Figure 3.15). A concentrated patch of $\delta^{13}C$ enriched material was centered at 300 m over the shelf break, possibly representing an advanced state of decay. This same patch was associated with very low C:N ratios, ≈3, as was much of the central water column over the shelf and slope. Once again these anomalously low values are attributed to instrument limitation and uncertainty in PON determination. The surface and bottom nepheloid layers on the other hand showed more reasonable C:N ratios of ≈6.5 and 5.5 respectively. In these high POM layers, where PON determinations were accurate, the ratios suggest that nitrogen is more rapidly recycled than carbon.

3.3.3.3 Dissolved Organic Matter

The general pattern of DOC concentrations in August 2006 was similar to that in June. However, the concentrations inshore near the surface had decreased dramatically, to 1200 $\mu g.l^{-1}$. Further offshore, surface concentrations ranged from 650-815 $\mu g.l^{-1}$, also lower than

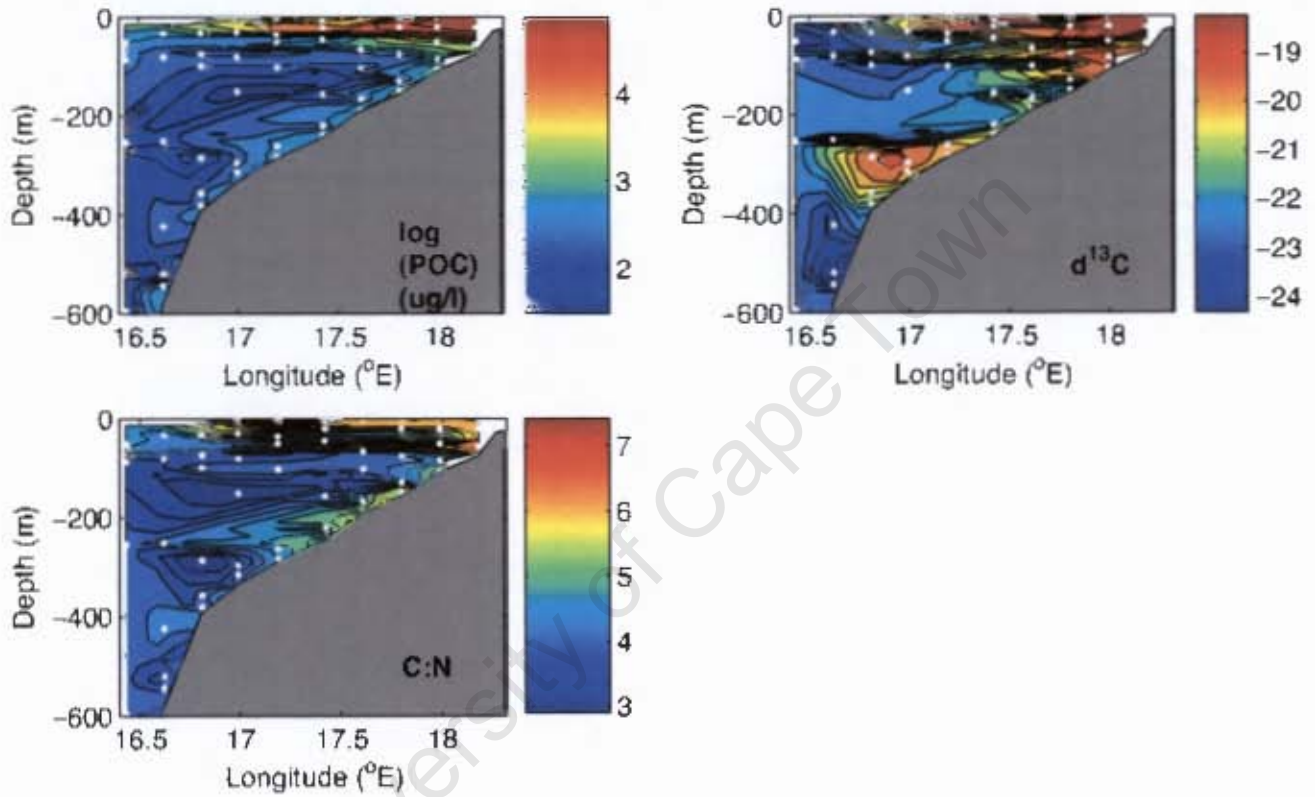

Figure 3.15: Characteristics of POM in the water column during the SHBML in June 2006.

POC is contoured on a log scale. White dots mark bottle sample positions. Highest concentrations are confined to the surface 50 m, although a secondary maximum in POC is evident as a bottom layer stretching across the shelf. By contrast, mid-water column and offshore concentrations are low. $\delta^{13}C$ values are enriched near the surface (-19), close to the coast, and at the bottom near the shelf break (-20), while they are depleted (<-22) in the central water column and offshore. C:N ratios are anomalously low (<4) offshore in the central water column and offshore, but are higher (6-7) in the regions of maximum POC, at the surface and near the bottom.

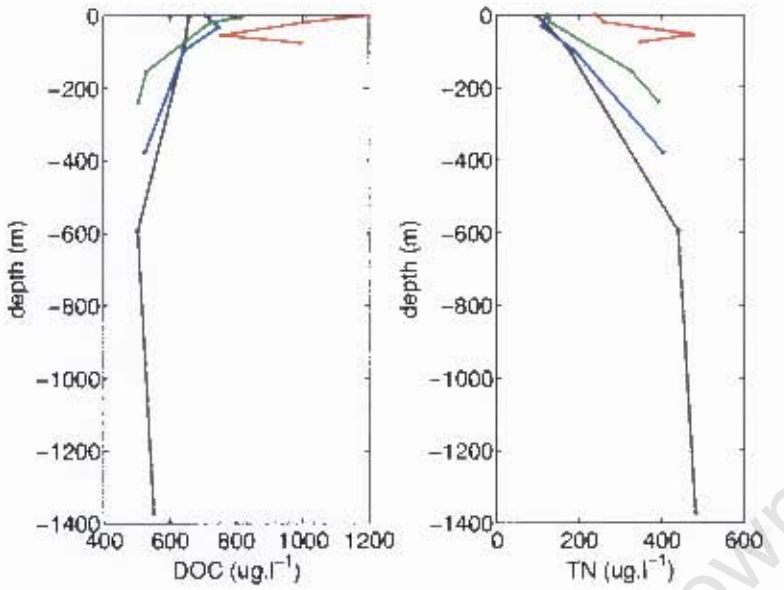

Figure 3.16: DOC and Total nitrogen (TN) at four Stations of the SHBML (12 (black); 10 (blue); 7 (green); 3 (red)) during August 2006.

DOC concentrations are highest inshore near the surface (1200 μg.l^{-1}), but closer to 500 μg.l^{-1} offshore, where concentrations tend to decrease with depth. Note that bottom concentrations increase from Station 7 to 12. Overall, DOC values are far lower than during June, representing depletion occurring at the end of winter. Total nitrogen values on the other hand are similar to the June values, indicting that inorganic forms are the dominant pool. Values of TN are higher at depth than at the surface, and increase towards the coast

in June. In general there was a decrease in DOC from surface to depth, except at Station 3, where a bottom accumulation reaching 995 μg.l^{-1} was evident. An interesting feature of the profiles was that the DOC concentration at the bottom of the water column increased by 40 μg.l^{-1} from Station 7 to Station 12, suggesting an enrichment across the shelf. The total nitrogen profiles converged at the surface to a value near 100 μg.l^{-1} at the outer 3 Stations measured, but concentrations were higher inshore. The profiles at each Station showed significantly higher concentrations at depth than at the surface, and bottom concentrations increased steadily with proximity to the coast, as in June.

3.4 Discussion

3.4.1 The seasonal signal

The biogeochemical characteristics of the water column display a clear seasonal signal in the southern Benguela (Andrews and Hutchings, 1980; Brown, 1992; Field and Shillington, 2004). During March, the end of austral summer, biomass was a maximum. POC was on average five times higher on the March SHBML, than during the two subsequent winter cruises, and the decrease was marked in the surface layer, the middle of the water column and in the BNL. The $\delta^{13}C$ values of surface organic matter were more enriched in March. This can be attributed to higher primary production, stripping DIC out of the surface waters, thus leaving phytoplankton less able to discriminate against the lighter isotope during this period (Bickert, 2000). Between June and August, although maximum POC concentrations increased at the surface, on average the amount of POC decreased slightly in the water column. This small decrease in POC over the course of winter was however overshadowed by a huge drop in DOC concentrations, particularly near the surface inshore, but averaging 300 $\mu g.l^{-1}$.

Close inshore, oxygen concentrations increased from March to June, but then fell to their lowest values during the August cruise, despite the deep winter mixing evident offshore. Oxygen concentrations could be expected to decrease during winter, owing to less photosynthetic activity (e.g. Andrews and Hutchings, 1980; Chapman and Shannon, 1985; Lalli and Parsons, 1997), although intensified mixing through strong winds and a deepened wave base inshore could lead to the opposite effect. Here it is suggested that deep reaching winter swells could have increased inshore oxygen concentrations during June. Despite the higher wind speeds observed surrounding the August cruise, the falling oxygen concentrations in the water column could be attributed to the oxidation of DOC (Lalli and Parsons, 1997; Jørgensen, 2000; Tréguer et al., 2003). Thus on the whole it appears from the decreasing organic matter (POC + DOC) and oxygen concentrations that the southern Benguela water column is in a state of net heterotrophy during winter. This maybe expected from the known seasonality

of the large scale wind forcing and upwelling (Andrews and Hutchings, 1980; Shannon, 1985; Shannon and Nelson, 1996; Field and Shillington, 2004; Shillington et al., 2006). Indeed nutrient concentrations at the surface and at depth were far higher during March, than during June, when surface nutrients were almost fully depleted. A reduced nutrient supply, deeper mixing, and decreased insolation would all contribute to lowering primary production during winter, facilitating net heterotrophy (Lalli and Parsons, 1997; Falkowski et al., 2003). By contrast, in spring and summer, the system must be net autotrophic, in order to allow for the accumulation of the observed high levels of organic matter. Such seasonal contrasts are a commonly observed feature on continental shelves (Rowe et al., 1986; Falkowski et al., 1988).

3.4.2 Inter-system comparison of organic matter concentrations

The POC concentrations observed over the shelf during March 2006 were far in excess (>5×) of those observed on the NW European margin (Wollast and Chou, 2001b; Gago et al., 2003), the East China Sea (ECS; Hung et al., 2000), and those observed in the NW Atlantic and NE Pacific (Bauer and Druffel, 1998; Sherr et al., 2002). POC concentrations at Station 12, the slope, were more in agreement with those measured adjacent to the other systems. The POC concentrations presented here are however consistent with previous observations in the Benguela (Andrews and Hutchings, 1980; Brown et al., 1991; Walker and Pitcher, 1991; Inthorn, 2006a). During the winter months, POC concentrations fell closer to those in the ECS, but remained higher than observed concentrations off Europe.

In general, the measured DOC concentrations in the southern Benguela were comparable with those measured on other continental margins (Bauer and Druffel, 1998; Hung et al., 2000; Hopkinson Jr. and Nolin, 2002; Gago et al., 2003). Particularly at Station 12, values are nearly in-line with the ocean background (see below; Hansell, 2002). However, at the surface inshore, particularly during June, concentrations are far higher (≈4×) than those reported in the other systems (Bauer and Druffel, 1998; Hung et al., 2000; Hopkinson Jr. and Nolin, 2002). This may be surprising, since upwelling areas often exhibit lower DOC concentrations than others (Hung et al., 2000; Hansell, 2002). Nonetheless, the values are

taken to be valid, and are thought to be fuelled by the remarkably high production of the Benguela system (e.g. Brown et al., 1991; Carr, 2002; Hansell, 2002).

For more direct comparison the DOC and TN concentrations during June and August at the outer Station (12) of the SHBML, on the edge of the Benguela system, have been plotted alongside data from a similar latitude, but in the center of the South Atlantic gyre (Figure 3.17). DOC concentrations can be seen to have been higher by up to 180 $\mu g.l^{-1}$ near the surface in the Benguela, as opposed to the central gyre. At mid depths, the concentrations are very similar between the two, but at depth of 1500 m, the edge of the Benguela exhibits concentrations 100-180 $\mu g.l^{-1}$ more enriched than the central South Atlantic. The Benguela samples represent near bottom values on the upper continental slope, where a carbon enriched nepheloid layer exists (see 3.4.4). In the upper 700 m, the Benguela edge exhibits more enriched TN values than the central South Atlantic which is likely representative of increased biological activity, as opposed to upwelling of inorganic nitrogen, which only occurs over the upper 300 m. At depth the TN concentrations at the edge of the Benguela are in line with those in the central gyre.

The extremely high concentrations of organic carbon in the southern Benguela system, when compared to other continental margins (Bauer and Druffel, 1998; Hung et al., 2000; Wollast and Chou, 2001b; Hopkinson Jr. and Nolin, 2002; Sherr et al., 2002; Gago et al., 2003), and the open ocean, suggest that it could contribute significantly to global biogeochemical cycles. The strong carbon gradients between the Benguela shelf and open ocean suggest that a significant lateral export of carbon could occur under favourable circulation patterns, as has been previously suggested here (Rowe, 1987; Waldron et al., 1998; Swart et al., 2007) and in other systems Walsh et al. (1981); Hung et al. (2000); McCave et al. (2001); Hopkinson Jr. and Nolin (2002). This concept is pursued further below, and is directly addressed in Chapter 4.

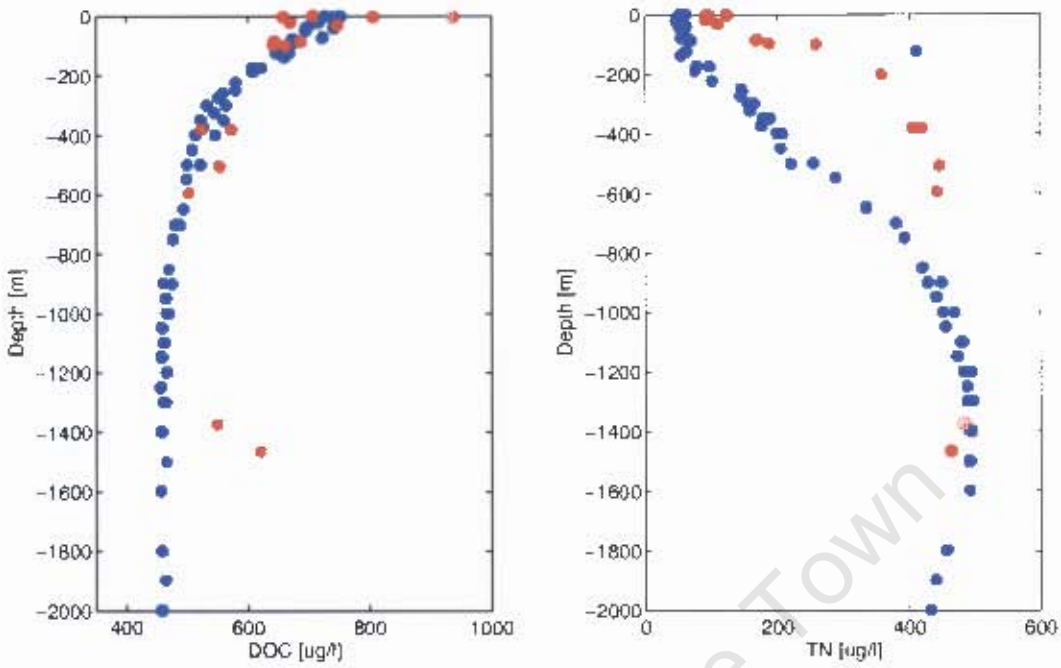

Figure 3.17: Comparison of DOC (top) and TN (bottom) concentrations between the edge of the Benguela upwelling system (Station 12 of SHBML; red) and the central South Atlantic (≈ 25°W; blue; see text for details).

3.4.3 Denitrification

About half of the total oceanic primary production is channeled through bacteria, and the 'microbial loop' (Azam, 1998). Bacteria can be classified according to their metabolism, or differentiated between those which live in the presence of oxygen (aerobic), and those who live without oxygen (anaerobic; Jørgensen, 2000). In much of the water column and surface sediments aerobic respiration leads to the oxidation of organic matter to CO_2 using oxygen. In hypoxic waters and deeper within the sediments, anaerobic organisms can use nitrate for oxidation instead (Jørgensen, 2000), although in some region both processes may overlap (Tyrrell and Lucas, 2002). Under hypoxic conditions, the so-called denitrifying bacteria reduce nitrate through nitrite to N_2, which is subsequently lost to the atmosphere (Jørgensen, 2000; Tyrrell and Lucas, 2002; Kuypers et al., 2005). During this 'denitrification' process, some ammonium is also accumulated (Kuypers et al., 2005).

Denitrification has been shown to occur in oxygen minimum zones around the world (Gruber and Sarmiento, 1997; Kuypers et al., 2005), and has been previously observed in the Benguela

system, particularly in the Central part (Calvert and Price, 1971; Andrews and Hutchings, 1980; Bailey and Chapman, 1991; Tyrrell and Lucas, 2002). Furthermore, nitrogen losses can be induced by anaerobic ammonium oxidation (anammox), which has been shown to be prevalent in the central Benguela (Kuypers et al., 2005). The clear nitrate deficit which occurred during March 2006 (Section 3.3.1.2) suggests that denitrification was occurring. Nitrate deficits of a similar amplitude ($40\,\mu M$) have been previously observed in the Benguela, and attributed to denitrification (Tyrrell and Lucas, 2002). The case for denitrification is further supported by the statistically significant inverse correlation between N* and NO_2. Lowest values of N*, where denitrification would have been greatest, were associated with highest values of NO_2, which is consistent with the denitrification process ($NO_3 \rightarrow NO_2 \rightarrow N_2$; Jørgensen, 2000). Furthermore it would be expected that the denitrification would have been occurring in hypoxic waters. A near bottom hypoxic zone was present inshore during the March SHBML, and is likely the region where denitrification was occurring. This is clearly illustrated by the relationship between N* and O_2 (Figure 3.18), with low N* values, and thus denitrification, coinciding with low oxygen concentrations during the March SHBML.

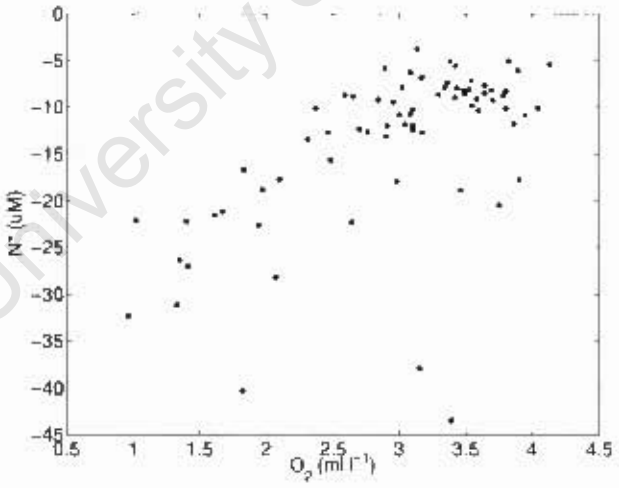

Figure 3.18: N* vs. oxygen concentrations for the March SHBML.
Lowest values of N* occur at low oxygen concentrations. This is consistent with the nitrogen deficit (low N*) being caused by denitrification in hypoxic waters.

By contrast, no nitrate deficiency, or denitrification signal was detected during the June cruise 3.3.2.2. This is most likely because oxygen concentrations were on average higher during June

than March, and a significant bottom confined hypoxic zone did not exist during the June period. However some hypoxic waters were evident in the cross shelf O_2 distribution (Figure 3.8). It is submitted here that enhanced mixing by surface waves, as discussed above, would ventilate inshore waters during winter, and suppress denitrification in these shallow waters. During August, when oxygen concentrations were lowest, and a distinct inshore bottom hypoxic zone was evident, there is unfortunately no nutrient data available to consider.

Since ammonium was not measured, it is not possible to conclude that the observed nitrogen loss was due solely to denitrification, as opposed to anammox (Kuypers et al., 2005). However, accumulation of N in the ammonium pool, due to zooplankton excretion for example, could not account for the observed nitrogen deficit. The observed nitrogen deficit during March 2006 reached 40 μM, while previously observed NH_4 concentrations in the southern Benguela are of the order 5 μM (Chapman and Shannon, 1985; Bailey, 1987; Bailey and Chapman, 1991). The detection of denitrification during late summer in the southern Benguela has significant biogeochemical implications. Firstly, by reducing the amount of nutrients available to phytoplankton, it hinders the ability of photosynthesis to draw down DIC concentrations in surface waters (Sarmiento and Bender, 1994; Lalli and Parsons, 1997). This in turn pushes the system towards outgassing CO_2 to the atmosphere (Watson et al., 2000). Secondly, nitrogen losses alter the C:N ratio in the inorganic pool, which renders the use of typical 'Redfield' stoichiometry problematic in the system (Monteiro, 1996; Tréguer et al., 2003). Such an impact implies that previous carbon sequestration estimates for the southern Benguela (Waldron et al., 1992, 1998; Swart et al., 2007), based on nitrogen budgets, represent overestimates.

3.4.4 The biogeochemical significance of nepheloid layers

Each of the three SHBML cruises revealed clearly defined surface and bottom nepheloid layers, present in both the turbidity and POC distributions. The surface nepheloid layer was typically 50 m thick, strongest inshore, and decreasing in POC concentration, turbidity and fluorescence with distance across the shelf. Since river input is almost nil in the region

(Shillington, 1998), the SNL owed its existence to biological particles (McCave, 2002), which is supported by the turbidity-POC correlation below. The biological activity in the SNL depleted inorganic nutrients and total nitrogen concentrations, and produced the highest observed concentrations of DOC and oxygen.

The importance of BNLs in meeting the requirements of benthic carbon demand (Thomsen and van Weering, 1998; Thomsen, 1999; Rutgers van der Loeff et al., 2002; van Weering and McCave, 2002), affecting fisheries (Monteiro et al., 2005) and naval operations (Johnson et al., 2001), and as a conduit for shelf-ocean exchange of biogeochemical constituents has been conclusively shown (Thomsen and van Weering, 1998; McCave et al., 2001; van Weering et al., 2001; Thomsen, 2002; Wollast, 2002; Inthorn et al., 2006). However, little work has been done on the BNL in the southern Benguela. Our turbidity observations show that the bottom nepheloid layer was ubiquitous. It was also the region where oxygen minima occurred, the likely region of denitrification, and is a known critical interface for sediment water column interactions, including nutrient regeneration (Bailey, 1987; Thomsen and van Weering, 1998; Thomsen, 1999, 2002). POC concentrations in the BNL were often double those in the central water column, and certain Stations show accumulations of DOC near the bottom too. The $\delta^{13}C$ values of POC coincident with the BNL were in all cases comparatively enriched, and the C:N ratios were generally higher. These observations could potentially be explained by bacterial oxidation of organic matter, with a preference for the lighter isotope (Bickert, 2000) and more rapid recycling of N over C (Toggweiler, 1993; Rullkötter, 2000).

The BNL varied in its vertical extent and tended to be intensified near the shelf break. Whether the material in the BNL is supplied from vertical input from the surface, or through bottom resuspension and lateral advection, turbulence is required to maintain the particles in the water column (Cacchione and Drake, 1986; Thomsen and McCave, 2000; Johnson et al., 2001; McCave, 2002; Thomsen, 2002). Internal tides are frequently cited as the source of this turbulence (Cacchione and Drake, 1986; Johnson et al., 2001; McPhee-Shaw and Kunze, 2002; McPhee-Shaw et al., 2004; Inthorn, 2006a). The presence of internal tides in the study region and the focusing of energy near the bottom in areas of critical topography near the

shelf break was discussed in Chapter 2. Breaking internal waves on critical topography, and the consequent turbulent motion could account for the increased intensity of the BNL near the shelf break, particularly through enhanced sediment resuspension, as documented elsewhere (Shannon, 1985; Inthorn, 2006a). The fact that the tidal range was greatest during the March cruise which occurred close to the spring tide, would have led to the more vigorous internal tidal activity during the March SHBML, than the other cruises, when the tidal range was less. This turbulence generating mechanism then provides an appealing explanation for why the BNL was thicker in March (100 m) than in June and August (50 m).

Focusing on the cross shelf variation in POC in the BNL (Figure 3.19 top), it is evident that highest concentrations occur inshore in the region of high primary production. Discounting the maximum which occurs near the shelf break (≈16.8°E), concentrations tend to decrease with increasing distance from the coast, typically by >20 $\mu g.l^{-1}$ between the coast and the shelf edge. Another marked decrease tends to occur between the shelf break and offshore. The general decrease of POC in the BNL with distance from the coast could be related to decreased input fluxes from the surface, since biomass and production generally increase towards the coast (Shannon and Pillar, 1986; Brown et al., 1991; Brown, 1992; Pitcher et al., 1992).

Alternatively, the decrease could be attributed to the continuous bacterial oxidation of organic matter in the BNL (Azam, 1998; Jørgensen, 2000; Azam and Long, 2001; Lochte et al., 2003). For this model to explain the observed pattern, it is required that organic matter is input to the BNL in the highly productive inshore region, and subsequently advected across the shelf, all the while undergoing continuous losses to oxidation. Long distance lateral transport and alteration of organic matter in BNLs, via resuspension-deposition cycles and microbial action is an established process (e.g. Thomsen, 1999; Thomsen and McCave, 2000; McCave, 2002; Thomsen, 2002). The distribution of $\delta^{13}C$ and C:N ratios also provides support for this 'advection and alteration' model. Furthermore the cross shelf variation of DOC in the BNL exhibits a fascinating pattern (Figure 3.19). While initially DOC concentrations fall rapidly with increasing distance from the coast, seawards of 17.4°E, DOC concentrations increase

by around 50 $\mu g.l^{-1}$. A plausible explanation for this increase could be related to the release of DOC during the bacterial decomposition of POC (Azam, 1998; Azam and Long, 2001; Carlson, 2002). In this context, the observed decreasing cross-shelf concentrations of POC maybe caused by bacterial respiration and channelling of POC into the DOC pool. However, the decrease in POC, and increase in DOC are not spatially coherent. Furthermore, such sustained bacterial activity in a water parcel crossing the shelf would deplete oxygen concentrations (Jørgensen, 2000). The cross shelf oxygen distribution does not show a decrease in the BNL with distance from the coast, but rather the opposite.

It seems likely that both changes in vertical supply, and oxidation during cross-shelf advection might explain the observed patterns in BNL POC and DOC. The elevated concentrations of POC in the BNL together with the tendency for off-shelf flow in the BBL (Chapter 2) make the region a prime candidate for shelf-ocean exchanges (Thomsen and van Weering, 1998; Thomsen, 1999; McCave et al., 2001; van Weering et al., 2001; McCave, 2002; Thomsen, 2002; Wollast, 2002; Inthorn et al., 2006). Furthermore the cross-shelf enrichment of DOC in the BNL contributes to the 100-180 $\mu g.l^{-1}$ DOC gradient between the Benguela edge and the open ocean at around 1400 m. Such gradients have been suggested to lead to significant exports of DOC to the deep ocean, in the region below the permanent thermocline during periods of off-shelf advection (McCave et al., 2001; Hopkinson Jr. and Nolin, 2002). The temporal characteristics of the BNL, and its role in shelf carbon export to the open ocean are considered further in Chapter 4.

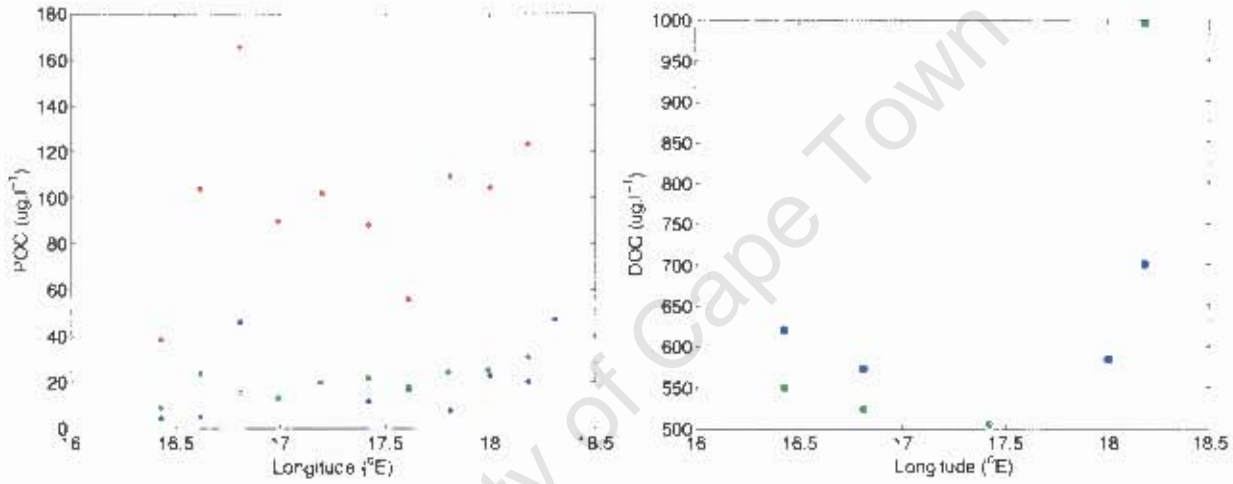

Figure 3.19: Cross-shelf variation in bottom POC and DOC.

The top panel shows the change in POC with longitude at the bottom on the SHBML during March (red), June (blue) and August (green) 2006. In general, concentrations drop by $\approx 20 \mu g.l^{-1}$ moving offshore, with secondary maxima occurring near the shelf break during March and June. Bottom DOC concentrations, shown in the bottom panel, initially decrease rapidly away from the coast, but then shown an increase from mid-shelf ($\approx$500 $\mu g.l^{-1}$) to Station 12 (550-620 $\mu g.l^{-1}$) at 16.4°E. Increasing cross shelf DOC concentrations near the bottom may be related to the release of DOC as POC is decayed in the bottom nepheloid layer, although the opposing trends in POC and DOC concentrations are not spatially coherent.

3.4.5 The calibration of turbidity with POC

It has emerged over the course of several large studies, that turbidity sensor data, usually beam attenuation, correlates with particulate suspended matter (Hall et al., 2000; McCave and Hall, 2002) and particulate organic carbon (Bishop, 1999; Hall et al., 2000; Gardner et al., 2003; Mishonov et al., 2003; Gardner et al., 2006). Furthermore, light scattering, as measured by the fluorometer in this study, has been shown to be correlated with beam attenuation and POC (Hall et al., 2000; McCave et al., 2001; Inthorn, 2006a). Using such correlations, optical sensors on CTDs and moorings can provide a wealth of information on the fine spatial scale, and long term temporal scale, of variations in POC in the ocean, not accessible through low resolution bottle samples and intermittent cruises (Bishop, 1999; Gardner et al., 2003; Inthorn, 2006a). High resolution data are particularly useful when investigating bottom nepheloid layers (e.g. McCave et al., 2001; Inthorn, 2006a), which have been shown here to be of particular biogeochemical importance in the southern Benguela. The optical sensors response is sensitive to the size distribution of particles in the water column, with beam attenuation responding most intensively to large fresh biogenic particles (Inthorn, 2006a). The fluorometers by contrast, have been shown to be more sensitive to smaller particles (McCave et al., 2001; Inthorn, 2006a), and display their greatest response in BNLs and INLs, where fine particles comprising of refractory organic matter dominate (Inthorn, 2006a). Thus it seems that for the purpose of investigating BNLs in the southern Benguela, the light scattering response from the fluorometer aboard the CTD should provide a good predictor for POC.

Because of the dependence of light scattering on the size and shape of particles, it is not possible to use one equation to relate light scattering (hereon called turbidity for convenience) to POC (McCave et al., 2001). Data from the highly turbid SNL and BNL present during the SHBML in March, June and August 2006 have been extracted and plotted in Figure 3.20. Normalized values $[z = (x - mean(x))/standard\,deviation(x)]$ have been used to remove the influence of seasonality on POC concentrations. The solid line represents the linear regression between the variables, which is statistically significant at the 1% level (see Table 3.1 for details

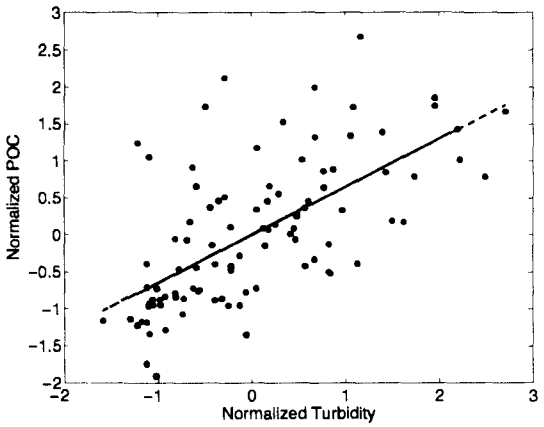

Figure 3.20: POC vs. turbidity in nepheloid layers on the SHBML

The correlation between POC and turbidity (light scattering), for data in the regions of high turbidity (surface and bottom nepheloid layers), in the Benguela. Turbidity and POC have been normalized to remove seasonal influences between cruises (higher concentrations in summer). The correlation is statistically significant at the 1% level, indicating that turbidity is in general a good predictor for POC in high turbidity regions of the water column. Individual regression relations on a per cruise basis are given below.

of the regression). This suggests that on the whole turbidity is a good predictor for POC in regions of high particles concentration in the study region.

Nonetheless, to be able to use turbidity values to predict POC concentrations, it is necessary to describe individual relationships for different parts of the water column (SNL vs. BNL) and seasons, because of the variation in particle size characteristics with depth and time (Pitcher et al., 1992; Inthorn, 2006a). Since we are primarily interested in the BNL, due to its biogeochemical significance and potential for lateral carbon advection, we can consider data from the bottom 20 m of the water column during the three sampled SHBML cruises. Figure 3.21 shows the relations, and linear regressions, the equations and statistics of which are provided in Table 3.1. In all cases the relationships are significant to at least the 5% level, and better during winter. The data spreads and regression relationships are very similar between the June and August cruises. Thus, for long term POC estimation purposes, it seems appropriate to use the relationship defined for March during summer, and an average of the June and August coefficients during winter. These relations are used in conjunction with a time series of turbidity over the southern Benguela shelf to quantify lateral POC in the BNL in Chapter 4.

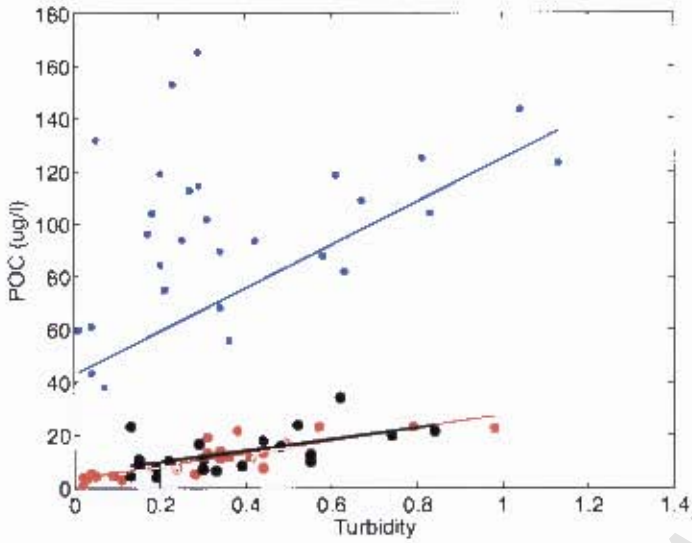

Figure 3.21: POC vs. Turbidity in the bottom 20 m of the water column on the SHBML during March (blue), June (red) and August (black) 2006. All of the linear regressions (solid lines) are statistically significant to at least the 5% level (see Table for the regression relationships).

X	Y	Sample	Number	Equation	R^2	p
Light Scattering	POC	All (normalized)	100	y=0.65x	0.42	<0.01
		BNL March	28	y=82x+42.7	0.16	0.03
		BNL June	24	y=3.3x+5.5	0.73	<0.01
		BNL August	23	y=5.8x+21.4	0.33	<0.01
		BNL winter average	47	y=4.5x+22.9		

Table 3.1: Regression equations and statistics of light scattering against POC, as shown in Figures 3.20 and 3.21.

3.5 Conclusions

The southern Benguela upwelling system exhibits a strong seasonality in its biogeochemical characteristics. At the end of summer, when biomass is a maximum, bottom hypoxia may develop inshore. During March 2006, there was clear evidence of nitrogen loss, probably from denitrification in the hypoxic Section of the water column. During winter, wind and wave mixing tends to reduce inshore bottom hypoxia, and no evidence for denitrification was found during July 2006. Over the course of winter, there is a large decrease in both particulate and dissolved organic matter concentrations in the water column, which is net heterotrophic. This oxidation of organic matter during winter may counteract the effects of mixing, and lead to oxygen depletion, as was observed in August 2006. During all seasons,

strongly developed surface and bottom nepheloid layers were present over the continental shelf and slope, and were found to be of elevated biogeochemical significance. The bottom nepheloid layer, rich in POC and DOC, may form a conduit for lateral export of carbon from the Benguela shelf to the deep ocean. This export could be significant, because the southern Benguela shelf contains higher concentrations of organic matter than those observed on many other continental margins, and exhibits strong gradients with the open ocean. A statistically robust predictor for POC is provided by optical backscatter, which can provide high resolution information about POC variations in the water column.

Chapter 4

Nepheloid layers and lateral carbon export from the southern Benguela upwelling system

4.1 Introduction

4.1.1 Nepheloid layers

Nepheloid layers are zones of elevated particulate concentration within the water column, commonly found overlying the continental shelves and slopes of the global ocean (Cacchione and Drake, 1986; Thomsen and van Weering, 1998; Johnson et al., 2001; McCave et al., 2001; McCave and Hall, 2002; Rutgers van der Loeff et al., 2002; McPhee-Shaw et al., 2004; Inthorn, 2006a). They are usually observed near the surface, where they are associated with biological matter, and at the bottom of the water column (Bottom Nepheloid Layers), where turbulence keeps particles in suspension, and erodes and resuspends material from the seafloor (see Figure 4.1; Cacchione and Drake, 1986; Johnson et al., 2001; McCave et al., 2001; van Weering et al., 2001; Rutgers van der Loeff et al., 2002; Thomsen, 2002; van Weering and McCave, 2002; Inthorn et al., 2006). Mechanisms of bottom turbulence generation,

such as internal waves, tides and bottom boundary layer currents were discussed in Chapter 2. Bottom nepheloid layers may extend in range from tens (McCave, 2002; McPhee-Shaw et al., 2004) to hundreds of meters off the bottom (Rutgers van der Loeff et al., 2002; Inthorn, 2006a), thereby often exceeding the height of the well mixed benthic boundary layer. Particles in the BNL typically remain in suspension for periods of 1-2 months (Rutgers van der Loeff et al., 2002; Inthorn, 2006a), their sinking characteristics being determined by aggregate formation (Thomsen and McCave, 2000), and a dynamic resuspension loop modulated by shear stresses (Thomsen and van Weering, 1998; Thomsen, 1999; Rutgers van der Loeff et al., 2002; Thomsen, 2002). In association with low frequency currents in the BBL (Thomsen, 1999; Hill and McCave, 2001), or with higher frequency, asymmetrical oscillations (barotropic tides and internal waves; Cacchione and Drake, 1986; Johnson et al., 2001; McCave et al., 2001; van Weering et al., 2001; Wollast, 2002; McPhee-Shaw et al., 2004; Monteiro et al., 2005), BNLs may propagate across the shelf, advecting with them their load of suspended particulate matter and solutes. Long distance lateral transport and alteration of organic matter in BNLs, via resuspension-deposition cycles and microbial action has been thoroughly documented (Figure 4.1; e.g. Thomsen, 1999; Thomsen and McCave, 2000; McCave, 2002; Thomsen, 2002). Moreover in certain regions, particularly on continental slopes critical with respect to internal tides, BNLs may become detached from the bottom, and form intermediate nepheloid layers (INLs), which tend to spread out laterally along isopycnals (McCave et al., 2001; McPhee-Shaw and Kunze, 2002; McPhee-Shaw et al., 2004).

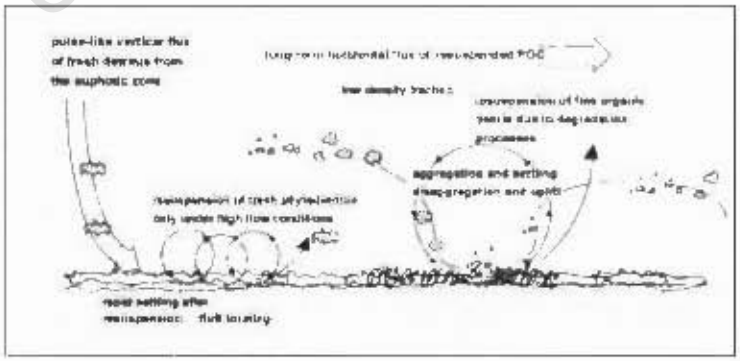

Figure 4.1: Schematic model of processes acting at different time scales that control the carbon input to the benthos at continental margins (After Thomsen and van Weering, 1998, Figure 5).

Bottom nepheloid layers are important because through their lateral advection they may form a conduit for shelf-ocean exchange of biogeochemical constituents (Cacchione and Drake, 1986; Thomsen and van Weering, 1998; McCave et al., 2001; van Weering et al., 2001; Thomsen, 2002; Wollast, 2002; Inthorn et al., 2006). This fact has been recognized by a host of continental margin flux studies, undertaken over a diverse range of oceanographic settings, including in upwelling areas, and western boundary currents (Falkowski et al., 1988; Walsh et al., 1988a; Walsh, 1991; Biscaye et al., 1994; Thomsen and van Weering, 1998; Thomsen, 1999; Hung et al., 2000; McCave et al., 2001; van Weering et al., 2001; Wollast and Chou, 2001b; van Weering et al., 2002; van Weering and McCave, 2002). It has also been shown that the benthic carbon demand on the outer shelf and slope cannot be met by the vertical carbon flux. Lateral carbon transport, typically in bottom nepheloid layers, is therefore a vital mechanism for sustaining the active benthos (Thomsen and van Weering, 1998; Thomsen, 1999; Rutgers van der Loeff et al., 2002; van Weering and McCave, 2002). Furthermore, the elevated turbidities present in the BNL can have an impact on fisheries (Monteiro et al., 2005), and potentially affect naval operations (Johnson et al., 2001). The turbidity observations presented in Chapter 3 showed that the bottom nepheloid layer was an ubiquitous feature of the southern Benguela continental shelf during March, June and August 2006. The southern Benguela BNL also appeared to be a region of elevated biogeochemical significance. It was where the oxygen minima occurred, the likely region of denitrification, and it contained elevated concentrations of POC, DOC and nutrients, the latter likely owing to regeneration from the sediments (Bailey, 1987). In this Chapter, the bottom nepheloid layers of the southern Benguela are characterized in their cross-shelf, vertical, and temporal variability using a time series of optical backscatter measurements from the SHBML. These observations are then used to consider the potential lateral export of carbon from the southern Benguela shelf.

4.1.2 Lateral carbon export from the Benguela

The significant role that the continental margins can play in global biogeochemical cycles through their exchanges with the continents, the atmosphere and the open ocean was com-

prehensively discussed in Chapter 1 (Walsh et al., 1981; Walsh, 1991; Sarmiento and Bender, 1994; Bauer and Druffel, 1998; Wollast, 1998; Liu et al., 2000; Sigman and Boyle, 2000; Chen et al., 2003). According to current understanding, as a region of coastal upwelling, the southern Benguela qualifies as a system which is likely to export matter from the shelf to the open ocean (Chen et al., 2003). It is known that the Benguela has one of the highest photosynthetic carbon fixation rates in the global ocean (Brown et al., 1991; Carr, 2002), and it has been proposed that this carbon is not fully consumed or buried on the shelf (Rowe, 1987; Hutchings et al., 1991; Verheye, 1991; Pitcher et al., 1991; Waldron et al., 1998; Touratier et al., 2003). Simultaneously, rates of shelf-ocean exchange are elevated in dynamically bounded eastern boundary currents (Brink, 1998). None more so than in the southern Benguela, the only EBC to be bordered on its poleward edge by a highly unstable western boundary current (Shillington, 1998; Field and Shillington, 2004; Shillington et al., 2006). Agulhas rings, a meandering upwelling front, and an offshore oriented bottom boundary layer are all mechanisms for cross-shelf exchange, which were identified in the southern Benguela and lengthily discussed in Chapter 2.

These points considered, the potential for the southern Benguela to laterally export organic carbon was identified in Chapter 1 (Waldron et al., 1992, 1998; Swart et al., 2007), together with the debate over the magnitude of this potential export (Monteiro, 1996). The foundation of the previous potential lateral carbon export estimates for the southern Benguela were nitrogen budgets which assumed Redfield stoichiometry (Waldron et al., 1998; Swart et al., 2007) the validity of which has previously been questioned (Monteiro, 1996; Tyrrell and Lucas, 2002). The results presented in Chapter 3, provided convincing evidence that denitrification occurs in the southern Benguela, rendering the use of Redfield stoichiometry problematic in the system. Indeed, departures from Redfield stoichiometry, and the inappropriateness of its use in the coastal zone have been documented before (e.g. Toggweiler, 1993; Tréguer et al., 2003). These findings imply that the previous carbon sequestration estimates based on nitrogen budgets (Waldron et al., 1992, 1998; Swart et al., 2007), represent overestimates, as suggested (Monteiro, 1996).

Nonetheless it was also found in the previous Chapter that the southern Benguela contained remarkably high concentrations of organic carbon when compared to other continental margins (Bauer and Druffel, 1998; Hung et al., 2000; Wollast and Chou, 2001b; Hopkinson Jr. and Nolin, 2002; Sherr et al., 2002; Gago et al., 2003), and the open ocean. These steep gradients in both POC and DOC between the Benguela shelf and open ocean suggest that a significant lateral export of carbon could occur under favourable circulation patterns (see Chapter 2), albeit at a lower rate than has been previously estimated (Rowe, 1987; Waldron et al., 1998; Swart et al., 2007). Indeed, an examination of the total organic carbon (TOC) content of the sediments supports such an export (Figure 4.2). The sediment TOC distribution shows a band of high values reaching nearly 6% inshore, corresponding to the mudbelt. The mid and outer shelf by contrast have extremely little carbon, generally less than 1%. However, the upper continental slope is a secondary maximum in TOC, with values around 2%, and higher in specific locations. The presence of this upper continental slope carbon depocenter suggests that there maybe a lateral export of organic carbon from the continental shelf, to the slope sediments, as it did elsewhere (Walsh et al., 1988a).

The recognized role of nepheloid layers in lateral carbon transport across shelves and slopes (Thomsen and van Weering, 1998; Thomsen, 1999; McCave et al., 2001; van Weering et al., 2001; McCave, 2002; Thomsen, 2002; Wollast, 2002; Inthorn et al., 2006), together with the identification of prominent such layers in the southern Benguela where biogeochemical gradients with the open ocean are greatest (Chapter 3, and below), strongly suggests a 'nepheloid conveyor' type mechanism maybe in operation. The offshore export of carbon from the southern Benguela at the surface was reliably estimated by Waldron et al. (1998) using remote sensing. However, it is the subsurface lateral export below the permanent thermocline which is of relevance to atmospheric CO_2 (Sarmiento and Bender, 1994; Wollast and Chou, 2001b; Watson and Orr, 2003). Furthermore it is this subsurface flux which has been a matter of conjecture in nitrogen budgets (Waldron et al., 1998; Swart et al., 2007) and biogeochemical models (Monteiro, 1996) of the southern Benguela. In the second part of this Chapter a model describing the lateral export of POC from the shelf to the open ocean,

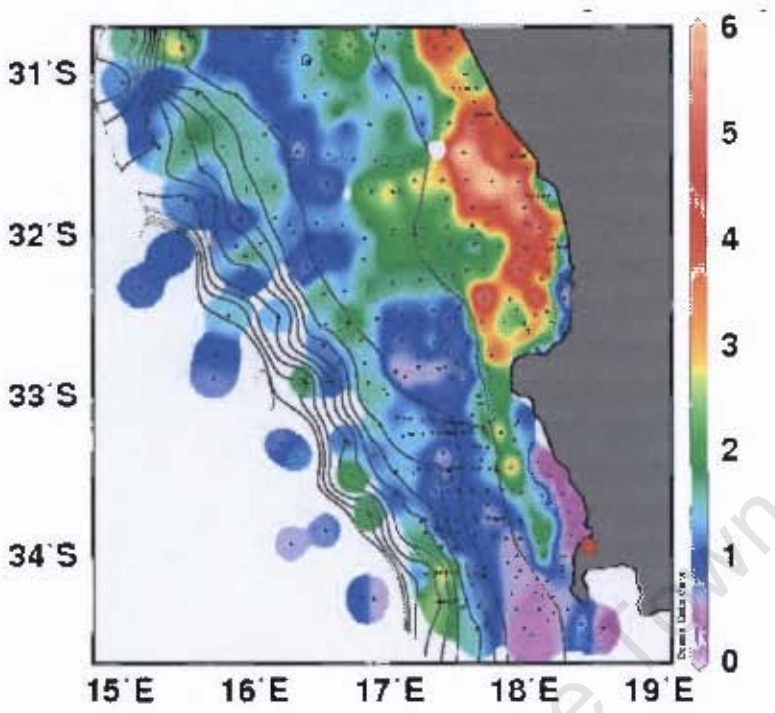

Figure 4.2: The total organic carbon content (weight %) of the sediments in the southern Benguela. Data were obtained from the online material associated with the article by Inthorn et al. (2006). The large red dot marks the position of Cape Town. The solid black lines are bathymetric contours at 200 m, 500m, and at 500 m intervals to 4500 m.

via the BNL mechanism, is developed. The model, based on SHBML turbidity data, is then used to quantify the lateral carbon flux from the southern Benguela in the BNL.

4.2 Data

Full depth hydrographic and turbidity data for all available cruises since the inception, in 2000, of the ≈monthly sampled SHBML was obtained from Marine and Coastal Management, South Africa. However many of the early cruises did not collect turbidity data. Furthermore some cruises had full resolution CTD data available, but for others the data were only available at the discrete depths of Niskin bottle samples. While characterising the vertical extent of the BNL in Section 4.3.1, only the full resolution turbidity data are used, however, when considering the time series in the BNL (Section 4.3.2), both the full resolution and discrete depth data are used. The appendix is furnished with a full list of the data utilized. Where

turbidity data were collected, they were a measure of optical backscatter from a Chelsea Instruments fluorometer. In most instances the CTD was deployed to within 5 m of the bottom, although in instances where that was not the case the data for that Station was discarded. In Chapter 3, a seasonal and depth dependent relationship between turbidity and POC was derived, and is used here to convert turbidity data into POC concentrations.

4.3 Results and discussion

4.3.1 Nepheloid layer distribution

In Chapter 3 cross shelf turbidity distributions were presented which showed very well developed bottom nepheloid layers over the southern Benguela shelf. The BNLs were present during both the summer and winter cruises, were regions of elevated POC and DOC concentrations and were also recognized as being of enhanced biogeochemical significance. To further investigate the presence of BNLs over the southern Benguela shelf, full resolution CTD optical backscatter data from 9 SHBML cruises (see appendix) are analysed here using an automated algorithm designed to detect the presence and vertical extent of BNLs. The algorithm defines a clear water turbidity value, $\mathrm{Tr}_{(\mathrm{cw})}$, as the minimum turbidity at each Station. A nepheloid layer is defined as a region whose turbidity exceeds 2.5× the clear water turbidity value ($Tr > 2.5 \times Tr_{(cw)}$). This limit of $2.5 \times Tr_{(cw)}$ is subjectively chosen, and can be adjusted to improve the performance of the algorithm. The thickness of the bottom nepheloid layer was defined as the height off the bottom where turbidity decreased below $2.5 \times Tr_{(cw)}$. If bottom concentrations were not in excess of $2.5 \times Tr_{(cw)}$ BNL thickness was defined as zero. Figure 4.3 shows four example turbidity profiles from the SHBML data, each of which exhibit a marked BNL. The thickness of the BNL, as determined using the criterion above, is marked by red dots, which show that the algorithm accurately determines the vertical extent of the BNL.

The cross shelf distribution of mean turbidity values at the bottom of the water column

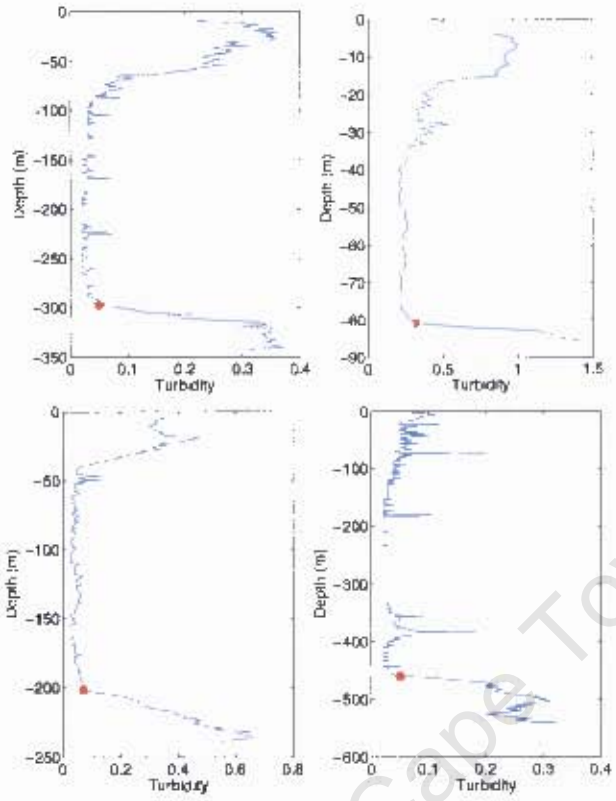

Figure 4.3: Bottom nepheloid layer thickness algorithm performance.

Four example profiles of turbidity, from top left, Station 10 (12/2004), Station 4 (04/2004), Station 7 (07/2003) and Station 11 (08/2003). The red dot marks the position of the top of the BNL, as determined by the algorithm used to derive BNL thickness. For these four Stations, and on the whole, the algorithm appears effective at determining the vertical extent of the BNL.

at each SHBML Station (Figure 4.4) show that turbidity was highest near the coast, and decreased logarithmically with distance across the shelf. A second rapid decrease in turbidity occurred from the shelf break (Station 10) out to Station 12. Turbidity values were also most variable at Station 3, close to the coast, and became progressively less variable with increasing distance offshore. By Station 12, the turbidity at the bottom of the water column was close to zero, and displayed little variability. The cross shelf distribution of turbidity in the BNL resembles the POC distribution presented in Chapter 3, as would be expected from the POC:turbidity correlation. However, the intensified (and highly variable) POC concentrations observed near the shelf break (Figure 4.4; Chapter 3) do not reflect in the mean turbidity intensities. This is also in contrast to observations off Namibia, which show elevated turbidities near the shelf break (Inthorn, 2006a). The reason for the discrepancy

remains unclear, however other measures of BNL variability are a maximum at Station 11, as discussed below.

In Chapter 3, two possible explanations were offered for the observed cross shelf decrease in POC concentrations. The first was that there was a decrease in vertical input of organic matter with increasing distance from the coast, corresponding to the observed decrease in primary productivity (Shannon and Pillar, 1986; Brown et al., 1991; Brown, 1992; Pitcher et al., 1992). The second possible explanation, which drew support from the $\delta^{13}C$ and C:N data, suggested that organic matter was input to the BNL in the highly productive region near the coast, leading to the high concentrations there. Subsequently, the organic matter was proposed to be advected across the shelf, all the while undergoing oxidation, which lead to decreasing concentrations with increasing distance offshore. Since much of the turbidity signal in the BNL is due to POC, the same conceptual models can be applied to explain the cross shelf decrease in optical backscatter. The two competing explanations are considered in detail in Section 4.3.2.

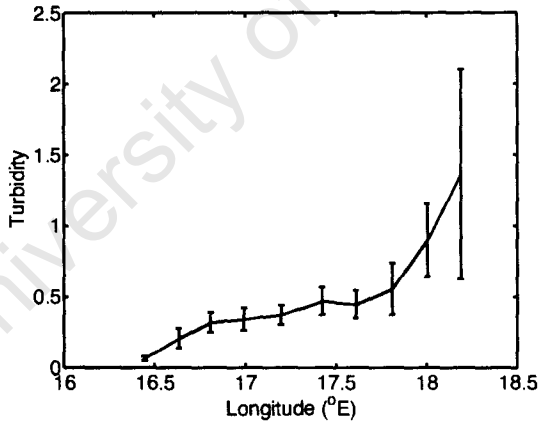

Figure 4.4: Mean and one mean absolute deviation of turbidity at the bottom of the water column across the shelf The solid line marks the mean turbidity at Stations Station 3 (18.2°E) to 12 (16.4°E) on the SHBML, based on continuous and discrete data, and error bars indicate one mean absolute deviation. Turbidity values are highest (and most variable) near the coast at Station 3, and then can be seen to decrease logarithmically, reaching a minimum offshore at Station 12.

The frequency distribution of BNL thickness for the 77 profiles analysed is shown in Figure 4.5. Since the CTD did not reach right to the bottom, BNLs thinner than ~5 m would not have been detected, and would be defined here as zero. A BNL was present over 95%

of the time, with a typical thickness of 20-70 m. The mean thickness of the BNL for the analysed profiles was 56 m, and the median thickness was 47 m. On approximately 10% of occasions, the BNL was thicker than 100 m, and it reached a maximum thickness of 220 m. These BNL thicknesses are typical, and in line with those observed in the central Benguela (Inthorn, 2006a) and on other continental shelves (Cacchione and Drake, 1986; McCave and Hall, 2002).

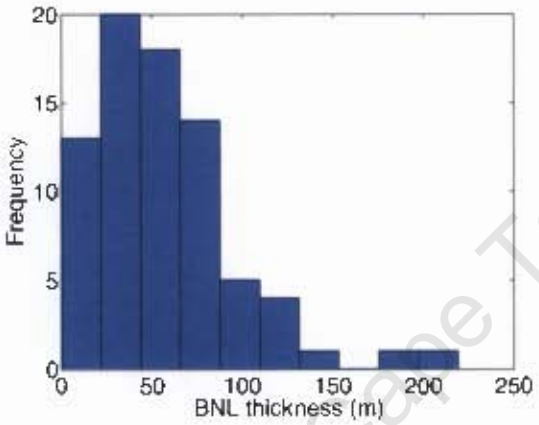

Figure 4.5: Bottom nepheloid layer thickness frequency distribution

Bins are approximately 22 m. At all Stations across the shelf, the BNL has a mean thickness of 56 m, and a median of 47 m. The distribution is heavily skewed towards the right.

The cross shelf distribution of the mean thickness of the BNL (Figure 4.6) reveals that the BNL increases in its vertical extent with increasing distance from the coast. Station 12 has been excluded, because there the CTD was often not deployed to the full depth. The upper slope exhibits the thickest mean BNL (~130 m), there was an intriguing local minimum near the shelf break (16.8°E), and then a near monotonic decrease in BNL thickness from Station 8 (17.2°E) towards the coast. The increase in BNL thickness across the shelf then directly translates into a correlation between BNL thickness and water depth (Figure 4.6, right). The slope of the regression line (not shown) reveals that the thickness of the BNL was typically 20% of the total water depth. The thickness of the BNL can also be seen to have generally increased with increasing bottom boundary layer thickness (as determined from density in Chapter 2; Figure 4.7). However, the BNL was almost always thicker than the BBL (values above the dashed line, which represents a 1:1 relationship), and even on occasions when there

was a thin, or no BBL, a BNL was often still present. Indeed, some of the maximum BNL thicknesses (>100 m) occurred when the BBL was less than 10 m thick.

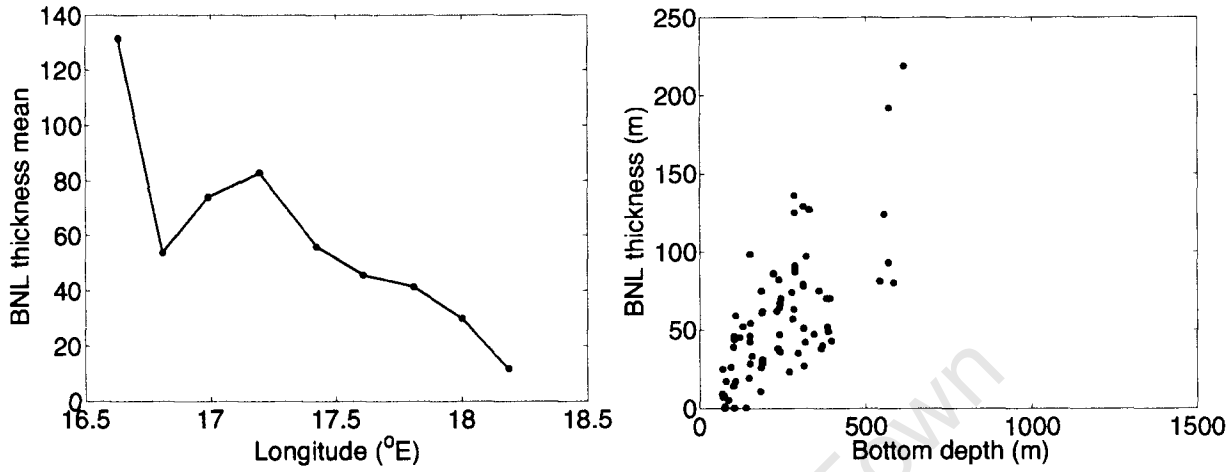

Figure 4.6: The mean thickness of the BNL across the shelf (left) and compared to bottom depth (right) The dots in the left panel mark Station positions on the SHBML, and only Station 3 (18.2°E) to 11 (16.6°E) are shown. The thickness of the BNL can be seen to increase in general across the shelf, reaching its maximum of ≈130 m at Station 11. An intriguing local minimum occurred near the shelf break at Station 10. The vertical extent of the BNL can be seen to be strongly related to the total depth of the water column (right panel). Points from Station 12 have been excluded. For the error estimate associated with this mean, see the Mean Absolute Deviation in BNL thickness shown in Figure 4.8.

The Mean Absolute Deviation in the thickness of the BNL (Figure 4.8), shows a similar pattern to BNL thickness. The MAD was a maximum of 50 m at Station 11 (16.6°E), markedly lower at the adjacent Station 10, and then decreased from the higher variability at Station 9 (17°E) towards the coast. An interesting mid-shelf minimum variability in BNL thickness also occurred at Station 7 (17.4°E). The variability in the thickness of the BBL was also a maximum at Station 11 (Chapter 2), suggesting an intermittent mechanism of enhanced mixing at this location.

In Figure 4.9 the thickness of the BNL is compared to the average buoyancy frequency (N) in the bottom 40 m of the water column at the Station, calculated from the density profile as described in Chapter 2. The minimum BNL thickness increased with decreasing buoyancy frequency, and reduced stability. The maximum BNL thicknesses however displayed a more complicated pattern. The largest BNL thicknesses of ~140 m were found at a buoyancy frequency of around 1.5 cph. Both above and below the N=1.5 cph, the maximum thickness

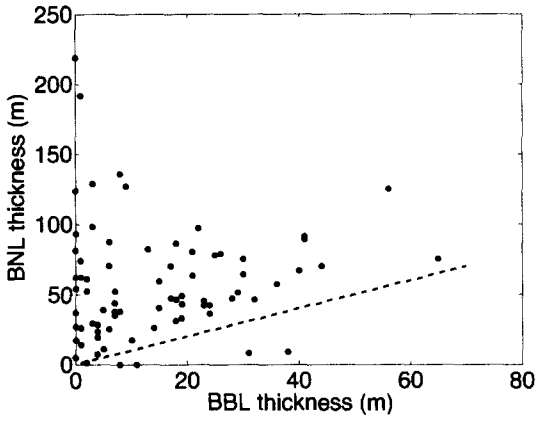

Figure 4.7: The thickness of the BNL vs. the thickness of the bottom boundary layer. The BBL thicknesses are determined from density profiles, as described in Chapter 1. BNL thicknesses are determined from the algorithm described in the text. There is a general increase in the thickness of the BNL as the BBL thickness increases, although it is evident that the BNL is almost always thicker than the BBL (values above the dashed line, representing the 1:1 relationship).

of the BNL decreases. Below N=1 cph, the BNL was never less than 40 m thick. However for N>1.5 cph, the maximum BNL thickness prominently decreases, and in cases reaches zero. The decreasing thickness of the BNL under increasing N relates to enhanced stability suppressing vertical mixing, and is unsurprising (Pond and Pickard, 1983). Similarly, the increasing minimum thickness of the BNL with decreasing N relates to decreased stability and enhanced vertical mixing. However, there is an apparent paradox in the observation that maximum BNL thickness decreases as N decreases below 1.5 cph, which is resolved below.

In Chapter 2, the angle of the bathymetry (λ) in the southern Benguela was compared to the angle of propagation of the internal tide characteristics (c). Figure 4.10 shows the mean λ/c at the SHBML Stations 3-11 for all the available density data. The entire southern Benguela continental shelf is transmissive ($\lambda/c<1$), but on the upper slope, at Station 11, λ/c jumps to very near the critical angle for internal tides. On individual occasions, Station 11 can be critical, and at other times super-critical and therefore reflective, with respect to internal tide propagation. Thus it appears that the region of the upper slope in the southern Benguela could be a site of enhanced internal tide energy dissipation, as discussed in Chapter 2, and shown previously for the central Benguela (Monteiro et al., 2005). In this region the bottom trapped baroclinic tidal energy, creating intensified velocities and shear stresses, would lead

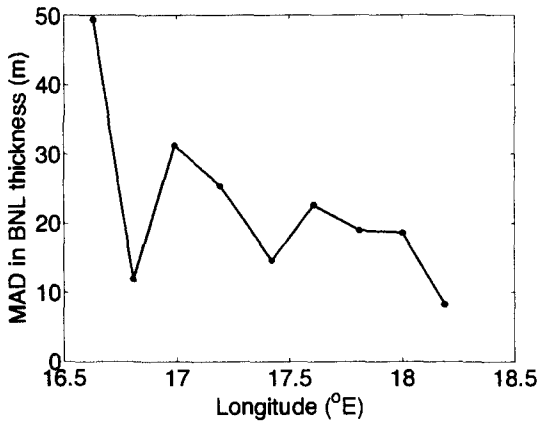

Figure 4.8: The MAD in the thickness of the BNL across the shelf
The dots mark Station positions on the SHBML, and only Station 3 (18.2°E) to 11 (16.6°E) are shown. BNL thickness variability is a maximum at Station 11, on the upper slope, anomalously low at the adjacent shelf break Station (10; 16.8°E) and then generally decreases inshore to Station 3.

to enhanced vertical mixing and potentially resuspend sediments, creating BNLs (Pond and Pickard, 1983; Cacchione and Drake, 1986; McPhee-Shaw and Kunze, 2002). Indeed, the formation and maintenance of BNLs by internal tides has been documented farther north in the Benguela (Inthorn, 2006a), and on many continental shelves and slopes around the world (Cacchione and Drake, 1986; Johnson et al., 2001; McCave and Hall, 2002).

The internal tide mechanism then provides an attractive explanation for why the BNL is so much thicker at Station 11 (Figure 4.6) than elsewhere, and particularly why the variability in BNL thickness (Figure 4.8) is so high at Station 11 compared with the rest of the shelf. The apparent relation between nepheloid layer thickness and internal tides is further supported by the observation in Chapter 3, that the BNL was thicker in March 2006, when the cruise nearly coincided with spring tide, than during the June and August cruises which experienced a smaller tidal range. The fact that near critical conditions for internal tide propagation can occur on the upper slope of the southern Benguela does not preclude the same phenomena from affecting BNL thickness on the rest of the continental shelf. It is known that under transmissive conditions ($\lambda/c<1$), internal tide bottom velocities increase up-slope, until the waves become nonlinear, and eventually break, dissipating their energy in a zone of turbulent mixing (Cacchione and Drake, 1986, p. 148). Thus, when internal tidal

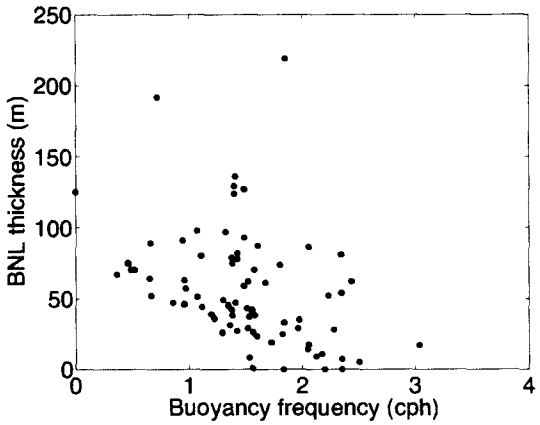

Figure 4.9: The thickness of the BNL vs. the average buoyancy frequency in the bottom 40 m of the water column. It is evident that the minimum BNL thickness is strongly related to the stability of the water column. At high buoyancy frequencies (N) the BNL is zero, while at N below 1.5 cph there is always a BNL present, being over 50 m thick at low N. Maximum BNL thicknesses however exhibit an fascinatingly different pattern. The maximum BNL thicknesses are found near the apparently threshold N value of 1.5 cph. Both above and below N of 1.5, the maximum BNL thickness decreases (see text for a discussion).

energy is not reflected from or focused on the upper continental slope, it could propagate onto the shelf of the southern Benguela, potentially resuspending sediments and generating the observed bottom nepheloid layers (Cacchione and Drake, 1986). Furthermore the paradox of decreasing maximum BNL thickness under decreasing N can be reconciled, if it is considered that the propagation of internal tides is dependent on the buoyancy frequency.

Under weak stratification, internal tidal energy will be reduced, and the internal tidal characteristics will travel at an angle (c) which is very steep, because c and N are inversely proportional (see Chapter 2 for a review on internal tidal characteristics; Cacchione et al., 2002; Pond and Pickard, 1983; Cacchione and Drake, 1986). Thus, below N=1.5 cph where $\lambda/c < 1$, internal tides maybe transmitted across the southern Benguela slope, without dissipating their energy at the bottom, leading to no resuspension or BNL formation. So while decreasing N maybe expected to favour BNL thickening by decreasing stability, it in fact reduces the maximum BNL thickness by reducing baroclinic tidal energy dissipation. However, under increasing stratification (N), the angle of internal tidal propagation will reduce, and in the case where it is coincident with the angle of the local bathymetry (critical), the internal tidal energy will be trapped along the bottom, intensifying velocities and shear stresses (Pond

and Pickard, 1983; Cacchione and Drake, 1986; Cacchione et al., 2002; McPhee-Shaw and Kunze, 2002). If internal tide bottom trapping occurs at a N of around 1.5 cph in the study region, then the associated turbulence and resuspension could explain why BNLs are at a maximum thickness at a N of 1.5 cph. Increasing N further however, would lead to the local bathymetry being reflective of internal tides ($\lambda/c > 1$), minimizing the energy dissipated at the bottom. Such reflection, together with enhanced stability, would then explain the decrease in BNL maximum thickness at N>1.5 cph. Thus on the whole internal tides seem to play a vital role in maintaining the ubiquitous BNLs of the southern Benguela shelf and slope.

The observation that the thickness (and variability) of the BNL decreases towards the coast may be explained by the fact that the N averaged over the water column tends to increase in this direction (Chapter 2). Thus higher stability, which suppresses vertical mixing (Pond and Pickard, 1983), limits the vertical extent of BNLs on the continental shelf. Other factors which affect the thickness of the BNL would be high velocity currents in the BBL, BBL turbulence (see Chapter 2), mixing induced by the barotropic tide, and closer to the coast surface gravity waves which interact with the bottom causing resuspension (Thomsen, 1999, 2002). In reality, all of these mechanisms would combine with the bottom turbulence created by internal tides, to resuspend matter from the seafloor, and keep particulates in suspension in the BNL. BNLs are recognized conduits for shelf ocean exchange of particulates and solutes (Cacchione and Drake, 1986; Thomsen and van Weering, 1998; McCave et al., 2001; van Weering et al., 2001; McCave and Hall, 2002; Thomsen, 2002; Wollast, 2002) and the central Benguela has recently been shown to laterally export organic matter via nepheloid layers (Inthorn et al., 2006). The nepheloid layers, flow field and particle transport in the central Benguela is represented schematically in Figure 4.11. Considering the ubiquitous nature of BNLs in the southern Benguela, documented above and in Chapter 3, and the observed tendency for off-shelf flows in the BBL (Chapter 2), it can be asserted that there should also be a lateral export of matter from the southern Benguela shelf. Such lateral export, particularly with regard to organic carbon, is considered in detail below.

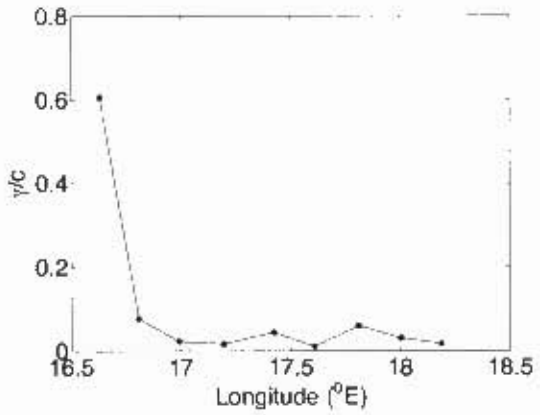

Figure 4.10: The mean cross shelf λ/c for semi-diurnal internal tidal frequencies. The dots mark Station positions on the SHBML, and only Station 3 (18.2°E) to 11 (16.6°E) are shown. The vast majority of the continental shelf is transmissive ($\gamma/c<1$), but at Station 11 on the upper slope near the shelf break, γ/c is close to the critical angle for internal tides (1). Thus internal tidal energy would be bottom focused and intensified near Station 11.

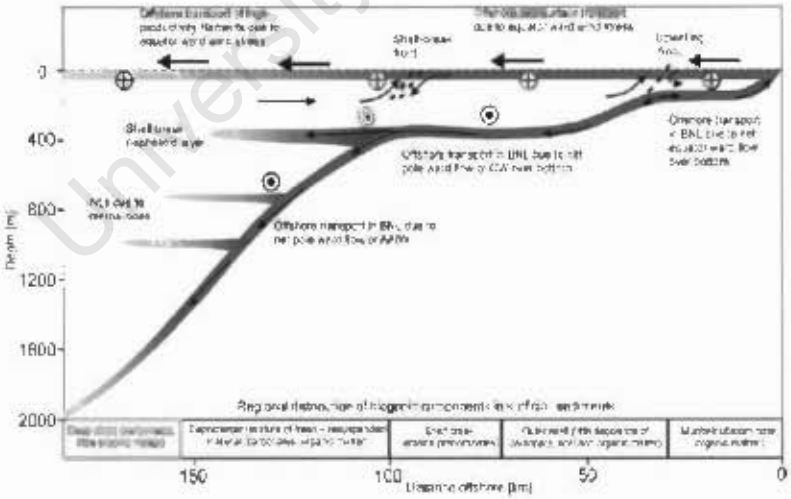

Figure 4.11: Cartoon representation of nepheloid layers, the flow field and particle transport in the central Benguela (from Inthorn (2006a)).

4.3.2 Quantifying lateral carbon export in the bottom nepheloid layer

The mean and mean absolute deviation in turbidity are compared between summer and winter for the surface nepheloid layer and bottom nepheloid layer across the southern Benguela shelf in Figure 4.12. Winter was defined as May-October and summer as November-April. T-tests at the 5% level reveal that at the surface (left), the summer values are significantly higher than the winter values over the shelf (Stations 3-10), but not statistically different over the slope (Stations 11 and 12). In the BNL, despite a small difference evident between the summer and winter distribution inshore, there is not a statistically significant seasonal signal in turbidity concentrations. The same result is produced using a Wilcoxon rank sum test for equal medians (also at the 5% level). The seasonal variation in the SNL, and the perennial nature and lack of seasonality in the BNL strongly suggest that factors other than vertical input from surface primary production maintain the elevated particle concentrations in the BNL. These factors could include resuspension of bottom sediments by turbulence (Chapter 2 and above), as well as lateral advection of particles in the BNL, from the highly productive inshore region, as was suggested above, in Chapter 3, and in other locations (Thomsen and van Weering, 1998; Thomsen, 1999; McCave et al., 2001; van Weering et al., 2001; McCave and Hall, 2002; Thomsen, 2002; Wollast, 2002; Inthorn, 2006a). This result also precludes any other mechanisms that vary with a seasonal cycle from modulating the intensity of the BNL. Such mechanisms include seasonal shifts in the internal wave climate due to changes in buoyancy frequency, or the seasonal shift in bottom turbulence associated with the shelf current structure.

A 4 year time series of turbidity at the bottom of the water column across the southern Benguela shelf is presented in Figure 4.13. What is most evident in the Hovmöller plot is that turbidity concentrations are high inshore, and decrease with distance across the shelf. The outstanding features however, are the tongues of high turbidity which stretch seaward across the shelf in time. It is shown below that these tongues represent pulses of high

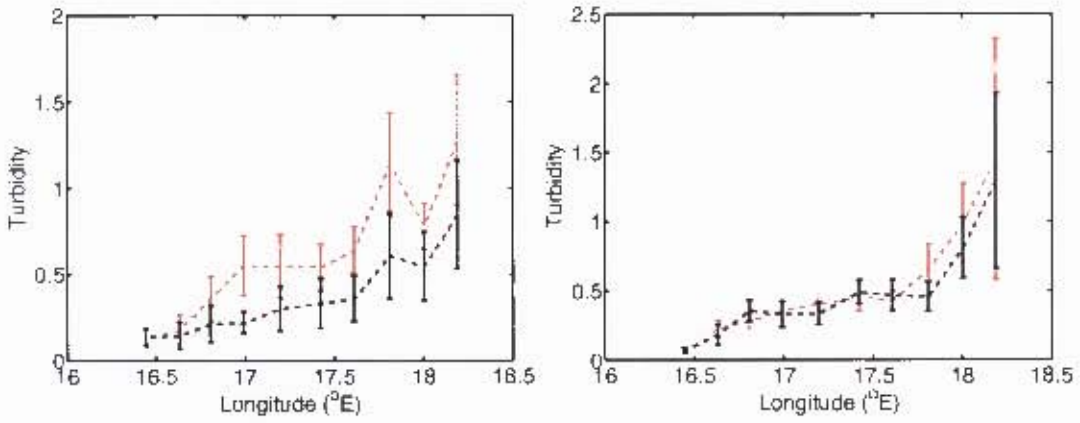

Figure 4.12: Seasonality of nepheloid layers in the southern Benguela

The cross shelf distribution of mean turbidity and variability in the surface nepheloid layer (left) and bottom nepheloid layer (right) during summer (red) and winter (black). Error bars represent one mean absolute deviation. T-tests reveal that at the surface (left), that the summer values are significantly different from the winter values, at Stations 3-10, but not statistically different at Stations 11 and 12. In the bottom nepheloid layer (right), the mean summer and winter distributions are not statistically different. These results illustrate that there is a seasonal signal in turbidity at the surface, corresponding to the seasonality in biological productivity. However in the BNL, there is no clear seasonality in the cross shelf turbidity distribution, indicating that particulate input to the BNL is maintained by sources other than surface productivity alone.

turbidity propagating across the shelf towards the open ocean. Several of the tongues have been marked by eye with solid black lines and the fact that these lines are all nearly parallel indicates that the pulses propagate at a characteristic speed. It can be estimated from the lines that the pulses move seaward by 1 Station on the SHBML (~10 Nm) in a period of two months, corresponding to a speed of just 0.0035 $m.s^{-1}$. The presence of pulses of turbidity propagating from the coast seaward in the bottom turbidity distribution further supports the suggestion that lateral advection plays a role in maintaining the BNL. Furthermore it strongly suggests that off-shelf advection in the BNL could export particulates and organic matter to the deep ocean, as has been previously been suggested in the Benguela (Inthorn et al., 2006; Swart et al., 2007) and elsewhere (Walsh et al., 1988b; Thomsen and van Weering, 1998; Hung et al., 2000; McCave et al., 2001; McCave and Hall, 2002).

The correlation between turbidity and POC confirms that the turbidity pulses would be associated with elevated concentrations of POC (Chapter 3). The critical question becomes whether these pulses transect the shelf break (near Station 10) and enter the deep ocean. This question can be neatly addressed by considering the relationship between salinity and

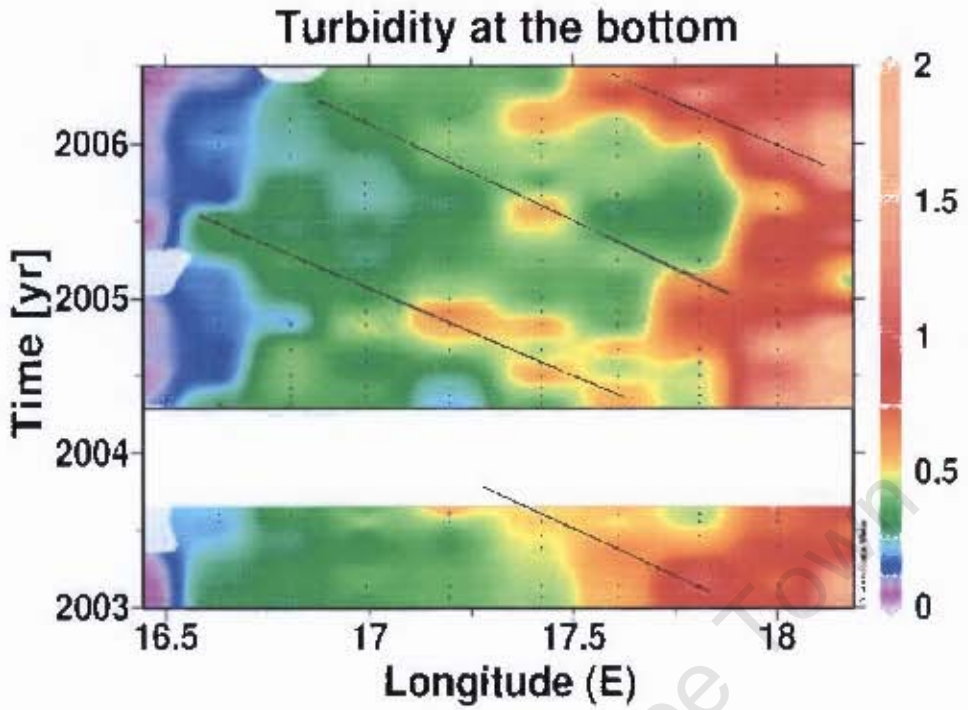

Figure 4.13: Hovmller plot of cross shelf bottom turbidity on the SHBML from 2003-2006
Black dots mark samples positions, and the coast is on the right of the diagram. Turbidity is high near the coast, and rapidly decreases with distance across the shelf, as in Figure 4.4. Tongues of high turbidity can be seen stretching across the shelf, propagating offshore with time. Several such tongues have been marked with solid black lines by eye. The lines are all approximately parallel, indicating that the pulses of high turbidity propagate offshore with a characteristic speed.

turbidity at the bottom of the water column on the upper continental slope, offshore of the shelf break (Station 11). The cross shelf salinity distribution in Figure 4.14 reveals a patch of very fresh water (<34.4) at the base of Station 11, and extending seaward. This layer of fresh water centered at 600 m represents Antarctic Intermediate Water. By contrast, the bottom waters on the continental shelf itself are considerably more saline, reaching over 34.6. Figure 4.14 also shows that salinity and turbidity are significantly correlated (p 0.004) at the base of Station 11. This correlation can be explained by extrusions of high salinity shelf water, which contain elevated turbidities, displacing the fresh AAIW. This evidence then strongly suggests that the observed pulses of turbidity do in fact cross the shelf break and enter the deep ocean. Furthermore, by associating increasing turbidities with water mass changes, this result confirms that it is indeed lateral advection which is responsible for the tongues of high turbidity in Figure 4.13.

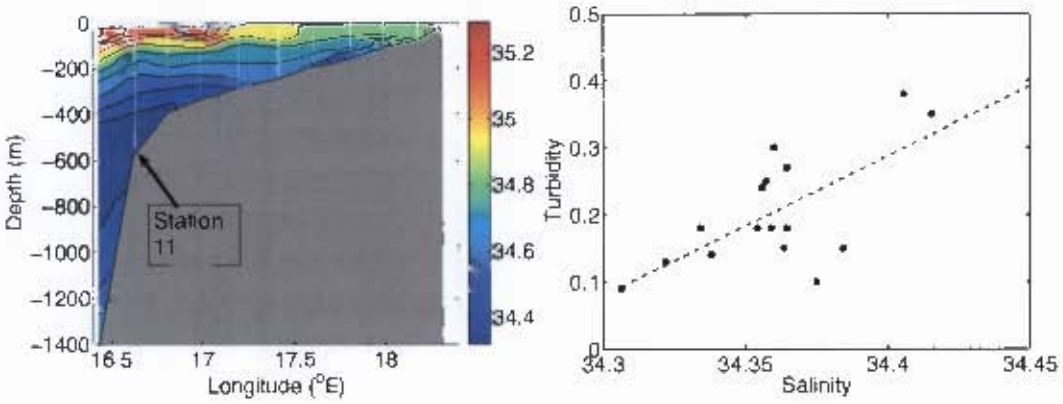

Figure 4.14: The June salinity cross Section as an example (left) and turbidity vs. salinity at the bottom of Station 11 (right). The layer of very fresh (salinity<34.4) water near the bottom at Station 11 is due to the presence of Antarctic Intermediate Water at depths of ~600 m. The water at the bottom, over the shelf, can be seen to be considerably more saline in comparison. At Station 11, turbidity and salinity are correlated (R^2=0.45, p=0.004). This can be explained by high salinity shelf water, displacing the low salinity AAIW at Station 11, and bringing with it high turbidities. This correlation suggests that the pulses of turbidity seen crossing the shelf in Figure 4.13, do in fact cross the shelf break and enter the deep ocean.

To finally confirm the significance of lateral advection in maintaining BNLs, a statistical model of BNL turbidity concentrations (intensity) can be constructed (Table 4.1). Distance from the coast exerts the single strongest influence on BNL intensity, however this was not included in the model, because it seeks to determine the relative importance of vertical input of particles from surface production as opposed to lateral advection. The predictor variables chosen were surface oxygen, surface turbidity, bottom oxygen and lateral advection. The predictor lateral advection was based on the observation above of propagating pulses of high turbidity crossing the shelf at a rate of 1 SHBML Station per two months. Thus the predictor lateral advection for any observation was defined as the turbidity value at the adjacent Station (on the coastal side), two months prior. Naturally this led to Station 3 being excluded from the analysis because it is the Station closest to the coast, and the predictor lateral advection is therefore undefined. The model was built using a forward stepwise regression technique, and in the end the predictor variables surface oxygen, bottom oxygen, and lateral advection were included. This model could explain about 60% of the observed variability in BNL intensity, which is deemed to be impressive, since no term for resuspension was included. The predictor surface turbidity was excluded. This is because it was highly correlated with surface oxygen, and was not useful in explaining any of the additional variability in BNL

intensity once surface oxygen was included. Surface oxygen represents a measure of primary production, and therefore becomes a proxy for vertical input of particulate organic matter to the BNL. Bottom oxygen by contrast likely represents organic matter degradation, and with low bottom oxygens being associated with high organic matter concentrations.

The overwhelmingly clear result of the stepwise regression, shown in the magnitude of the coefficients and t-test statistics, is that lateral advection is the most important and significant predictor of BNL intensity on the southern Benguela shelf. Nonetheless, surface input, and biogeochemical processes near the bottom also play a role. Additionally, the unexplained portion of the variability in BNL intensity by the model suggests that other processes not included, such as resuspension, must also contribute to maintaining the BNL. However, the propagating pulses of turbidity shown in Figure 4.13 above cannot be explained by movements of the bottom turbulence associated with the shelf current structure, or shifts in the internal wave climate or other similar mechanisms which would vary with a seasonal cycle. This point was shown above by the non-seasonality in the intensity of the BNL. Thus lateral advection remains the most likely candidate to explain the tongues of high turbidity, as has been shown here statistically. Overall, the observation of pulses of bottom turbidity propagating across the shelf, the evidence that they enter the deep ocean, the statistical confirmation of the importance of lateral advection in the BNL together with the correlation between POC and turbidity provides convincing evidence that organic matter is exported from the southern Benguela shelf to the deep ocean. The problem becomes quantifying this BNL lateral export flux of organic carbon and assessing its biological and geochemical significance.

The bottom turbidity concentrations across the shelf are considered on a cruise by cruise basis in Figure 4.15. An example from the November 2004 SHBML shows that turbidity does not decrease logarithmically across the shelf as is expected (see Figure 4.4), but is rather interrupted by unexpectedly high turbidities at Stations 7-9. It can be seen from the time-series (Figure 4.15), where the cruise is marked by the horizontal black line, that the anomalously high mid shelf turbidities are caused by one of the propagating pulses of high turbidity. Thus, it becomes evident that the occasional arrival of turbidity pulses at

Regression statistics	
R^2	0.61
R^2 adjusted	0.57
F	18.4
Significance F (p)	0.000
Observations	55

Predictor	Co-efficients	Standard error	t-stat	p-value
Intercept	0.21	-	-	-
Surface Turbidity	0.00	0.16	-0.82	0.42
Surface oxygen	0.06	0.02	2.66	0.01
Lateral advection	0.37	0.09	3.94	0.00
Bottom oxygen	-0.08	0.02	-3.36	0.00

Table 4.1: Predictors of bottom nepheloid layer intensity: stepwise regression
The predictor variable chosen were surface turbidity, surface oxygen, lateral advection (represented by time lagged turbidity from the next most inshore Station; see text for details) and bottom oxygen. It can be seen that the three predictors which were entered into the model were lateral advection, surface oxygen and bottom oxygen. Overall the model can explain nearly 60% of the variability in turbidity in the bottom nepheloid layer. Lateral advection from coast is the most significant predictor of bottom turbidity at any Station, followed by bottom oxygen concentration and then surface oxygen concentration. Surface oxygen concentration is thought to represent primary productivity, and therefore vertical input of organic particles (Surface oxygen is significantly correlated with surface turbidity, thus the latter is excluded from the model). Bottom oxygen concentration has a negative co-efficient, implying that high turbidity values are associated with low oxygen concentrations.

the Stations across the shelf would serve to increase the variability in the turbidity. In an attempt to remove any seasonal or event scale variability caused by periodic injections of POC from the surface, we can normalize (divide) the turbidity values at each Station, by the value at Station 3. This was done for each cruise. Then, reconsidering the cross shelf distribution of turbidity of all the data (Figure 4.15 bottom), we can see that there is a high variability at most stations on the shelf as given by the one mean absolute deviation error bars.

If we instead choose to consider the cross shelf distribution of normalized turbidity in individual water parcels which propagate across the shelf, then the influence of the turbidity pulses would be eliminated. This would then minimize the variability in turbidity at each Station. This approach is equivalent to rotating the line in Figure 4.15, so that it no longer falls upon an individual cruise, but rather slopes with respect to time, as shown in the example in Figure 4.16. If the turbidity data along the sloping black line in Figure 4.16 are normalized by the value at Station 3, and plotted, they would display the expected logarithmic decrease with distance across the shelf. By experimenting with lines of different slopes (which corre-

sponds to different propagation speeds for water parcels crossing the shelf), the one which minimizes the variability in bottom turbidity at all the SHBML Stations, should correspond to the 'true' propagation speed of water parcels crossing the shelf. This is the case, because such a slope would follow water parcels from the coast, where organic matter in input, across the shelf, and the influence of pulses on turbidity would be completely removed. Such an exercise was undertaken by testing many propagation speeds (or line slopes), and measuring the variability using Mean Absolute Deviation (MAD) of turbidity at SHBML Stations 4-12 (since all turbidities were normalized by the value at Station 3, the values at Station 3 became 1 everywhere, and were not included). The result, shown in Figure 4.17, shows that by far the lowest average variability in turbidity is achieved by using a line slope of 2. That is, the water parcel would propagate 1 Station across the shelf in a period of 2 months. This is independent of, but exactly equal to the slope and propagation speed of pulses which was chosen by eye in Figure 4.13 and both approaches affirm each other. The distribution of the mean and mean absolute deviation in turbidity across the shelf, when considered using the water parcel approach and a slope of 2, is shown in Figure 4.16 right. The red line represents in the decay in turbidity in a water parcel as it cross the shelf in time. The variability at all Stations is noticeably lower than when the data are considered on a cruise by cruise basis, as in Figure 4.15.

Having developed the concept of a cross shelf propagation of turbidity and POC in the BNL, it is possible to develop a model which predicts the turbidity at any position across the shelf, and by extension of the linear correlation in Chapter 3, the POC concentration (P.J.S. Franks, pers. comm.). The model, is given by

$$POC_{(x)} = POC_{(0)}.e^{-\frac{\lambda}{u}.x} \quad (1)$$

where $POC_{(x)}$ is the POC concentration ($g\,C.m^{-3}$) in the BNL at a distance x across the shelf in meters; $POC_{(0)}$ is the POC concentration ($g\,C.m^{-3}$) at the coast, where the organic matter in input to the BNL; u is the propagation speed of the water parcel across the shelf in $m.s^{-1}$, determined from the slope of the line; λ is the linearized rate of decay of POC in water parcel as it crosses the shelf and is given by $\lambda = -u.ln\left(\frac{Turbidity_{(x)}}{Turbidity_{(0)}}\right)$. The $\left(\frac{Turbidity_{(x)}}{Turbidity_{(0)}}\right)$

term in λ was taken directly from Figure 4.16. λ is shown in Figure 4.18, and its value at any distance x across the shelf is described by the function

$\lambda_{(x)} = 1.53\times10^{-5}x + 0.55$ (2)

($R^2 = 0.76$; p=0.000).

A typical value for $POC_{(0)}$ during summer was taken as the 75th percentile of the turbidity values at Station 3, and converted from turbidity to POC using the relationship for summer obtained in Chapter 3. The turbidity value was 1.94, and converted to a POC of 0.188 $g\,C.m^{-3}$ (note the change in units from $\mu g.l^{-1}$). The accuracy of the calculations below are subject to the errors associated with this prediction of $POC_{(0)}$. It can be noted in this regard that the value used here 0.188 $g\,C.m^{-3}$ is equivalent to 188 $\mu g.l^{-1}$, which is typical of the actual measured POC concentrations near the coast (Chapter 3). Thus, the error associated with this prediction of $POC_{(0)}$ will not dramatically influence the first order model results presented here. The modelled $POC_{(x)}$ (Figure 4.19), corresponding to this summer value for $POC_{(0)}$, u=0.0035 $m.s^{-1}$, and $\lambda_{(x)}$ as defined in equation 2, shows the logarithmic decay in POC in a water parcel as it transects the shelf. In the model result, there is still POC present in the water parcel once it has been advected past the shelf break. The model only takes into consideration lateral advection and decay in POC with time, and therefore this result shows there is an export of organic carbon from the shelf to the open ocean in the BNL. The model result can be integrated to obtain the amount of POC (gC) on the shelf (green area), and the amount of POC (gC) which has been exported from the shelf (red area) as follows:

$POC_{shelf} = \int_0^{180000} POC_{(x)}dx$ (3)

$POC_{exported} = \int_{180000}^{\infty} POC_{(x)}dx$ (4)

In practise, $POC_{(x)}$ has decayed to very nearly zero by 350 000 m offshore and this can be used as the upper limit to the integral in 4. The results which are derived correspond to the concentrations per meter of nepheloid layer thickness and per meter along the shelf. These can subsequently be scaled up to represent a (typical) 50 m thick nepheloid layer, and a 1500 km long coastline for the southern Benguela. This assumes that the nepheloid layers

present on the SHBML are ubiquitous on the southern Benguela shelf, that the rest of the shelf contains similar POC concentrations, and that water parcels propagate across the shelf in a similar manner everywhere.

From the above considerations it is possible to derive a flux of POC across the shelf break ($g\,C.s^{-1}$), defined as

$$POC_{flux} = u.\frac{POC_{exported}}{\delta x}$$

where u is the characteristic water parcel propagation velocity, and δx is the distance between the shelf break and where $POC_{(x)}$ decays to zero (350 000 m offshore). This calculated lateral carbon flux for the BNL in the southern Benguela, can then be scaled to an annual estimate ($\times 365 \times 24 \times 60 \times 60$). The final annual export of organic carbon in the BNL calculated in this way is 6.32×10^{10} g C.yr^{-1}. This lateral export flux corresponds to only a tiny fraction (<1%) of southern Benguela annual primary production (7.7×10^{13} g C; Brown et al., 1991). The flux estimate could be refined by integrating separately for summer and winter values of $POC_{(0)}$, but this would only serve to decrease the estimate flux further.

While this estimate of the lateral carbon export in the BNL appears very small, it neglects any export which may occur in intermediate nepheloid layers, which are occasionally evident of the southern Benguela slope. Furthermore, since conditions were assumed to be uniform along the shelf, no account was taken for the additional export which may occur in regions of enhanced shelf-ocean exchange, such as canyons (van Weering and McCave, 2002), or during periods of intensified off-shelf flow when velocities would have been larger than 0.0035 $m.s^{-1}$ (Chapter 2). Indeed, careful consideration of the sediment TOC distribution (Figure 4.2) reveals abnormally high values on the slope coinciding with the mouth of the Cape Canyon (near 34.1°S, 17.5°E). The down-canyon flow noted in Chapter 2 likely carries organic carbon down the canyon, until it is deposited near the mouth, leading to the elevated TOC concentrations. This further suggests the canyon as a preferential conduit for shelf-ocean exchange. Furthermore, it should be emphasized that the calculation here also assumes that the turbidity signal on the southern Benguela shelf was fully modulated by lateral advection. While it is known from the stepwise regression that lateral advection was the most important

process, the modulation of the turbidity signal by other processes not accounted for introduces an error into the estimates made here. It is asserted however, that even if this error was large, either doubling or halving the estimated export - the conclusion that less than 5% of primary production was exported remains robust.

Nonetheless it has been the finding of the majority of the continental margin exchange programs that the vast majority of organic matter is oxidized on the shelf, and that only a small fraction is exported to the open ocean (Rowe et al., 1986; Falkowski et al., 1988; Biscaye et al., 1994; Wollast and Chou, 2001b; Verity et al., 2002). Furthermore, estimates of bacterial consumption for the southern Benguela system suggest that 86-147% of primary production is consumed on the shelf, leaving little for lateral export (Brown et al., 1991). This has also been supported by the findings of a previous modeling study, which found that primary production is fully consumed by heterotrophs on the southern Benguela shelf, and that there is only a marginal export of POC through fecal pellets (Monteiro, 1996). Consideration of the accumulation of organic carbon in the slope sediments of the southern Benguela over the period of the Holocene (Compton, Holocene terrestrial-marine organic carbon fluxes estimated for the western continental margin of South Africa, in prep.) show that ≈0.22 Gt C OC have accumulated over the 10 000 year period. This is only 35% of the potential lateral export during the period, obtained if the annual figure calculated above is scaled to the length of the Holocene (6.32×10^{10} g C.yr$^{-1}\times$10 000 years=6.32×10^{14} g C). Since a large fraction of the export flux of POC from the shelf would be lost during early diagenesis (Lochte et al., 2003), these figures are actually in good agreement, and suggest that the major fraction of OC preserved on the continental slope in the southern Benguela may be supplied by lateral advection as opposed to vertical input. This has, for example, been shown to be the case in the central Benguela region (Inthorn, 2006a). Furthermore, what has not been discussed thus far, is the role in the lateral POC flux in meeting benthic carbon demand over the continental slope. Lateral input of carbon via BNLs has been shown to be a vital factor for maintaining the active benthos on other continental slopes (Thomsen and van Weering, 1998; Thomsen, 1999; Rutgers van der Loeff et al., 2002; van Weering and McCave, 2002). Estimates of ben-

thic carbon demand from the Barents sea, at a similar depth to the southern Benguela slope, were 50 $mg\,C.m^{-2}.day^{-1}$ (Thomsen, 1999). The area of the southern Benguela continental shelf can be estimated at $1.2\times10^5\,km^2$ (1500 km × 80 km) giving an annual benthic carbon demand for the southern Benguela slope of 2.2×10^{12}g C. Thus the calculated lateral export of POC could account for only ~3% of benthic carbon demand calculated in this way, and the remainder would have to be supplied by vertical input, or from other sources.

What has not been considered here, is the flux of DOC. The observations in Chapter 3, as well as previous carbon flow models (Touratier et al., 2003), have shown that there is a large flux from primary production into the DOC pool. The large gradient in DOC between the Benguela shelf and the open ocean ($>100\mu g\,C.l^{-1}$; see Chapter 3) near the bottom of the water column, together with the documented off-shelf flow at depth, dictate that there should be an export of DOC from the system to the open ocean. For a 50 m thick BNL, a 1500 km long coastline, and an off-shelf propagation speed of 0.0035 $m.s^{-1}$, this could lead to a flux of $8.27\times10^{11}\,g\,C.yr^{-1}$ or about 1% of total primary production. Thus, in the BNL, the potential lateral export flux of DOC is an order or magnitude greater than the potential POC flux. This dominant role of DOC over POC in export fluxes has been recognized in previous studies off the east coast of the USA, the East China Sea, and in general (Hung et al., 2000; Álvarez-Salgado et al., 2001; Hopkinson Jr. and Nolin, 2002; Chen et al., 2003). Added together, the POC and DOC lateral export fluxes derived here remain a small portion (<2%) of annual primary production in the southern Benguela, in stark contrast to previous system budgets which estimated the potential flux at close to 60% of annual new production (Waldron et al., 1998; Swart et al., 2007). By far and large, it seems that the southern Benguela is consistent with other continental margins, by oxidizing the majority of annual primary production on the shelf, and laterally exporting only a small fraction of the photosynthetically fixed organic carbon (Chen et al., 2003). From the results of Monteiro (1996), it can be calculated that the SACW upwelling in the southern Benguela has a total CO_2 concentration which is approximately 100 $\mu mol.m^{-3}$ in excess of the value required for water at the typical temperature of 18°C and 35 psu, to be in partial pressure CO_2 equilibrium

with the atmosphere. From this it can be approximated that about $3.6\times10^{12}\,gC.yr^{-1}$ of primary production must be permanently exported to make the system carbon neutral with respect to the atmosphere. The POC + DOC flux of $\approx 8.5 \times 10^{11}\,gC.yr^{-1}$ calculated above for the bottom nepheloid layer can account for about 23% of this value. Export in the intermediate levels of the water column, or burial of organic carbon in the shelf sediments could help to fill the remainder of the required export quota to achieve a carbon neutral system. Indeed, it has been shown that the southern Benguela is a marginal CO_2 sink (Monteiro, 1996), suggesting the total export flux of primary production in fact exceeds the value required to make the system neutral with respect to the atmosphere.

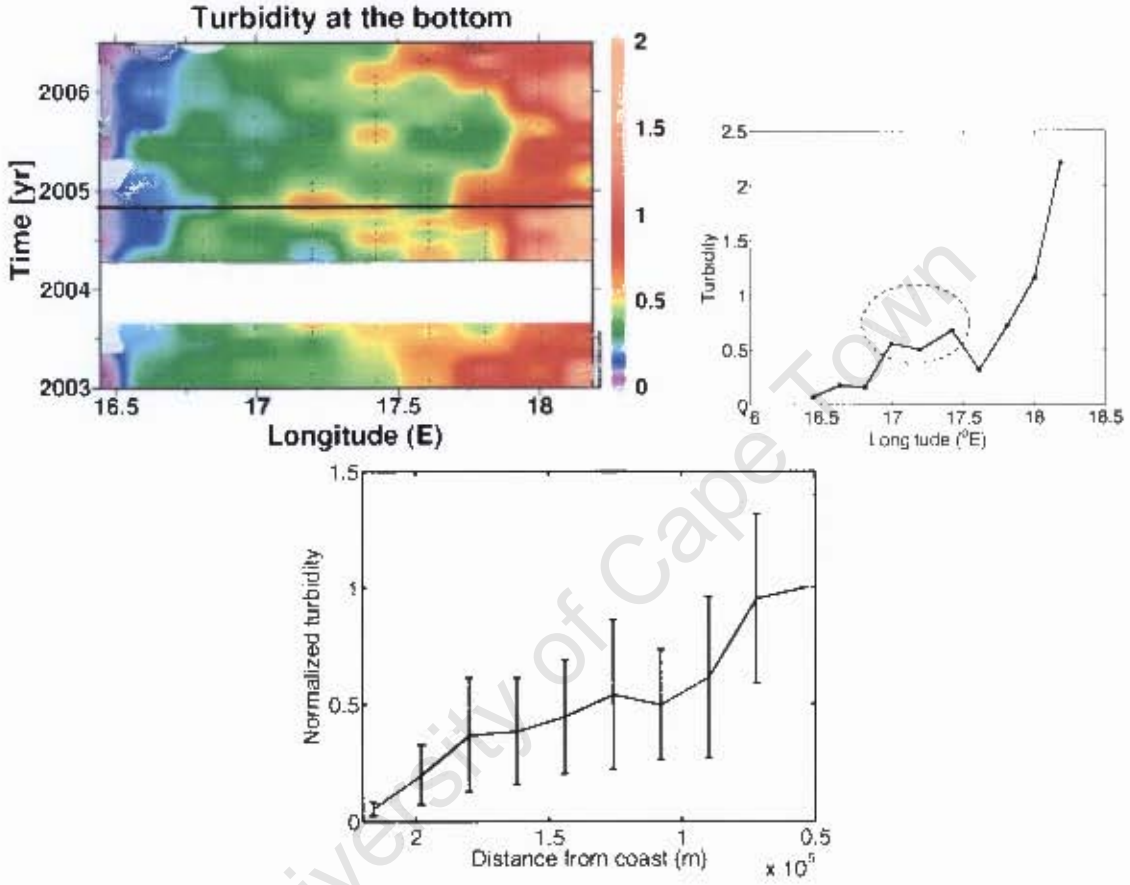

Figure 4.15: Variability in cross shelf BNL turbidity by cruise

The cross shelf distribution of turbidity considered on a cruise by cruise basis. The cross shelf turbidity distribution during the SHBML of November 2004 is shown on the top right (corresponding to the solid black horizontal line on the Hovmöller plot). It can be seen that at Stations 7, 8 and 9, turbidity values are significantly higher than would be expected from the characteristics 'logarithmic decay' shown in Figure 4.4. It can be seen from the hovmöller (top left), that the high values at these Stations are caused by one of the propagating pulses of turbidity which transect the shelf. These pulses tend to cause high variability in turbidity values at all the Stations on the shelf. This is evident in the large mean absolute deviations at each Station given by the error bars in the bottom panel. The solid line represents the mean cross shelf turbidity of the SHBML data. The values for each cruise were normalized by the turbidity value at Station 3 for that cruise, to remove seasonal variations.

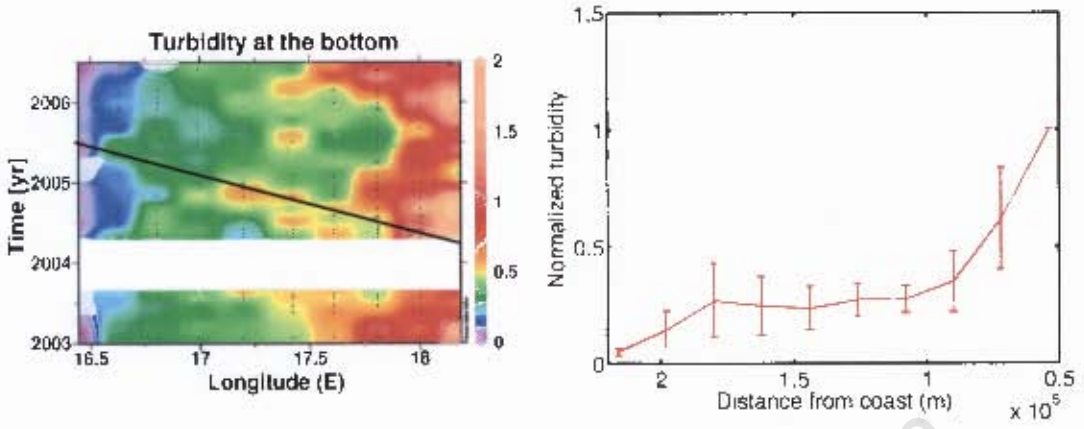

Figure 4.16: Variability in cross shelf BNL turbidity by water parcel.

By following water parcels as they propagate from the coast across the shelf (e.g. solid black line, left panel), the influence of the pulses of turbidity can be removed from the cross shelf distribution. The right panel shows the mean, and one mean absolute deviation (error bars) in turbidity at each Station, obtained by following water parcels across the shelf, as opposed to considering turbidity on a cruise by cruise basis. It can be seen that as the water parcel crosses the shelf, turbidity within the water decays logarithmically. The values have been normalized by the turbidity at the coast (Station 3), and thus the red line corresponds to $\frac{Turbidity_{(x)}}{Turbidity_{(0)}}$. See text for details on tracking the water parcels across the shelf.

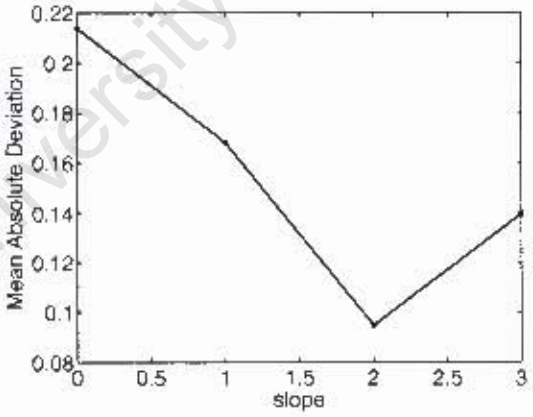

Figure 4.17: Minimizing cross shelf variability in BNL turbidity.

Mean absolute deviation (y axis) represents the mean variability in BNL turbidity at all 12 SHBML Stations. By following individual water parcels across the shelf in the BNL, the variability in turbidity at each Station should be minimized because the influence of propagating pulses of high turbidity is removed. Various propagation speeds (corresponding to the steepness of the slope of the line in 4.16) were tested. The mean absolute deviation in turbidity of all 12 SHBML Stations shows a minimum when a slope of 2 is used. This corresponds to a water parcel moving laterally 1 Station in a period of 2 months, or at 0.0035 $m.s^{-1}$. Interestingly, a slope of 2 was also selected when following the pulses of turbidity by eye (Figure 4.13).

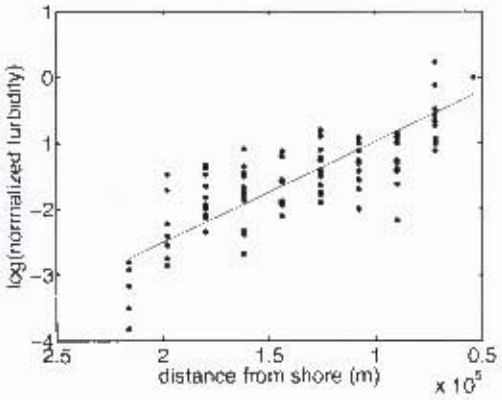

Figure 4.18: Turbidity decay function (λ)

The decay in turbidity in water parcels propagating across the shelf in the BNL at a speed of 0.0035 $m.s^{-1}$ (see Figure 4.17 and 4.16). The decay has been given as a function of distance across the shelf, and the values of turbidity have been logged so as a linear relationship could be derived. The turbidity values in each water parcel were normalized by the value in the water parcel at Station 3. The linear regression (dashed line), is given by the relation: $\lambda_{(x)} = 1.53 \times 10^{-5} x + 0.55$ ($R^2 = 0.76$; $p = 0.000$).

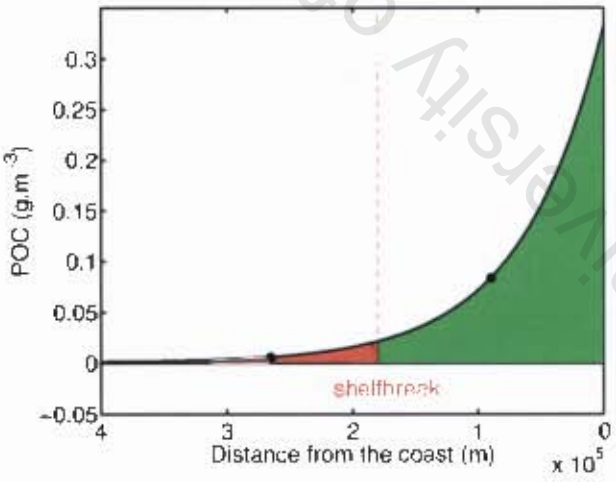

Figure 4.19: Modelled POC decay and export from the southern Benguela shelf.

The solid black line shows the predicted logarithmic decay in POC in a water parcel in the BNL as it crosses the shelf, given by the model (see text). The green area represents the integrated POC between the coast and the shelf break, the red area represents the integrated POC between the shelf break and where is decays to zero (~350 km). This red area represents the amount of POC which is exported from the southern Benguela shelf to the open ocean, per meter of continental margin, and per meter thickness of the BNL. The black dots mark the central positions of the shelf (90 km), and the exported POC (265 km).

4.4 Summary and Conclusions

Bottom nepheloid layers are ubiquitous features of the southern Benguela continental shelf and slope, being present in both summer and winter, and displaying no seasonality in their intensity. Particle concentrations are highest adjacent to the coast, where vertical input from surface production is greatest, and decrease logarithmically with increasing distance across the shelf. The BNL is typically 50 m thick, although thickness increases with distance across the shelf and hence with water depth. Particles in the BNL are kept in suspension through turbulence generated by currents in the BBL, barotropic tides, and surface gravity waves. They appear to be predominantly controlled however, by the shear stresses associated with internal tides. Bottom dissipation of internal tidal energy is concentrated on the upper slope, where the angle of the bathymetry is close to the angle of propagation of the internal tide. This leads to the BNL being thickest, and most variable in height over the upper continental slope, in about 600 m of water. Internal tides which are transmitted onto the shelf may also become critical, break, and cause resuspension of bottom sediments in zones of active turbulence. On the shelf, the thickness of the BNL decreases as stability in the water column increases and suppresses vertical mixing.

Particle concentrations in the BNL were shown statistically to be maintained by lateral advection rather than vertical input. The presence of a seasonal signal in surface layer particle concentrations, and the lack of a seasonal signal in the BNL further confirms this finding. Hovmöller plots of bottom turbidity times series on the SHBML reveal that pulses high turbidity propagate seaward across the southern Benguela shelf at a characteristic speed. These pulses of turbidity are known to be associated with elevated POC concentrations, and furthermore were shown to transect the shelf break and enter the deep ocean. The lateral export flux of POC in the BNL associated with cross shelf movement was quantified using a power model, and shown to comprise only a small fraction of southern Benguela annual primary production. The flux is however in good agreement with the sedimentation rate of OC on the continental slope over geological time. The lateral POC flux is only able to meet a fraction of the benthic carbon demand on the continental slope, assuming that the benthos

of the southern Benguela has similar requirements to that of the Barents Sea. The known gradients in DOC between the southern Benguela and the open ocean could lead to an export flux of an order of magnitude greater than the POC flux, but would still only represent a small fraction of total annual production. In the southern Benguela, as on most continental shelves that have been observed, the majority of photosynthetically fixed organic carbon is oxidized on the shelf. Thus export in the BNL accounts for less than one quarter of the flux required to make the southern Benguela carbon neutral with respect to the atmosphere.

Chapter 5

Highlights, conclusions and recommendations

The global ocean is the most important player in regulating the level of atmospheric carbon dioxide on millennial timescales. The critical feature of the ocean carbon reservoir is the vertical gradient in DIC, which maintains vast quantities of carbon at depth, isolating them from atmospheric exchange. Three quarters of the observed vertical DIC gradient is maintained through the action of the oceans biota and the biological pump. Furthermore certain regions of the ocean exhibit enhanced biological productivity, which acts to photosynthetically draw down atmospheric carbon dioxide. In particular, the continental margins account for a disproportionally large fraction of the total ocean carbon fixation, and biogeochemical cycling. Thus it has been recognized for some time that lateral fluxes of organic carbon from the continental margins into the deep ocean could play a significant role in the biological pump. Nonetheless, global carbon cycle models tend to ignore the biological component, and where they do account for it, it is parametrized erroneously as a purely vertical flux. The southern Benguela upwelling system is by area one of the most productive and biogeochemically active ecosystems in the global ocean. However, previous studies have disagreed on the potentially significant ability of the system to laterally export organic carbon to the deep ocean. It is within the context of this debate that the current study undertook to examine the physical

and biogeochemical aspects of a lateral carbon flux from the southern Benguela upwelling system.

While several potential physical mechanisms capable of inducing seaward advection were discussed, it was recognized from studies on other continental margins and previous work in the Benguela that the bottom boundary layer was the most likely region of lateral carbon flux. Although the BBL had been previously recognized in the system, here the first attempt to characterize its vertical extent, cross-shelf distribution and flow characteristics was made using historical hydrographic and current meter data. It emerged from the analysis that the BBL was a persistent feature of the southern Benguela shelf and slope, its vertical extent and variability being controlled by water column stability and the presence of turbulence generating mechanisms. Off-shelf flow in the BBL was predicted theoretically to occur during poleward flow regimes, owing to cyclonic Ekman veering caused by bottom friction. Analysis of near bottom recording current meter records showed that this was indeed the case over much of the shelf and slope. Particular regions, most notably the Cape Canyon, experienced unprecedented off-shelf velocities at all times, highlighting such regions as conduits of shelf-ocean exchange. The forcing mechanisms responsible for modulating these cross-shelf fluxes varied spatially, but coastal trapped waves, tides and anonymous low frequency processes dominated the energy spectrum's of the RCM records. In addition to its importance for lateral biogeochemical exchanges, the BBL is significant because it influences benthic dwelling organisms, and commercially important bottom dwelling fish species such as Hake, not to mention its role in bottom energy dissipation, as well as shelf-ocean hydrographic, tracer and pollutant exchange. Despite this, almost none of the historic RCM moorings contained instruments within the bottom few meters. It is suggested that in order to fully quantify lateral advection and turbulence dissipation in the BBL, moorings with near bottom upward facing ADCPs should be deployed during future studies, especially in the data-sparse region of the shelf break.

Internal waves are another phenomenon which had previously been identified as crucial to vertical mixing, nutrient exchange and tidal energy dissipation in the Benguela, but little

studied. Here, for the first time, the characteristics of internal tide propagation over the bathymetry of the southern Benguela was examined with the aid of historic density profiles. The results showed that the semi-diurnal internal tide should preferentially dissipate its energy on the upper continental slope, perhaps even becoming completely bottom trapped in this region. Significant baroclinic velocities at internal tidal frequencies were evident on the upper continental slope in one RCM record. Such energy dissipation and turbulent mixing would be critically important for sediment resuspension and bottom nepheloid layer formation, not to mention lateral advection caused by asymmetry in the tidal flows. The semi-diurnal tides were more likely to propagate onto the shelf in summer, and clear evidence of such waves at tidal frequencies was evident in near-shore fluctuations in the height of the thermocline. Thus, shoaling internal tides were also recognized as a mechanism controlling bottom mixing over much of the continental shelf. Despite the interesting information which this study revealed regarding internal tide propagation on the southern Benguela shelf, it could be significantly improved by using a higher resolution bathymetric database in future studies. Furthermore, in the event that future studies deploy moorings, positioning current meters at several depths, including near the bottom and near the surface, together with a thermistor string, would reveal valuable information on internal wave dynamics, provided that the sampling interval was sufficient.

While many studies have been conducted on biogeochemical aspects of the southern Benguela system, none of them to date has been fully inclusive. This is particularly true of denitrification, which although identified as relevant in the central part of the system, has been given less attention in the southern Benguela. Here use of the tracer N* using nutrient data from sampled cruises revealed that a nitrogen deficit exists in the system, at least seasonally. The nitrogen deficit was correlated with oxygen deficiency and elevated nitrite concentrations, which supported the hypothesis that denitrification was occurring, although it was not possible to eliminate the possibility that anammox was causing the signal. Indeed, all the biogeochemical variables measured showed a marked seasonal signal. This included particulate organic carbon, which it was found occurs in substantially higher concentrations in

the southern Benguela, than on other continental margins. Furthermore, the strong horizontal POC gradients which were evident suggested that a significant lateral export of organic carbon was possible during off-shelf flow conditions. Overall the largest gap in previous observational research in the southern Benguela has been the neglect of dissolved organic matter. A highlight of this study was the documentation of the first known reliable estimates of DOC and total nitrogen for the system. These variables too showed a significant seasonal variation, accumulating over summer and decaying over winter. The high concentrations of DOC identified it as the dominant organic carbon pool in the southern Benguela, and the horizontal gradients between the Benguela edge and the central South Atlantic suggested DOC as the best candidate to induce a lateral carbon flux. Within the water column, the bottom nepheloid layer was identified as a biogeochemical hotspot, because it was the preferential site of oxygen deficiency, denitrification, organic matter accumulation and it exhibited the strongest horizontal gradients.

Bottom nepheloid layers have been identified and described previously in the central Benguela, but their existence has only been alluded to in the southern system. Optical techniques which have proved successful elsewhere were used to provided a characterization of bottom nepheloid layer vertical extent and cross shelf distribution for the first time in the southern Benguela. These results showed that the BNL was ubiquitous over the shelf and slope, thicker than the BBL, and modulated by a complex interaction between water column stability and turbulence generation. Significantly it was found that the BNL was not seasonal, and that it was maintained through lateral advection rather than vertical input of particulate matter. Indeed, a unique and intriguing time series of turbidity extending across the shelf showed pulses of turbidity propagating across the shelf in time. It was known that such pulses were associated with elevated levels of particulate organic carbon, because a statistically significant relationship was derived between the two variables. Furthermore, by combining the time series results with concurrent hydrographic data, it was shown that the particulate matter pulses transected the shelf break and entered the deep ocean. Despite the significance of these results, the data were only available at a monthly period, and for one transect across

the shelf. Higher frequency events and alongshore variability would have been completely missed in the analysis here. While more frequent or extensive cruises are cost prohibited, future studies could obtain higher temporal resolution optical backscatter data by deploying a mooring with a turbidity sensor near the bottom. Such a dataset could significantly refine our perceptions of particulate matter dynamics at the shelf slope interface. Through a cross-shelf carbon flux model based on the turbidity time series, it was possibly to quantify the annual lateral export flux of POC from the southern Benguela continental shelf to the deep ocean. Although the model could be improved, the result indicated that the vast majority of organic carbon was oxidized on the continental shelf, and that only a small fraction (<1%) of primary production was exported seaward of the shelf break as POC. Despite the small magnitude of the lateral POC flux, it was in good agreement with geological rates of organic carbon accumulation on the upper continental slope. The potential lateral DOC flux was estimated as an order of magnitude greater than the POC flux, but still a negligible fraction of total primary production. These results from the southern Benguela agree with those obtained on other continental margins, which suggest that lateral organic carbon export is a small fraction of primary production, because the majority of organic matter is oxidized on the shelf. Thus the BNL export fulfilled only about one quarter of the organic carbon export flux required to make the system carbon neutral with respect to the atmosphere. Nonetheless many new interesting questions have been raised. To name a few, the nature of internal waves, the dynamics of nutrient cycling and denitrification and the characteristics of DOM in the southern Benguela are all deserving of further attention.

Bibliography

Alley, R., 2000. Ice-core evidence of abrupt climate changes. Proceedings of the National Academy of Sciences of the USA 97 (4), 1331–1334.

Álvarez-Salgado, X., Doval, M., Borges, A., Joint, I., Frankignoulle, M., Woodward, E., Figueiras, F., 2001. Off-shelf fluxes of labile materials by an upwelling filament in the NW Iberian Upwelling System. Progress in Oceanography 51, 321–337.

Andrews, W., Hutchings, L., 1980. Upwelling in the southern Benguela current. Progress in Oceanography 9, 1–81.

Azam, F., 1998. Microbial Control of Oceanic Carbon Flux: The Plot Thickens. Science 280 (5364), 694–696.

Azam, F., Long, R., 2001. Sea snow microcosms. Nature 414, 495–498.

Bailey, G., 1987. The role of regeneration from the sediments in the supply of nutrients to the euphotic zone in the southern Benguela system. South African Journal of Marine Science 5, 273–285.

Bailey, G., Chapman, P., 1991. Short term variability during an anchor station study in the southern Benguela upwelling system: Chemical and physical oceanography. Progress in Oceanography 28, 9–35.

Bauer, J., Druffel, E., 1998. Ocean margins as a significant source of organic matter to the deep ocean. Nature 392, 482–485.

Behrenfeld, M., Falkowksi, P., 1997. Photosynthetic rates derived from satellite-based chlorophyll concentration. Limnology and Oceanography 42 (1), 1–20.

Berelson, W., 2001. The flux of Particulate Organic Carbon into the ocean interior. Oceanography 14 (4), 59–67.

Bergman, N., Lenton, T., Watson, A., 2004. Copse: A new model of biogeochemical cycling over Phanerozoic time. American Journal of Science 304, 397–437.

Berner, R., 2005. A history of atmospheric CO_2 and its effects on plants, animals and ecosystems. No. 1. Springer, New York, Ch. 1, pp. 1–7.

Berner, R., Kothavala, Z., 2001. GeocarbIII: A revised model of Atmospheric CO_2 over Phanerozoic time. American Journal of Science 301, 182–204.

Bickert, T., 2000. Marine Geochemistry. Springer, Berlin, Ch. 10, pp. 309–333.

Biscaye, P., Flagg, C., Falkowski, P., 1994. The Shelf Edge Exchange Processes experiment, SEEP-II: an introduction to hypotheses, results and conclusions. Deep-Sea Research II 41, 231–252.

Bishop, J., 1999. Transmissometer measurement of POC. Deep-Sea Research I 46, 353–369.

Blunier, T., Brook, E., 2001. Timing of millenial-scale climate change in Antarctica and Greenland during the last glacial period. Science 291, 109–112.

Blunier, T., Monnin, E., Barnola, J., 2005. A history of atmospheric CO_2 and its effects on plants, animals and ecosystems. Springer, New York, Ch. 4, pp. 63–82.

Brink, K., 1987. Upwelling fronts: Implications and unknowns. South African Journal of Marine Science 5, 3–9.

Brink, K., 1998. The Global Coastal Ocean: Processes and Methods. Vol. 10 of The Sea. John Wiley & Sons, Ch. 6, pp. 151–170.

Broeker, W., 2003. Does the trigger for abrupt climate change reside in the ocean or in the atmosphere? Science 300, 1519–1522.

Brown, P., 1992. Spatial and seasonal variation in chlorophyll distribution in the upper 30 m of the photic zone in the southern Benguela/Agulhas ecosystem. In: Payne, A., Brink, K., Mann, K., Hillborn, R. (Eds.), Benguela Trophic Functioning. Vol. 12. pp. 515–525.

Brown, P., Hutchings, L., 1987. The development and decline of phytoplankton bloms in the southern Benguela upwelling system. 1. Drogue movements, hydrography and bloom development. South African Journal of Marine Science 5, 357–391.

Brown, P., Painting, S., Cochrane, K., 1991. Estimates of the phytoplankton and bacterial biomass and production in the northern and southern Benguela ecosystems. South African Journal of Marine Science 11, 537–564.

Cacchione, D., Drake, D., 1986. Nepheloid layers and internal waves over continental shelves and slopes. Geo-Marine Letters 6, 147–152.

Cacchione, D., Pratson, L., Ogston, A., April 2002. The shaping of continental slopes by internal tides. Science 296, 724–727.

Calvert, S., Price, N., 1971. Upwelling and nutrient regeneration in the Benguela current. October, 1968. Deep-Sea Research 18, 505–523.

Carlson, C., 2002. Biogeochemistry of Marine Dissolved Organic Matter. Academic Press, San Diego, Ch. 4, pp. 91–141.

Carr, M., 2002. Estimation of potential productivity in Eastern Boundary Currents using remote sensing. Deep-Sea Research II 49, 59–80.

Chapman, P., Shannon, L., 1985. The Benguela ecosystem. Part II. Chemistry and related processes. Oceanography and Marine Biology Annual Review 23, 183–251.

Chen, C., Liu, K., Macdonald, R., 2003. Ocean biogeochemistry: a synthesis of the Joint Global Ocean Flux Study (JGOFS). Springer-Verlag, New York, Ch. 3, pp. 53–95.

Cullen, J., Stewart, E., Renger, E., Eppley, R., Winant, C., 1983. Vertical motion of the thermocline, nitracline and chlorophyll maximum layers in relation to currents on the Southern California Shelf. Journal of Marine Research 41, 239–262.

Dade, W., Hogg, A., Boudreau, B., 2001. The Benthic Boundary Layer. Oxford University Press, Oxford, Ch. 2, pp. 4–43.

De La Rocha, C., Passow, U., 2007. Factors influencing the sinking of POC and the efficiency of the biological carbon pump. Deep-Sea Research II 54, 639–658.

Demarcq, H., Barlow, R., Hutchings, L., in prep. Variability in phytoplankton biomass in the Benguela ecosystem using a chlorophyll index derived from satellite data.

Duncombe Rae, C., Shillington, F., Agenbag, J., Taunton-Clark, J., Gründlingh, M., 1992. An Agulhas ring in the South Atlantic Ocean and its interaction with the Benguela upwelling frontal system. Deep-Sea Research I 39, 2009–2027.

EPICA members, 2004. Eight glacial cycles from an Antarctic ice core. Nature 429, 623–628.

Falkowski, P., Flagg, C., Rowe, G., Smith, S., Whitledge, T., Wirick, C., 1988. The fate of a spring phytoplankton bloom: export or oxidation? Continental Shelf Research 8, 457–484.

Falkowski, P., Laws, E., Barber, R., Murray, J., 2003. Ocean biogeochemistry: a synthesis of the Joint Global Ocean Flux Study (JGOFS). Springer-Verlag, New York, Ch. 4, pp. 99–121.

Falkowski, P., Scholes, R., Boyle, E., Canadell, J., Canfield, D., Elser, J., Gruber, N., Hibbard, K., Högberg, P., Linder, S., Mackenzie, F., Moore, B. I., Pedersen, T., Rosenthal, Y., Seitzinger, S., Smetacek, V., Steffen, W., 2000. The global carbon cycle: A test of our knowledge of the earth as a system. Science 290, 291–296.

Fedorov, A., Dekens, P., McCarthy, M., Ravelo, A., deMenocal, P., Barreiro, M., Pacanowski, R., Philander, S., 2006. The Pliocene paradox (Mechanisms for a permanent El Niño). Science 312, 1485–1489.

Field, J., Shillington, F., 2004. Vol. 14 of The Sea. President and Fellows of Harvard College, Ch. 21, pp. 833–861.

Fofonoff, P., Millard, R. J., 1983. Algorithms for computation of fundamental properties of seawater. Unesco Technical Papers in Marine Science 44, 53.

Gago, J., Álvarez-Salgado, X., Gilcoto, M., Pérez, F., 2003. Assessing the contrasting fate of dissolved and suspended organic carbon in a coastal upwelling system ('Ria de Vigo', NW Iberian Peninsula). Estuarine, Coastal and Shelf Science 56, 271–279.

Gardner, W., Mishonov, A., Richardson, M., 2006. Global POC concentrations from in-situ and satellite data. Deep-Sea Research II 53, 718–740.

Gardner, W., Richardson, M., Calson, C., Hansell, D., Mishonov, A., 2003. Determining true particulate organic carbon: bottles, pumps and methodologies. Deep-Sea Research II 50, 655–674.

Gerkema, T., Zimmerman, J., 1995. Generation of nonlinear internal tides and solitary waves. Journal of Physical Oceanography 25, 1081–1094.

Ghosh, P., Bhattacharya, S., Ghosh, P., 2005. A history of atmospheric CO_2 and its effects on plants, animals, and ecosystems. Springer, New York, Ch. 2, pp. 9–34.

Gill, A., 1982. Atmosphere-Ocean Dynamics. Vol. 30 of International Geophysical Series. Academic Press, San Diego.

Gruber, N., Sarmiento, J., 1997. Global patterns of marine nitrogen fixation and denitrification. Global Biogeochemical Cycles 11 (2), 235–266.

Hall, I., Schmidt, S., McCave, I., Reyss, J., 2000. Particulate matter distribution and $^{234}Th/^{238}U$ disequilibrium along the Northern Iberian Margin: implications for particulate organic carbon export. Deep-Sea Research I 17, 557–582.

Hansell, D., 2002. Biogeochemistry of Marine Dissolved Organic Matter. Academic Press, Ch. 15, pp. 685–714.

Hayes, J., 1982. Fractionation, et al.: An introduction to isotopic measurements and terminolgy. Spectra 8 (4), 3–8.

Hill, A., Hickey, B., Shillington, F., Strun, P., Brink, K., Barton, E., Thomas, A., 1998. The Global Coastal Ocean: Regional Studies and Syntheses. Vol. 11 of The Sea. John Wiley & Sons, Ch. 2, pp. 29–67.

Hill, P., McCave, I., 2001. The Benthic Boundary Layer. Oxford University Press, Oxford, Ch. 4, pp. 78–103.

Holloway, P., 1987. Internal hydraulic jumps and solitons at a shelf break region on the Australian North West shelf. Journal of Geophysical Research 92 (C5).

Hopkinson Jr., C.S. Vallino, J., Nolin, A., 2002. Decomposition of dissolved organic matter from the continental margin. Deep-Sea Research II 49, 4461–4478.

Hung, J., Lin, P., Liu, K., 2000. Dissolved and particulate organic carbon in the southern East China Sea. Continental Shelf Research 20, 545–569.

Hutchings, L., Pillar, S., Verheye, H., 1991. Estimates of standing stock, production, and consumption of meso- and macrozooplankton in the Benguela ecosystem. South African Journal of Marine Science 11, 499–512.

Huybers, P., Wunsch, C., 2005. Obliquity pacing of the late Pleistocene glacial terminations. Nature 434, 491–494.

Inthorn, M., 2006a. Lateral particle transport in nepheloid layers-a key factor for organic matter distribution and quality in the Benguela high-productivity area. Ph.D. thesis, Universitat Bremen, Bremen.

Inthorn, M., Wagner, T., Scheeder, G., Zabel, M., 2006. Lateral transport controls distribution, quality, and burial of organic matter along continental slopes in high-productivity areas. Geology 34 (3), 205–208.

IPCC, 2001. Climate Change 2001: The Scientific Basis. Contribution of Working Group I to the Third Assessment Report of the Intergovernmental Panel on Climate Change. Cambridge University Press, Cambridge and New York.

Jahnke, R., Jahnke, D., 2000. Rates of C, N, P and Si recycling and denitrification at the US Mid-Atlantic continental slope depocenter. Deep-Sea Research I 47, 1405–1428.

JGOFS, 1994. Protocols for the Joint Global Ocean Flux Study (JGOFS) core measurements. Intergovernmental Oceanographic Commision Manuals and Guides (29), 101–103.

Johnson, D., Weidemann, A., Pegau, W., 2001. Internal tidal bores and bottom nepheloid layers. Continental Shelf Research 21, 1473–1484.

Jørgensen, B., 2000. Marine Geochemistry. Springer, Ch. 5, pp. 173–200.

Keeling, C., Piper, S., Bacastow, R., Wahlen, M., Whorf, T., Heimann, M., Meijer, H., 2005. A history of atmospheric CO_2 and its effects on plants, animals and ecosystems. Springer, New York, Ch. 5, pp. 83–113.

Kóne, V., Machu, E., Penven, P., Anderson, V., Garçon, V., Fréon, P., Demarcq, H., 2005. Modeling the primary and secondary productions of the southern Benguela upwelling system: A comparitive study through two biogeochemical models. Global Biogeochemical Cycles 19, 1–22.

Kuypers, M., Lavik, G., Woebken, D., Schmid, M., Fuchs, B., Amann, R., Jørgensen, B., Jetten, M., 2005. Massive nitrogen loss from the Benguela upwelling system through anaerobic ammonium oxidation. Proceedings of the National Academy of Sciences of the USA 102 (18), 6478–6483.

Lalli, C., Parsons, T., 1997. Biological Oceanography: An Introduction, 2nd Edition. Butterworth-Heinemann, Oxford.

Lamy, F., Kaiser, J., Arz, H., Hebbeln, D., Ninnemann, U., Timm, O., Timmermann, A.,

Toggweiler, J., 2007. Modulation of the bipolar seesaw in the Southeast Pacific during Termination 1. Earth and Planetary Science Letters in press.

Lentz, S., Trowbridge, J., 1991. The bottom boundary layer over the Northern California shelf. Journal of Physical Oceanography 21, 1186–1201, pragtag.

Liu, K., Iseki, K., Chao, S., 2000. The changing ocean carbon cycle. Cambridge University Press, Cambridge, Ch. 7, pp. 187–239.

Lochte, K., Anderson, R., Francois, R., Jahnke, R., Shimmield, G., Vetrov, A., 2003. Ocean biogeochemistry: a synthesis of the Joint Global Ocean Flux Study (JGOFS). Springer-Verlag, New York, Ch. 8, pp. 195–216.

Lutjeharms, J., Stockton, P., 1987. Kinematics of the upwelling front off Southern Africa. South African Journal of Marine Science 5, 35–49.

Malone, T., Hopkins, T., Falkowski, P., Whitledge, T., 1983. Production and transport of phytoplankton biomass over the continental shelf of the New York Bight. Continental Shelf Research 1, 305–337.

Marinov, I., Gnanadesikan, A., Toggweiler, J., Sarmiento, J., 2006. The Southern Ocean biogeochemical divide. Nature 441, 964–967.

McCave, I., 2002. Ocean Margin Systems. Springer-Verlag, Berlin Heidelberg, Ch. Sedimentary settings on continental margins-an overview, pp. 1–14.

McCave, I., Hall, I., 2002. Turbidity of waters over the Northwest Iberian continental margin. Progress in Oceanography 52, 299–313.

McCave, I., Hall, I., Antia, A., Chou, L., Dehairs, F., Lampitt, R., Thomsen, L., van Weering, T., Wollast, R., 2001. Distribution, composition and flux of particulate material over the European margin at 47°-50°N. Deep-Sea Research II 48, 3107–3139.

McPhee-Shaw, E., Kunze, E., 2002. Boundary layer intrusions from a sloping bottom: A mechanism for generating intermediate nepheloid layers. Journal of Geophysical Research 107 (C6), 1–16.

McPhee-Shaw, E., Sternberg, R., Mullenbach, B., Ogston, A., 2004. Observations of intermediate nepheloid layers on the northern California continental margin. Continental Shelf Research 24, 693–720.

Mishonov, A., Gardner, W., Richardson, M., 2003. Remote sensing and surface POC concentration in the South Atlantic. Deep-Sea Research II 50, 2997–2015.

Moloney, C., 1992. Simulation studies of trophic flows and nutrient cycles in Benguela upwelling foodwebs. South African Journal of Marine Science 12, 457–476.

Monteiro, P., 1996. The oceanography, the biogeochemistry and the fluxes of carbon dioxide in the Benguela upwelling system. Ph.D. thesis, University of Cape Town, Rondebosch, 7700, South Africa.

Monteiro, P., Nelson, G., van der Plas, A., Mabille, E., G.W., B., Klingelhoeffer, E., 2005. Internal tide-shelf topography interactions as a forcing factor governing the large-scale distribution and burial fluxes of particulate organic matter (POM) in the Benguela upwelling system. Continental Shelf Research 25, 1864–1876.

Nakata, K., Doi, T., 2006. Estimation of primary production in the ocean using a physical-biological coupled ocean carbon cycle model. Environmental Modelling & Software 21, 204–228.

Nelson, G., 1989. Poleward Flows Along Eastern Ocean Boundaries. Springer-Verlag, New York, Ch. Poleward motion in the Benguela area, pp. 110–130.

Nelson, G., Hutchings, L., 1983. The Benguela Upwelling Area. Progress in Oceanography 12 (333-356).

Nelson, G., Polito, A., 1987. Information on currents in the Cape Penninsula area, South Africa. South African Journal of Marine Science 5, 287–304.

Pahnke, K., Zahn, R., 2005. Southern Hemisphere water mass conversion linked with North Atlantic climate variability. Science 307, 1741–1746.

Painting, S., Moloney, C., Probyn, T., Tibbles, B., 1992. Microheterotrophic pathways in the southern Benguela upwelling system. South African Journal of Marine Science 12, 527–543.

Petit, J., Jouzel, J., Raynaud, D., Barkov, N., Barnola, J., Basile, I., Bender, M., Chappellaz, J., Davis, M., Delaygue, G., Delmotte, M., Kotlyakov, V., Legrand, M., Lipenkov, V., Lorius, C., Pépin, L., Ritz, C., Saltzman, E., Stievenard, M., 1999. Climate and atmospheric history of the past 420, 000 years from the Vostok ice core, Antarctica. Nature 399, 429–436.

Pitcher, G., Boyd, A., Horstman, D., Mitchell-Innes, B., 1998. Subsurface dinoflagellate populations, frontal blooms and the formation of red tide in the southern Benguela upwelling system. Marine Ecology Progress Series 172, 253–264.

Pitcher, G., Brown, P., Mitchell-Innes, B., 1992. Spatio-temporal variability of phytoplankton in the southern Benguela upwelling system. South African Journal of Marine Science 12, 439–456.

Pitcher, G., Calder, D., 2000. Harmful algal blooms of the southern Benguela current: A review and appraisal of monitoring from 1989 to 1997. South African Journal of Marine Science 22, 255–271.

Pitcher, G., Walker, D., Mitchell-Innes, B., Moloney, C., 1991. Short-term variability during an anchor station study in the southern Benguela upwelling system: Phytoplankton dynamics. Progress in Oceanography 28, 39–64.

Pond, S., Pickard, G., 1983. Introductory Dynamical Oceanography, 2nd Edition. Elsevier Butterworth-Heinemann, Oxford.

Probyn, T., 1992. The inorganic nitrogen nutrition of phytoplankton in the southern Benguela: New production, phytoplankton size and implications for pelagic foodwebs. In: Payne, A., Brink, K., Mann, K., Hillborn, R. (Eds.), Benguela Trophic Functioning. Vol. 12. pp. 411–420.

Raven, J., Falkowski, P., 1999. Oceanic sinks for atmospheric CO_2. Plant, Cell and Environment 22, 741–755.

Roe, G., Allen, M., 1999. A comparison of competing explanations for the 100 000-yr ice age cycle. Geophysical Research Letters 26 (15), 2259–2262.

Rogers, J., Bremner, J., 1991. The Benguela Ecosystem. Part VII. Marine-geological aspects. Oceanography and Marine Biology Annual Review 29, 1–85.

Rowe, G., 1987. Seasonal growth and senescence in continental shelf ecosystems: A test of the SEEP hypothesis. South African Journal of Marine Science 5, 147–161.

Rowe, G., Smith, S., Falkowski, P., Whitledge, T., Theroux, R., Phoel, W., Ducklow, H., 1986. Do continental shelves export organic matter? Nature 324, 559–561.

Royer, D., Berner, R., Montañez, I., Tabor, N., Beerling, D., 2004. CO_2 as a primary driver of Phanerozoic climate. GSA Today 14 (3), 4–10.

Rullkötter, J., 2000. Marine Geochemistry. Springer, Berlin, Ch. 4, pp. 129–172.

Rutgers van der Loeff, M., Meyer, R., Rudels, B., Rachor, E., 2002. Resuspension and particle transport in the benthic nepheloid layer in and near Fram Strait in relation to faunal abundances and ^{234}Th depletion. Deep-Sea Research I 49, 1941–1958.

Sandstrom, H., Elliot, J., 1984. Internal tide and solitons on the Scotian Shelf: A nutrient pump at work. Journal of Geophysical Research 89, 6415–6426.

Sarmiento, J., May 31 1993. Ocean carbon cycle. Chemical and Engineering News, 30–42.

Sarmiento, J., Bender, M., 1994. Carbon biogeochemistry and climate change. Photosynthesis Research 39, 209–234.

Schimel, D., Enting, I., Heimann, M., Wigley, T., Raynaud, D., Alves, D., Siegenthaler, U., 2000. The Carbon Cycle. Cambridge University Press, Cambridge, Ch. 1, pp. 7–33.

Shannon, L., 1985. The Benguela ecosystem part I. Evolution of the Benguela, physical features and processes. Oceanography and Marine Biology Annual Review 23, 105–182.

Shannon, L., Nelson, G., 1996. The South Atlantic: Present and past circulation. Spinger-Verlag, Berlin Heidelberg, Ch. The Benguela: Large scale features and processes and system variability, pp. 163–210.

Shannon, L., Pillar, S., 1986. The Benguela ecosystem. Part III. Plankton. Oceanography and Marine Biology Annual Review 24, 65–170.

Sharp, J., Benner, R., Bennet, L., Carlson, C., Fitzwater, S., Peltzer, E., Tupas, L., 1995. Analyses of dissolved organic carbon in seawater: the JGOFS EqPac methods comparison. Marine Chemistry 48, 91–108.

Sharp, J., Carlson, C., Peltzer, E., Castle-Ward, D., Savidge, K., Rinker, K., 2002. Final dissolved organic carbon broad based community intercalibration and preliminary use of DOC reference materials. Marine Chemistry 77, 239–253.

Shaviv, N., Veizer, J., July 2003. Celestial driver of Phanerozoic climate? GSA Today.

Sherr, E., Sherr, B., Verity, P., 2002. Distribution and relation of total bacterial, active bacteria, bacterivory, and volume of organic detritus in Atlantic continental shelf waters off Cape Hatteras NC, USA. Deep-Sea Research II 49 (20), 4571–4585.

Shillington, F., 1998. The Global Coastal Ocean: Regional Studies. Vol. 11 of The Sea. John Wiley & Sons, Inc., New York, Ch. 20, pp. 583–604.

Shillington, F., Hutchings, L., Probyn, T., Waldron, H., Peterson, W., 1992. Filaments and the Benguela frontal zone: Offshore advection or recirculating loops? South African Journal of Marine Science 12, 207–218.

Shillington, F., Reason, C., Duncombe Rae, C., Florenchie, P., Penven, P., 2006. Benguela: Predicting a Large Marine Ecosystem. Vol. 14 of Large Marine Ecosystems. Elsevier B.V./Ltd., Ch. 4, pp. 47–68.

Siegenthaler, U., Sarmiento, J., 1993. Atmospheric carbon dioxide and the ocean. Nature 365, 119–125.

Sigman, D., Boyle, E., 2000. Glacial/interglacial variations in atmospheric carbon dioxide. Nature 407, 859–869.

Solomon, S., Qin, D., Manning, M., Alley, R., Berntsen, T., Bindoff, N., Chen, Z., Chidthaisong, A., Gregory, J., Hegerl, G., Heimann, M., Hewitson, B., Hoskins, B., Joos, F., Jouzel, J., Kattsov, V., Lohmann, U., Matsuno, T., Molina, M., Nicholls, N., Overpeck, J., Raga, G., Ramaswamy, V., Ren, J., Rusticucci, M., Somerville, R., Stocker, T., Whetton, P., Wood, R., Wratt, D., 2007. Climate Change 2007: The Physical Science Basis. Contribution of Working Group I to the Fourth Assessment Report of the Intergovernmental Panel on Climate Change. Cambridge University Press, Cambridge and New York, Ch. Technical Summary.

Soulsby, R., 1983. Physical Oceanography of coastal and shelf seas. Elsevier, Amsterdam, Ch. 5, pp. 189–266.

Stramma, L., Peterson, R., 1989. Geostrophic transport in the Benguela Current region. Journal of Physical Oceanography 19, 1440–1448.

Stuiver, M., Quay, P., Ostlund, H., 1983. Abyssal water carbon-14 distribution and the age of the world oceans. Science 219 (4586), 849–851.

Suess, E., 1980. Particulate organic carbon flux in the oceans - surface productivity and oxygen utilization. Nature 288, 260–263.

Swart, S., Waldron, H., Hutchings, L., 2007. Evidence of carbon transport between shelf and slope waters in the Benguela upwelling system. African Journal of Marine Science 29 (1), 137–139.

Thomsen, L., 1999. Processes in the benthic boundary layer at continental margins and their implication for the benthic carbon cycle. Journal of Sea Research 41, 73–86.

Thomsen, L., 2002. Ocean Margin Systems. Springer-Verlag, Berlin Heidelberg, Ch. The benthic boundary layer, pp. 143–155.

Thomsen, L., McCave, I., 2000. Aggregation processes in the benthic boundary layer at the Celtic Sea continental margin. Deep-Sea Research I 47, 1389–1404.

Thomsen, L., van Weering, T., 1998. Spatial and temporal variability of particulate matter in the benthic boundary layer at the N.W. European Continental Margin (Goban Spur). Progress in Oceanography 42, 61–76.

Toggweiler, J., 1993. Carbon overconsumption. Nature 363, 210–211.

Toggweiler, J., 1995. Anthropogenic CO_2: The natural carbon cycle reclaims center stage. Supplement to Reviews of Geophysics, 1249–1252.

Toggweiler, J., in press. Modest role for atmospheric CO_2 in the progression of ice ages.

Toggweiler, J., Russell, J., Carson, S., 2006. Midlatitude westerlies, atmospheric CO_2, and climate change during the ice ages. Paleoceanography 21, 1–15.

Touratier, F., Field, J., Moloney, C., 2003. Simulated carbon and nitrogen flows of the planktonic food web during an upwelling relaxation period in St Helena Bay (southern Benguela ecosystem). Progress in Oceanography 58, 1–41.

Tréguer, P., Legendre, L., Rivkin, R., Ragueneau, O., Dittert, N., 2003. Ocean biogeochemistry: a synthesis of the Joint Global Ocean Flux Study (JGOFS). Springer-Verlag, New York, Ch. 6, pp. 145–156.

Trowbridge, J., Chapman, D., Candela, J., 1998. The Global Coastal Ocean: Processes and Methods. Vol. 10 of The Sea. John Wiley & Sons, Inc., New York, Ch. 3, pp. 63–88.

Tsunogai, S., Watanabe, S., Sato, T., 1999. Is there a "continental shelf pump" for the absorption of atmospheric CO_2? Tellus 51, 701–712.

Tyrrell, T., Lucas, M., 2002. Geochemical evidence of denitrification in the Benguela upwelling system. Continental Shelf Research 22, 2497–2511.

van Weering, T., De Stigter, H., Balzer, W., Epping, E., Graf, G., Hall, I., Helder, W., Khripounoff, A., Lohse, L., McCave, I., Thomsen, L., Vangriesheim, A., 2001. Benthic dynamics and carbon fluxes on the NW European continental margin. Deep-Sea Research II 48, 3191–3221.

van Weering, T., de Stigter, H., Boer, W., de Haas, H., 2002. Recent sediment transport and accumulation on the NW Iberian margin. Progress in Oceanography 52, 349–371.

van Weering, T., McCave, I., 2002. Benthic processes and dynamics at the NW Iberian margin: an introduction. Progress in Oceanography 52, 123–128.

Veizer, J., Godderis, Y., François, L., 2000. Evidence for decoupling of atmospheric CO_2 and global climate during the Phanerozoic eon. Nature 408, 698–701.

Verdugo, P., Alldredge, A., Azam, F., Kirchman, D., Passow, U., Santschi, P., 2004. The oceanic gel phase: a bridge in the DOM-POM continuum. Marine Chemistry 92, 67–85.

Verheye, H., 1991. Short-term variability during an anchor station study in the southern Benguela upwelling system: Abundance, distribution and estimated production of mesozooplankton with special reference to Calanoides carinatus (krooyer, 1849). Progress in Oceanography 28, 91–119.

Verity, P., Bauer, J., Flagg, C., DeMaster, D., Repeta, D., 2002. The Ocean Margins Program: an interdisciplinary study of carbon sources, transformations, and sinks in a temperate continental margin system. Deep-Sea Research II 49, 4273–4295.

Waldron, H., Probyn, T., Brundrit, G., 1997. Preliminary annual estimates of regional nitrate supply in the southern Benguela using coastal sea level fluctuations as a proxy for upwelling. South African Journal of Marine Science 18, 93–106.

Waldron, H., Probyn, T., Brundrit, G., 1998. Carbon pathways and export associated with the southern Benguela upwelling system: A re-appraisal. South African Journal of Marine Science 19, 113–118.

Waldron, H., Probyn, T., Lutjeharms, J., Shillington, F., 1992. Carbon export associated with the Benguela upwelling system. South African Journal of Marine Science 12, 369–374.

Walker, D., Pitcher, G., 1991. The dynamics of phytoplankton populations, including a red-tide bloom, during a quiescent period in St Helena Bay, South Africa. South African Journal of Marine Science 10, 61–70.

Walsh, J., 1991. Importance of continental margins in the marine biogeochemical cycling of carbon and nitrogen. Nature 350, 53–55.

Walsh, J., Biscaye, P., Csanady, G., 1988a. The 1983-1984 Shelf Edge Exchange Processes (SEEP)-I experiment: hypotheses and highlights. Continental Shelf Research 8, 435–456.

Walsh, J., Dieterle, D., Meyers, M., 1988b. A simulation analysis of the fate of phytoplankton within the Mid-Atlantic Bight. Continental Shelf Research 8, 757–787.

Walsh, J., Rowe, G., Iverson, R., McRoy, C., May 1981. Biological export of shelf carbon is a sink of the global CO_2 cycle. Nature 291, 196–201.

Watson, A., Bakker, D., Ridgwell, A., Boyde, P., Law, C., 2000. Effect of iron supply on Southern Ocean CO_2 uptake and implications for glacial atmospheric CO_2. Nature 407, 730–733.

Watson, J., Orr, J., 2003. Ocean biogeochemistry: a synthesis of the Joint Global Ocean Flux Study (JGOFS). Springer-Verlag, New York, Ch. 5, pp. 124–143.

Wollast, R., 1998. The Global Coastal Ocean: Processes and Methods. Vol. 10 of The Sea. John Wiley & Sons, New York, Ch. 9, pp. 213–252.

Wollast, R., 2002. Ocean Margin Systems. Springer-Verlag, Berlin Heidelberg, Ch. Continental margins-Review of geochemical settings, pp. 15–31.

Wollast, R., Chou, L., 2001a. Ocean Margin EXchange in the Northern Gulf of Biscay: OMEX I. An Introduction. Deep-Sea Research II 48, 1971–2978.

Wollast, R., Chou, L., 2001b. The carbon cycle at the ocean margin in the northern Gulf of Biscay. Deep-Sea Research II 48, 3265–3293.

Wong, G., Chao, S., Li, Y., Shiah, F., 2000. The Kuroshio edge exchange processes (KEEP) study - an introduction to hypotheses and highlights. Continental Shelf Research 20, 335–347.

Zachos, J., Pagani, M., Sloan, L., Thomas, E., Billups, K., 2001. Trends, rhythms, and aberrations in global climate 65 ma to present. Science 292 (686), 686–693.

Zimmerman, C., Keefe, C., Bashe, J., 1997. Determination of Carbon and Nitrogen in sediments and particulates of estuarine/coastal waters using elemental analysis. U.S. Environmental Protection Agency, Cincinnati, Ohio, 1st Edition.

Appendix A

Year	Month	Cruise	Hydrographic data	Full resolution turbidity data	Bottle resolution turbidity data
2001	1	Alg089			
2001	2	Alg091	x		
2001	3	Alg093			
2001	4	Alg094	x		
2001	5	Alg095			
2001	6	Alg096	x		
2001	7	Alg097	x		
2001	8	Alg098	x		
2001	9				
2001	10	Alg099	x		
2001	11				
2001	12	Alg101			
2002	1	Alg102	x		
2002	2		x		
2002	3	Alg105			
2002	4	Afr167			
2002	5	Alg108	x		
2002	6	Alg110	x		
2002	7				
2002	8				
2002	9	Afr169	x		
2002	10	Afr171			
2002	11	Alg116			
2002	12	Alg118			
2003	1	Afr173	x	x	
2003	2	Afr174	x	x	
2003	3	Afr176			
2003	4				
2003	5	Afr178			x
2003	6	Afr179	x	x	
2003	7	Afr180	x	x	
2003	8	Afr181	x	x	

Year	Month	Cruise	Hydrographic data	Full resolution turbidity data	Bottle resolution turbidity data
2003	9	Afr184			
2003	10	Afr186			
2003	11	see above			
2003	12	Afr187	x		
2004	1	Afr188	x		
2004	2	Afr189	x		
2004	3	Afr190	x		
2004	4	Afr192	x	x	
2004	5	Afr193	x	x	
2004	6	Afr194			
2004	7	Afr196			x
2004	8	Afr197			x
2004	9	Afr199			
2004	10	as below			
2004	11	Afr201	x	x	
2004	12	Afr202	x	x	
2005	1	Afr203			x
2005	2	Afr204			x
2005	3	Afr205			
2005	4	Afr206			x
2005	5	Afr207			
2005	6	Alg136			
2005	7	Afr209			x
2005	8	Afr210			x
2005	9	Afr211			x
2005	10	Afr212			
2005	11				
2005	12	Afr213			x
2006	1	Afr214			x
2006	2	Afr215			x
2006	3	Afr216			x
2006	4	Afr217			
2006	5	Afr218			x
2006	6	Afr219			x

The data from the St Helena Bay Monitoring Line used in this study. Data was obtained from Marine and Coastal Management, Cape Town, South Africa. Hyrdographic data was used in calculating the thickness of the bottom boundary layer (Chapter 2), and to derive buoyancy frequency profiles (Chapter 2). Full resolution turbidity data was used to define the thickness of the bottom nepheloid layer (Chapter 4). Full resolution and bottle resolution turbidity data were used together to make the turbidity time series at the bottom of the water column (Chapter 4). Data marked with o was used in Chapter 3, to show the cross shelf profiles of temperature, salinity and turbidity.

Appendix B

Statistical methods

All statistics were computed using the native capabilities of Matlab (version 7.4) and the Matlab Statistics toolbox (version 6.0), as detailed below.

Fourier analysis

The Fourier power spectrum's presented for current meter data were calculated from a Matlab routine developed by Dr J.L. Melice, based on the fast Fourier transform (FFT) function.

- FFT(x) is the discrete Fourier transform (DFT) of vector x.
  - For length N input vector x, the DFT is a length N vector X, with elements
  - $\sum_{n=1}^{N} x(n) \times \exp^{[-j \times 2 \times \pi \times (k-1) \times (n-1)/N]}, 1 \leq k \leq N$
- The power spectrum was then calculated from X as follows:
  - power=abs(X(1:N/2))^2; power=power/max(power); corresponding to the frequencies:
  - frequency=(1:N/2)/(N/2)$\times$1/2

Standard deviation and Mean Absolute Deviation

Standard deviations were calculated using the function NANSTD.

- NANSTD(X)
  - returns the sample standard deviation of the values in X, treating NaNs as missing values.
  - The standard deviation is calculated as the square root of the variance, where variance is calculated as follows:
  - VAR(X) = SUM(RESID.×CONJ(RESID)) / (N-1)
  - where RESID = X - MEAN(X), N is LENGTH(X) and CONJ(X) is the complex conjugate of X.

Mean Absolute Deviations (suitable for non Gaussian distributions) were calculated using the MAD function. It should be noted that a MAD is always less than or equal to a standard deviation.

- Y = MAD(X)
  - returns the mean absolute deviation of the values in X.
  - Y is MEAN(ABS(X-MEAN(X)).
  - MAD treats NaNs as missing values, and removes them.
- Reference: L. Sachs, *Applied Statistics: A Handbook of Techniques*, Springer-Verlag, 1984, page 253.

Correlations, linear regressions, regression statistics (ρ, R^2)

In all cases quoted correlation statistics between variables were based on a linear regression between the variables concerned. Linear regressions between variables were performed using the REGRESS function.

- [B, BINT, R, RINT, STATS] = REGRESS(Y, X)
  - REGRESS is a multiple linear regression using least squares.
  - In the vector B are the regression coefficients in the linear model Y = X×B(1) + B(2).
  - X is an n-by-p design matrix, with rows corresponding to observations and columns to predictor variables. Y is an n-by-1 vector of response observations.
  - BINT is a matrix of 95% confidence intervals for B.
  - R is a vector of residuals
  - The vector STATS contains, in the following order, the R-square statistic, the F statistic and p value for the full model, and an estimate of the error variance.
  - The R-square value is one minus the ratio of the error sum of squares to the total sum of squares.
  - REGRESS treats NaNs in X or Y as missing values, and removes them.
- References:
  - [1] Chatterjee, S. and A.S. Hadi (1986), Influential Observations, High Leverage Points, and Outliers in Linear Regression, *Statistical Science* 1(3) :379-416.
  - [2] Draper N. and H. Smith (1981), *Applied Regression Analysis*, 2nd ed., Wiley.

Stepwise regression

The stepwise regression was conducted using the STEPWISE function. Only predictors which significantly improved the overall fit of the model were included (i.e. those which had co-efficients which).

- STEPWISE(X, Y)

- displays an interactive tool for creating a regression model to predict the vector Y using a subset of the predictors given by columns of the matrix X. Initially no predictors are included in the model, but you can click on predictors to switch them into and out of the model. STEPWISE automatically includes a constant term in all models. For each predictor in the model, its least squares coefficient is plotted with a blue filled circle. For each predictor not in the model, a filled red circle indicates the coefficient it would have if it were added to the model. Horizontal bars indicate 90% (colored) and 95% (black) confidence intervals.

- Reference: Draper, Norman and Smith, Harry, *Applied Regression Analysis*, Second Edition, John Wiley & Sons, Inc. 1981 pp. 307-312.

T-tests and Wilcoxon rank sum test

T-tests were performed with the function TTEST2. The test was performed either assuming equal, or unequal variances, based on the result of VARTEST2, described below.

- H = TTEST2(X, Y, ALPHA, TAIL,VARTYPE)

  - performs a T-test of the hypothesis that two independent samples, in the vectors X and Y, come from distributions with equal means, at the significance level (100×ALPHA)% and returns the result of the test in H.
  - When VARTYPE is 'equal', TTEST2 performs the default test assuming equal variances. When VARTYPE is 'unequal', TTEST2 performs the test assuming that the two samples come from normal distributions with unknown and unequal variances.

- Reference: E. Kreyszig, *Introductory Mathematical Statistics*, John Wiley, 1970, section 13.4. (Table 13.4.1 on page 210)

The equality of variances between two samples was tested using VARTEST2.

- H = VARTEST2(X, Y, ALPHA)
  - performs an F test of the hypothesis that two independent samples, in the vectors X and Y, come from normal distributions with the same variance, against the alternative that they come from normal distributions with different variances, at the significance level (100×ALPHA).

The Wilcoxon rank sum test for equal medians was performed using the function RANKSUM

- [P, H] = RANKSUM(X,Y)
  - performs a two-sided rank sum test of the hypothesis that two independent samples, in the vectors X and Y, come from distributions with equal medians. It returns the result of the hypothesis test, performed at the 0.05 significance level, in H. H=0 indicates that the null hypothesis ("medians are equal") cannot be rejected at the 5% level. H=1 indicates that the null hypothesis can be rejected at the 5% level.
- References:
  - [1] Hollander, M. and D. A. Wolfe. *Nonparametric Statistical Methods.* Wiley, 1973.
  - [2] Gibbons, J.D. *Nonparametric Statistical Inference*, 2nd ed. M. Dekker, 1985.

Percentiles

Percentiles were calculated using the function PRCTILE.

- Y = PRCTILE(X, P)
  - returns percentiles of the values in X. P is a scalar or a vector of percent values.

- Percentiles are specified using percentages, from 0 to 100. For an N element vector X, PRCTILE computes percentiles as follows:
  1. The sorted values in X are taken as the $100\times(0.5/N)$, $100\times(1.5/N)$, ..., $100\times((N-0.5)/N)$ percentiles.
  2. Linear interpolation is used to compute percentiles for percent values between $100\times(0.5/N)$ and $100\times((N-0.5)/N)$
  3. The minimum or maximum values in X are assigned to percentiles for percent values outside that range.
- PRCTILE treats NaNs as missing values, and removes them.

Data interpolation and contouring

All contour plots were produced using the Matlab functions CONTOUR and CONTOURF. Prior to plotting, data were interpolated onto regular grids using the function GRIDDATA. GRIDDATA uses linear Delaunay triangulation for interpolation.